Technical Report No. 121

MEASUREMENT OF SMALL SCALE TURBULENCE IN AN AXISYMMETRIC JET USING MOVING HOT WIRES

by

Hussein J. Hussein

Turbulence Research Laboratory
Faculty of Engineering and Applied Sciences
University at Buffalo/SUNY
Buffalo, NY 14260

September 1988

TABLE OF CONTENTS

ACKNOWLEDGMENTS

I thank all those who helped me with my dissertation at the Turbulence Research Laboratory. Most of all I thank my advisor, Professor W.K. Geroge for his friendship, support and advice over the course of this study. I also want to thank Professors D.B. Taulbee and W.J. Rae for their never ending encouragement, S.H. Woodward for his help with the experiments and for building the rotating wing apparatus. The above mentioned in addition to the other members of the the TRL have given a lot of themselves in making my stay at Buffalo both enjoyable and fulfilling.

My acknowledgment would not be complete without stating my gratitude to Mrs. Eileen Graber for her friendship and for typing this manuscript on such a short notice. I thank my family for their patience and understanding for all the years I was away from home. Finally this research was supported by the National Science Foundation under Grant No. MEA8316833, is gratefully acknowledged

ABSTRACT

The present work consists of an extensive investigation of an axisymmetric turbulent jet. The overall object is to provide a basis for evaluating turbulence closure hypotheses from measurements of the moments of the velocity and the rate of dissipation of turbulence energy. The secondary objectives are: a direct measurement of the dissipation, evaluation of hot-wire errors in this high turbulence intensity flow, evaluation of prior LDA data (Capp 1983), and assessment of Taylor's frozen field hypothesis.

The high turbulence intensity in a jet gives rise to cross-flow and rectification errors on hot-wires. These errors as well as the effect of the fluctuating convection velocity on the measured derivatives can be reduced by superimposing a velocity on the hot-wire, thereby reducing the effective turbulence intensity. This was accomplished by using hot-wires mounted on a rotating wing which reduced the effective turbulence intensity from 30% to 11% at the centerline of the jet and to a maximum of 38% at the outer edge.

Measurements of the dissipation in the past always relied on the assumption of Taylor's frozen field hypothesis and the assumption of local isotropy. The former is known to fail in high turbulence intensity flows while the latter has never been confirmed experimentally in laboratory shear flows. In this experiment, spatial velocity derivatives were measured using parallel single-wires and a new AXI-probe which consisted of 1-1/2 x-wires. The superposition of a mean velocity on the wires enabled both the evaluation of the effects of turbulence intensity on Taylor's hypothesis, and the use of this hypothesis to obtain the velocity derivative in the streamwise

direction. The derivative measurements showed that the flow could not be considered locally isotropic, but did satisfy the derivative relations for axisymmetric homogeneous turbulence.

The experimental results motivated a review of the theory of axisymmetric homogeneous turbulence. The concept of local axisymmetry was introduced and defined to mean that the derivative statistics satisfied the relations for axisymmetric homogeneous turbulence. The derivative relations and thus the dissipation and mean square vorticity, were shown to depend only on four invariants which could be directly measured with the AXI-probe. The experimental results together with the hypothesis of local axisymmetry were used to determine the dissipation directly.

LIST OF FIGURES

CHAPTER 1

Introduction

1.1 Historical Review

The axisymmetric jet represents a benchmark for research into the physics of turbulent fluid flow. Although experiments are complicated by the high turbulence intensities of this flow, theoretical study is simplified since the jet is a simple, free shear flow to which boundary-layer approximations can be applied. The contribution of the axisymmetric jet to the understanding of turbulence is evidenced by volumes of publications involving experimental data, mathematical analysis, and computational modeling.

Early experimental investigations of the jet include the work of Corrsin (1943), Corrsin and Uberoi (1949, 1951), Reichart (1951), Hinze and van der Hegge Zijnen (1949), and Corrsin and Kistler (1954). The failure of the turbulence intensities to attain self-preservation in these early works motivated the efforts of Wygnanski and Fiedler (1969) using linearized hot-wires. Their work became the standard reference for the quantitative description for profiles of mean velocities, turbulence stresses and triple correlation coefficients.

Questions concerning the validity of the data of Wygnanski and Fiedler (1969) were first raised by the Turbulence Research Laboratory of SUNY at Buffalo during the early 1980's. Baker (1980), while investigating the evolution of a hot axisymmetric turbulent jet into a turbulent plume using numerical methods and an eddy viscosity closure scheme, discovered that the data of Wygnanski and Fiedler (1969) failed to satisfy the momentum constraints of the integrated axial momentum equation (See also Baker 1980 and George et al.1982).

Seif's (1981) subsequent numerical study, using both k-ϵ and Reynolds stress models, also showed significant deviation from that data. These difficulties prompted the experimental study by Capp (1983) using LDA techniques to investigate the source of the discrepancy. Capp's work, established that the problem was facility-related, and that there could be a significant difference between a jet in a confined enclosure versus one in an infinite environment.

Occasionally researchers used the far field of the jet to evaluate new experimental methods or to examine the role of large-scale structures. Rodi (1975), investigating a new technique for analysing hot-wire signals, measured mean and second moments at a position 75 diameters from the jet exit. Lehrmann (1986) used different LDA seeding techniques to examine the entrainment process as evidenced by variations in profiles of mean velocity and turbulence intensities. For the most part, however, experimenters found it more convenient (because of the facility size and the difficulty of measuring highly turbulent flows with low mean velocities) to direct their attention to the near field region of the jet.

The jet has also been heavily studied by turbulent modelers. Tollmien's (1926) study based on Prandtl's mixing-length theory was the first theoretical treatment of the circular jet. Many other modeling studies have since followed (Rodi and Spaulding 1970, Launder et al. 1975, Seif 1981 and Taulbee 1988).

There have also been several recent re-examinations of jet theory. Schneider (1985) analysed the flow field with a multiple scaling approach using inner and outer expansions. He examined the effect of boundary conditions on the entrainment and the resulting

increase in the centerline velocity decay rate and the loss of momentum. His results applied to the jet of this experiment confirm the analysis of George et al. (1982) that the momentum integral should remain constant at its value at the jet exit. George et al. (1985) and George (1988a) considered the effect of external screens and a co-flowing stream on the flow and established conditions for their use.

In a separate study, George (1988b) discovered a flaw in the original similarity theory which assumed all jets to asymptotically behave as point sources of momentum. He showed that the self-preserving state was determined by the initial conditions and was not independent of them, as had been previously assumed (Townsend 1976). It also revealed that any x-variation of the jet transverse length scale satisfying $d\delta/dx \propto R_s/U_s^2$ where R_s and U_s are the scales for the Reynolds stress and mean velocity respectively, can result in a self-preserving jet, at least at the order of the mean momentum equation. This theory explained the exponential spread observed by Lee and Reynolds (1985), as well as many of the differences observed by different experimenters who used different initial conditions.

1.2 Governing Equation for Axisymmetric Jet Momentum Equation

Momentum Equation:

The momentum equation of incompressible isothermal steady state turbulent flow is obtained from the Navier-Stokes equations. For an axisymmetric jet with no swirl the turbulent shear stresses $\overline{uw}$ are zero, the azimuthal component of the velocity field W is also zero. The equation governing the mean velocity are:

$$U \frac{\partial U}{\partial x} + V \frac{\partial U}{\partial r} = - \frac{1}{\rho} \frac{\partial P}{\partial x} - \frac{1}{r} \frac{\partial}{\partial r} (\overline{ruv}) - \frac{\partial}{\partial x} \overline{u^2} \qquad (1.2.1)$$

$$U \frac{\partial V}{\partial x} + V \frac{\partial V}{\partial r} = - \frac{1}{\rho} \frac{\partial P}{\partial x} - \frac{1}{r} \frac{\partial}{\partial r} \overline{rv^2} - \frac{\partial}{\partial x} \overline{uv} + \frac{\overline{w^2}}{r} \qquad (1.2.2)$$

The velocity and lengths in the above equations scale as,

$$\frac{\partial U}{\partial x} \sim \frac{U}{L}$$

$$\frac{\partial}{\partial r} \sim \frac{1}{\delta}$$

For a jet issuing into a quiescent environment assuming a thin shear layer approximation $\delta/L << 1$, and scaling equations (1.2.1) and (1.2.2) the following first order momentum equation, is obtained.

$$U \frac{\partial U}{\partial x} + V \frac{\partial U}{\partial y} = - \frac{1}{r} \frac{\partial}{\partial r} \overline{ruv} - \frac{1}{\rho} \frac{\partial P}{\partial x}$$

$$\frac{P_\infty}{\rho} - \frac{P}{\rho} = - \int_r^\infty \frac{\partial \overline{v^2}}{\partial r} \partial r - \int_r^\infty \left[\frac{\overline{v^2} + \overline{w^2}}{r} \right]$$

the continuity equation is,

$$\frac{\partial U}{\partial x} + \frac{1}{r} \frac{\partial (rV)}{\partial r} = 0$$

The validity of the measured data can be verified by utilizing the integrated form of above equations (see Section 1.3).

The interest in measuring the terms in the momentum equation stem from the classical problem of the turbulence equations being an unclosed set of equations. The aim of modelers is to determine the mean velocity from the momentum equation. Because the presence of the Reynolds stress there are more unknowns than equations making it necessary to find a way of closing the equations.

Reynolds Stress Equations:

The transport equations for the Reynolds stresses are:

$$\frac{D\overline{u_i u_j}}{Dt} = -\frac{\partial}{\partial x_k}\left[\overline{u_i u_j u_k} + \frac{\overline{pu_i}}{\rho}\delta_{jk} + \frac{\overline{pu_j}}{\rho}\delta_{ik} - \nu\frac{\overline{\partial u_i\, u_j}}{\partial x_k}\right]$$

$$-\overline{u_i u_k}\frac{\partial U_j}{\partial x_k} - \overline{u_j u_k}\frac{\partial U_i}{\partial x_k} + \overline{\frac{p}{\rho}\left[\frac{\partial u_i}{\partial x_j} + \frac{\partial u_j}{\partial x_i}\right]} - \frac{2}{3}\epsilon\,\delta_{ij}$$

For high Reynolds number flow the viscous diffusion term is negligible. The third moments which represent the diffusion by the turbulent velocity fluctuations, $\overline{u_i u_j u_k}$, are modeled in terms of the Reynolds stress terms. The terms containing the diffusion of pressure correlations, $\overline{pu_k}$ are also modeled in terms of velocity correlations, Lumley (1978). The pressure-strain correlations $\overline{p(\partial u_i/\partial x_j + \partial u_j/\partial x_i)}/\rho$ are modeled in terms of an anisotropic stress tensor which can be related to the Reynolds stress.

In evaluating these models it is advantageous to measure as many terms as possible in the above equation which makes it crucial to measure the dissipation term directly. This direct measurement of the dissipation sheds light on the quality of these models.

Kinetic Energy Equation:

The equation for the transport of the kinetic energy is given by

$$\frac{Dk}{Dt} = -\frac{\partial}{\partial x_k}\left[\frac{1}{2}\overline{q^2 u_k} + \frac{\overline{pu_k}}{\rho} - \nu\frac{\partial k}{\partial x_k}\right] - \overline{u_i u_j}\frac{\partial U_i}{\partial x_j} - \epsilon$$

All the terms in the above equation except the pressure transport term (which is modeled) can be measured. Earlier investigators (Taulbee et al. 1987) used the dissipation as a closing term.

Measuring the dissipation directly, provides the data necessary to evaluate the terms involving the pressure.

1.3 The Integral Momentum Balance

The traditional equations for the axisymmetric jet containing first order terms are well documented and can be found in a number of basic fluid texts. However, the attempts by Baker to validate the experimental data of Wygnanski and Fiedler (1969) have confirmed the need to utilize equations with second order accuracy. A brief summary of their development is presented below.

In the U-momentum equation, all nonzero Reynolds stress terms are included and only the viscous terms are ignored. The only term that has been added to the traditional equation is the axial normal stress, $\overline{u^2}$.

$$U \frac{\partial U}{\partial x} + V \frac{\partial V}{\partial y} = -\left[\frac{1}{r} \frac{\partial (r\overline{uv})}{\partial r} + \frac{\partial \overline{u^2}}{\partial x}\right] - \frac{1}{\rho} \frac{\partial P}{\partial x} \qquad (1.3.1)$$

The continuity equation is unchanged.

$$\frac{\partial U}{\partial x} + \frac{1}{r} \frac{\partial}{\partial r} (rV) = 0 \qquad (1.3.2)$$

In the V-momentum equation, all terms are ignored except for the pressure gradient and the turbulent kinetic energy. This form is integrated from r to infinity to yield an expression for the pressure gradient.

$$P_\infty - P = \overline{v^2} + \int_r^\infty \frac{\overline{v^2} - \overline{w^2}}{r} \, dr \qquad (1.3.3)$$

Once differentiated with respect to x, it can be used to eliminate the dependence upon pressure in the U-momentum equation.

$$U\frac{\partial U}{\partial x} + V\frac{\partial U}{\partial y} = -\frac{1}{r}\frac{\partial(r\overline{uv})}{\partial r} - \frac{\partial \overline{u^2}}{\partial x} + \left[\frac{\partial \overline{v^2}}{\partial x} + \frac{\partial}{\partial x}\int_r^\infty \frac{\overline{v^2}-\overline{w^2}}{r}\,dr\right] \tag{1.3.4}$$

When multiplied by 2π r dr and integrated from 0 to infinity, the result is

$$2\pi\int_0^\infty \left[U^2 + \overline{u^2} - \frac{(\overline{v^2}+\overline{w^2})}{2}\right] r\,dr = \text{constant} = M_o \tag{1.3.5}$$

where ρM_o is the rate at which momentum is added at the source.

The integration of the U-momentum equation can be interpreted in terms of momentum conservation. From this viewpoint, U^2 and $\overline{u^2}$ are the flux of axial momentum across a plane perpendicular to the jet axis. The term $(\overline{v^2}+\overline{w^2})/2$, which has been obtained from integration of the V-momentum equation, represents the effect of the streamwise pressure gradient on the overall momentum balance. Note that because of the latter term, the momentum <u>flux</u> (and its integral) is greater than that at the source. Therefore, using the monentum flux alone as a verification for momentum conservation would be quite misleading and may result in the belief that momentum integral increases with increasing distance from the source. This increase is a natural consequence of the <u>constancy</u> of the <u>momentum integral.</u> Most important to this experiment is that the terms of equation (1.3.5) are directly measureable and thus provide a means of evaluating the accuracy of the measurements and the validity of the experiment.

1.4 Objective of this Work

This work presents detailed experimemtal data of the turbulent velocity and its derivatives in the axisymmetric jet. There are three objectives for this work:

The first objective is to obtain data to give new insight into the evaluation of turbulence closure hypotheses. Of particular interest is a direct measurement of the dissipation. Earlier evaluations of turbulence models relied on an analysis based on balancing this kinetic energy equation by modeling the pressure velocity correlation terms, using measured third moments and solving for the dissipation as a closing term (Taulbee et al. 1987). The data provided in this work enables verification of the model using a directly measured dissipation term.

The second objective of this work is to provide an evaluation of measured techniques in high turbulence intensity shear flows. An evaluation of both the effect of cross-flow errors on velocity moments and the effect of the fluctuating convection velocity on hot-wire measured velocity derivatives is presented. This work enables comparisons of the data obtained from stationary and moving hot-wires to that obtained using an LDA by earlier investigators (Capp 1983, Capp et al. 1988).

The third objective of this work is the assessment of local isotropy and local axisymmetry in this flow. The latter is accomplished by measuring numerous spatial and temporal derivatives, and comparing the results with that of the theory of axisymmetric homogeneous turbulent flows.

CHAPTER 2

Experimental Equipment

2.1 Jet facility

The jet facility used was the same as the one used by Capp (1983) in his investigation of the axisymmetric jet. The boundary conditions duplicate those of the jet flow of Wygnanski and Fiedler (1969). This was done not only because we wished to repeat their experiment as closely as possible, but also because we faced the same design criteria. It is desirable to maximize the exit velocity U_o since both the exit Reynolds number, Re_o, and the centerline velociy, U_m, measured at a fixed x/D are proportional to U_o. The smaller the diameter, the smaller the length of the facility. However, Re_o is also proportional to the exit diameter. We also wish the exit area of the jet A_o, to be large enough so that the boundary layer at the nozzle exit is insignificant when determining the source mass and momentum flux.

The jet apparatus was the same one utilized by Capp (1983), and is shown schematically in Figure 2.1.1. Driving the flow was a 1 h.p. motor and high pressure, paddle type blower. Swirl, spatial inhomogeneities in the mean flow and turbulence intensities were removed using wire screens and one section of plastic straws. The first contraction is 16:1 and its geometry was two matched cubics optimized for minimum pressure gradient as suggested by Morel (1975). To repeat the conditions of Wygnanski and Fiedler, a second contraction of 9:1 was added to bring the exit to the required one inch diameter. The last contraction was constructed using a fifth

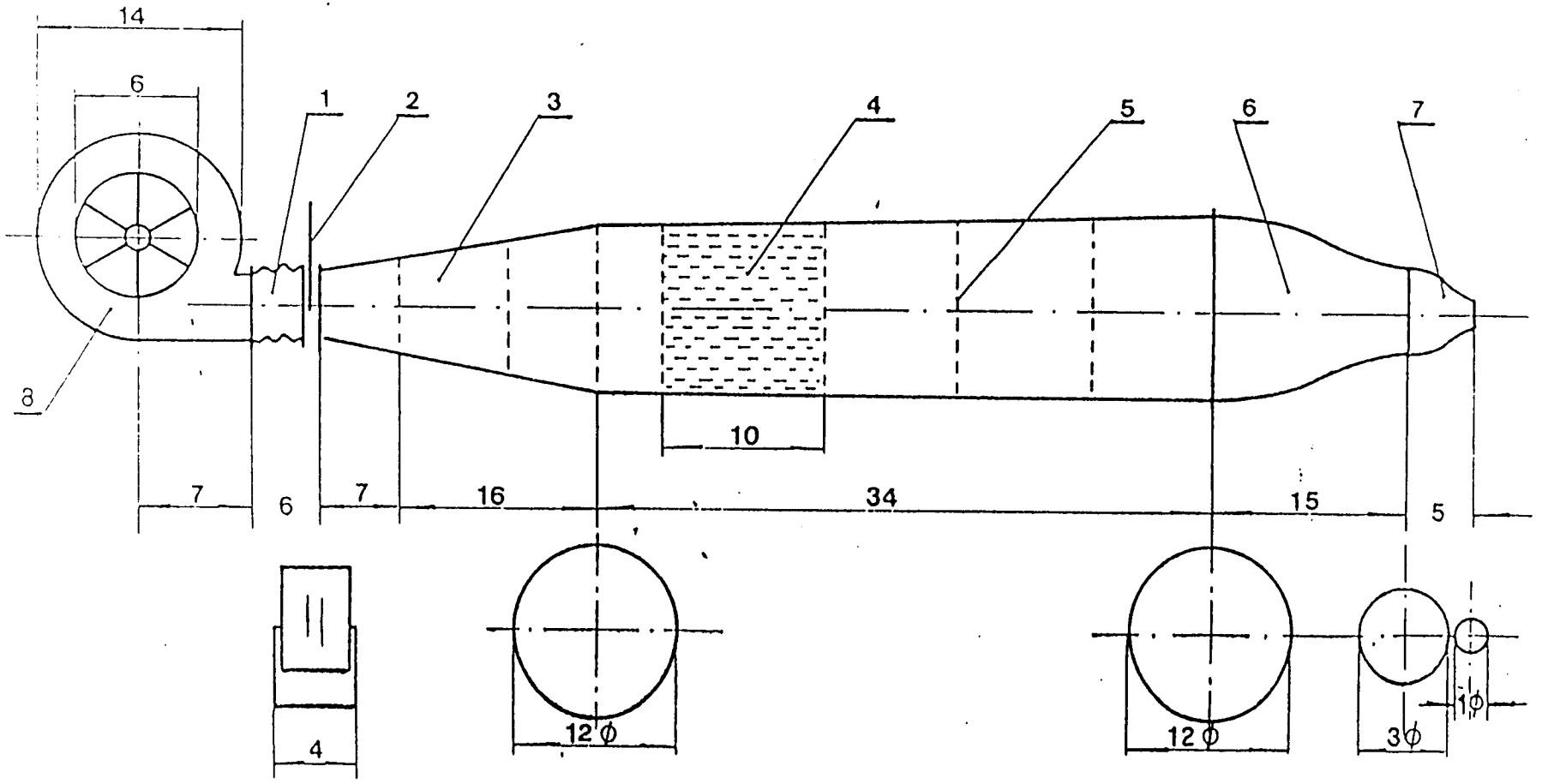

FIGURE: 2.1.1 JET FACILITY (ALL DIMENSIONS IN INCHES)

1. VIBRATION ISOLATION
2. SLOT AND PLATE
3. DIFFUSER
4. HONEY COMB
5. SCREEN
6. NOZZLE
7. JET
8. BLOWER

order polynomial. As demonstrated by Tan-Atichat (1980), such a curve produces a more uniform mean velocity distribution over a shorter length. The exit profile is shown in Figure 2.1.2. The measured profile had a velocity overshoot at the jet edges of 3% relative to the centerline velocity. This effect was balanced by the boundary layer thickness (approximately 2% of the exit radius). The error terms arising from the adoption of a top hat profile based upon the centerline velocity and the exit diameter may be accepted with an error of less than 3%. The exit conditions listed in Table 2.1.1 were used for all experimental measurements reported in this thesis.

TABLE 2.1.1

QUANTITY	SYMBOL	VALUE
Exit Diameter (inches)	D	1.0
Velocity (m/s)	U_o	55.0
Volume Flux (m^3/s)	m_o	0.277
Momentum Flux/Unit Mass (m^4/s^2)	M_o	1.51
Reynolds Number	Re_o	9.2×10^4

While the jet apparatus was the same as used by Capp (1983), the enclosure was different. In this experiment the apparatus was used in a large 5m x 5m x 25m room. The size of the room was determined using the criterion proposed by Capp (1983) to ensure that the momentum integral was constant to within 5% at 150 diameters. The jet was mounted on a table 2.5m above the floor to place the exit near the geometrical center of the room cross-section. The temperature of the room was monitored throughout the experiment and was constant to within $\pm 3^{o}C$.

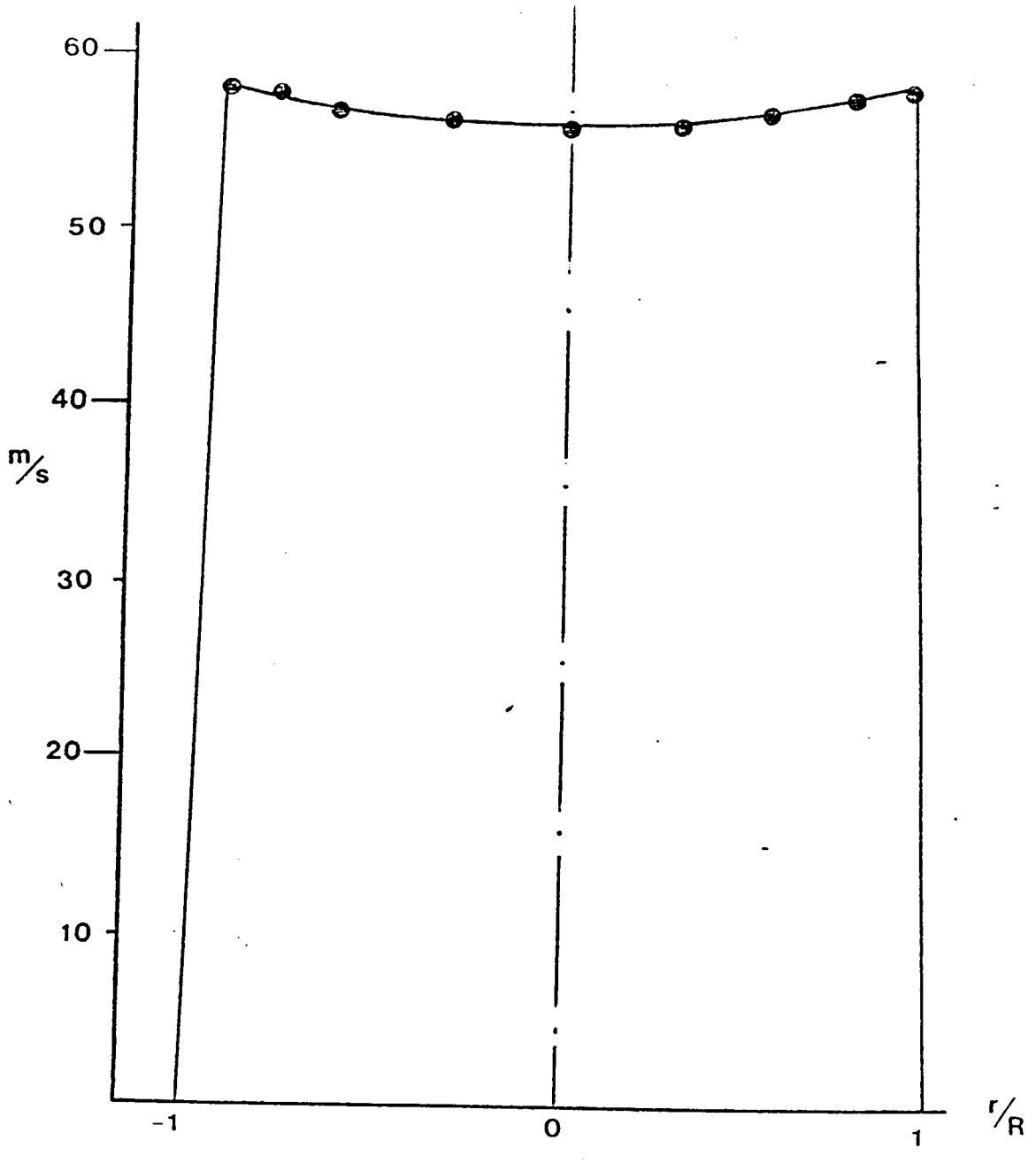

FIG. 2.1.2 JET EXIT PROFILE

2.2 The Nature of the Far Jet

Measurements were taken at 70 and 100 diameters downstream of the jet exit in the stationary probe experiment, and 70 diameters downstream with the moving probe. The collapse of the profiles when scaled with the centerline velocity and downstream distance indicates a well established similarity region. These are discussed in detail in Chapter 4.

The axisymmetry of the jet was very carfully documented. A three dimensional traversing system designed for this experiment was utilized to obtain velocity contours which show good axisymmetry. The contours shown in Figure 2.2.1 were measured at 50,60, and 70 diameters from the exit of the jet by Peng (1985) in a parallel experiment. The virtual origin of the jet was found to be 2.7 diameters from the exit.

Concurrent with these measurements was a parallel investigation by Capp using a two-component LDA in the same facility. These measurements will be described in detail elsewhere (Capp et al. 1988), but will be cited herein. The techniques utilized were identical to those used in Capp (1983).

2.3 Description of Hot-Wire Probes

The two different types of hot-wire probes used in this work were a standard parallel wire probe and a three wire probe that was designed for these experiments. All the wires used on the probes were Wollaston (Pt-10%Rh) with 2.5 micron diameter. Since the wires originally had a silver coating, a sensing element 0.2mm long was etched by a nitric acid solution. Compared to the Kolmogrov scales in

Figure 2.2.1a Contours of the mean velocity profile at x/D=50.

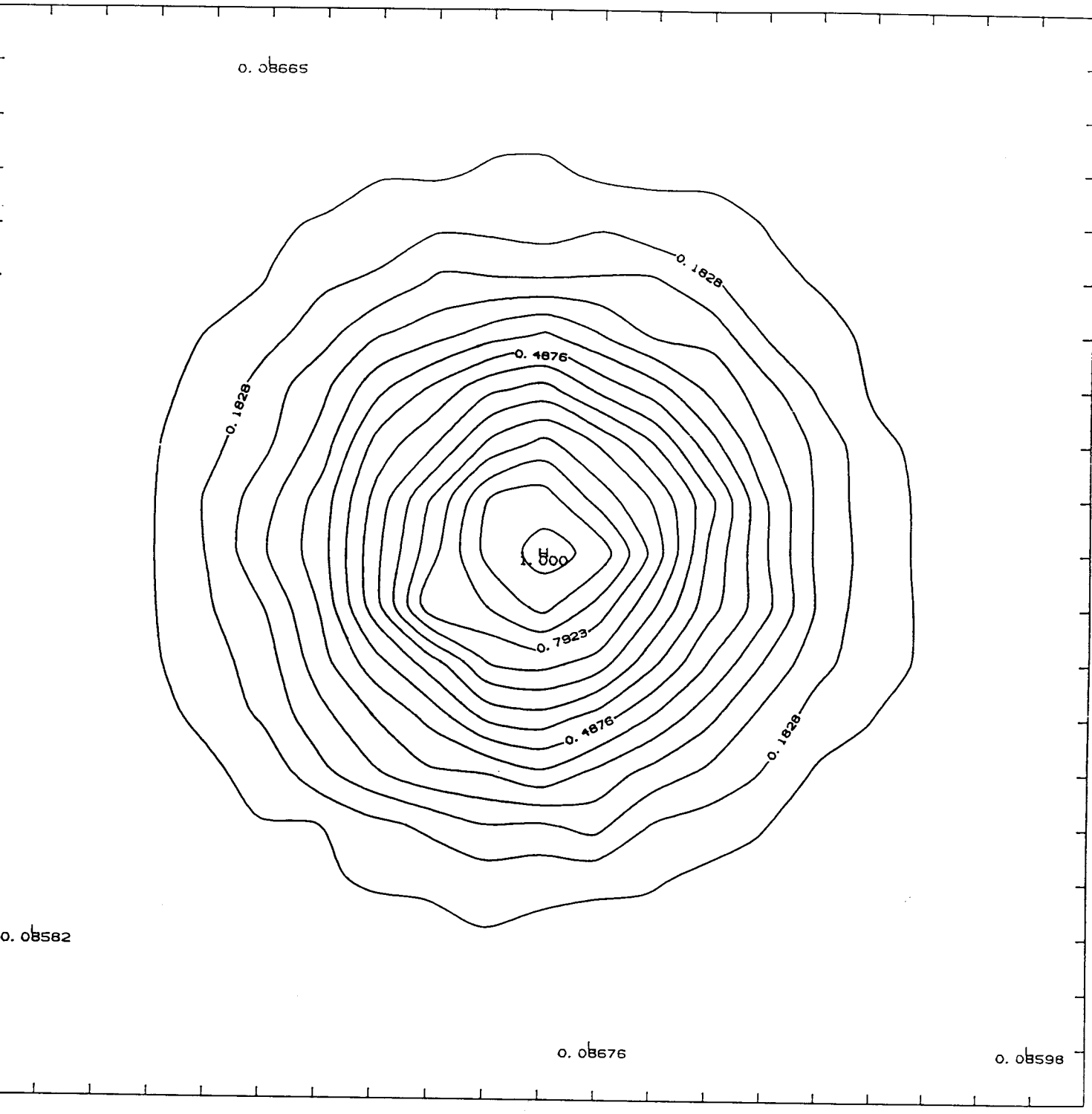

Figure 2.2.1b Contours of the mean velocity profile at x/D=60.

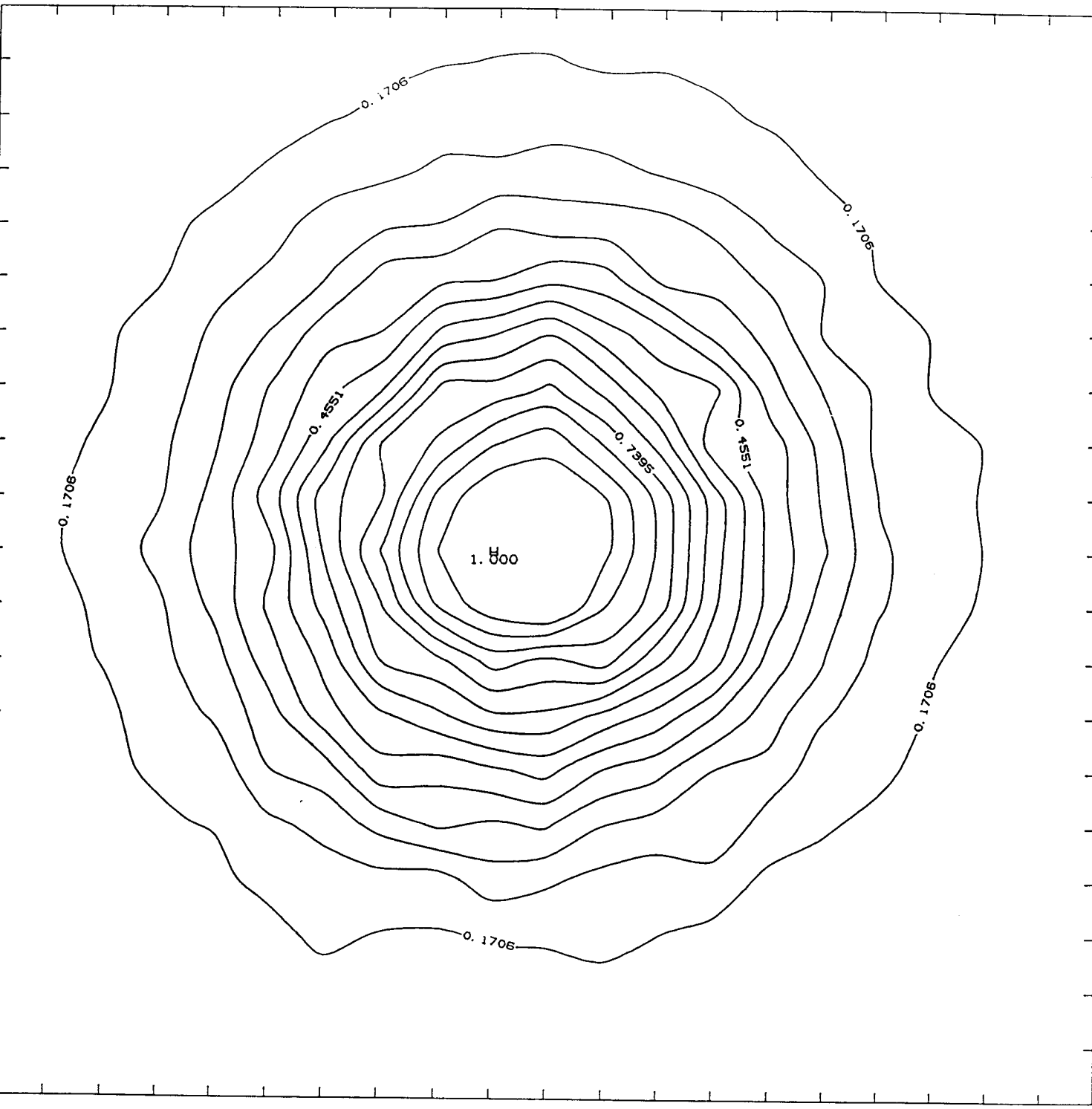

Figure 2.2.1c Contours of the mean velocity profile at x/D=70.

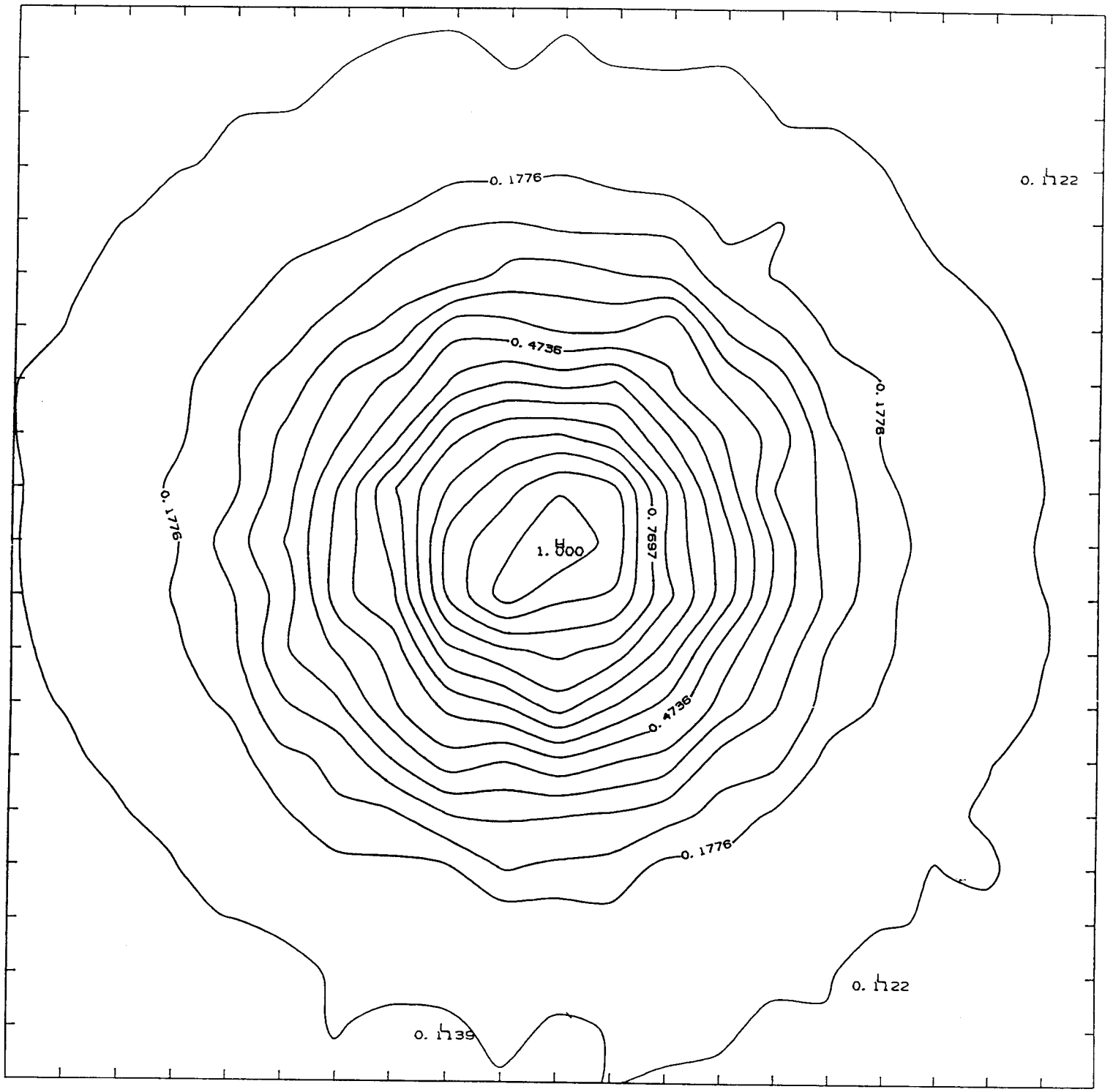

this flow which are about 0.16mm at the centerline of the jet, the wires were sufficiently short so that the variances of the measured derivatives were not affected by length effects. (See Section 3.5) The small diameter of the wires was chosen since smaller diameter wires have higher resistance and hence better signal to noise ratio (Doughman 1972).

The anemometers used were Dantec 55M constant temperature anemometers operated with 0.6 overheat ratio. To avoid aliasing of the signals, signal conditioners were used to low pass the signals. The highest frequency in the flow (corresponding to the Kolmogorov microscale) was 12 kHz, so the low pass setting for the filters was at 15 khz. This cutoff frequency was calculated using the sum of jet velocity and superimposed velocity as the convection velocity.

The parallel wire probe shown on Figure 2.3.1 was used in two different experiments. The first experiment (which will from here on be noted as Experiment 1) was performed with the probe oriented in such a way as to measure $\overline{(\partial u/\partial y)^2}$. This was done using the differencing technique described in Section 2.4 of this chapter. In addition to the spatial derivative, the time derivative of the velocity signal was also recorded. Experiment 2 was done with the probe rotated 90 degrees. In this orientation the probe was used to measure $\overline{(\partial u/\partial z)^2}$.

The triple wire probe used is shown in Figure 2.3.1. This probe was designed to measure all the terms in the dissipation equation assuming axisymmetric flow. The criteria used in design of this probe were that it has the least amount of probe interference, and acceptable spatial resolution for the derivative measurements. The probe was built from three angle wires. The wires used were 10% Rh.-Pt

Figure 2.3.1 Multiple Wire Probes

Triple wire AXI-probe

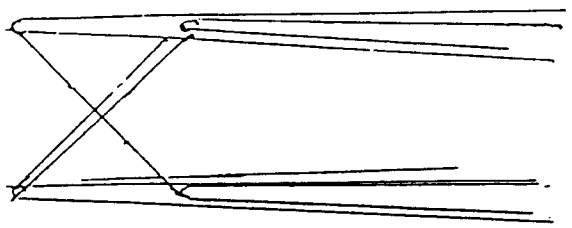

Parallel wire probe

with diameters of 2.5 microns. The sensing length of these wires was 0.2 mm. In this work the Kolmogrov scales are estimated to be about 0.16mm at the centerline of the jet. As pointed out earlier it is essential that the spacing of the wires be close enough in regards to this scale to avoid spatially filtering the derivative signal. (See Chapter 3) This probe was used in two different experiments which will be called experiments 3 and 4. In experiment 4 the probe was aligned with the jet in such a way that the the terms $\overline{(\partial u/\partial x)^2}$, $\overline{(\partial v/\partial x)^2}$, $\overline{(\partial v/\partial z)^2}$, $\overline{(\partial u/\partial z)^2}$ were measured. For experiment 4, the probe was rotated 90 degrees to obtain $\overline{(\partial u/\partial x)^2}$; $\overline{(\partial w/\partial x)^2}$, $\overline{(\partial w/\partial y)^2}$, $\overline{(\partial u/\partial y)^2}$.

2.4 Data Acquisition and Sampling Consideration

The hot-wire signals were digitized using a 15 bit, 16 channel A/D converter with a throughput rate of 150 kHz. The anti-aliasing filters used were Bessel Low-Pass Filters (manufactured by Frequency Devices, Model 848 P8105) and were tunable over a frequency range of 200 Hz to 51.2 kHz.

Measurements of all of the components of the velocity were made and all the moments to the fourth order were computed. Care was taken to ensure that record lengths were long enough to ensure that statistical convergence was achieved, and that the dynamical ranges were adequate to minimize adversely affecting the higher moments by clipping the tails of the probability distributions. To obtain the proper record length for the convergence of measured moments it is necessary to know the integral time scale, τ, of the flow which is related to the effective number of independent realizations, N, by the following formula:

$$N = \frac{T}{2\tau} \tag{2.4.1}$$

where T is the record length. The integral scale of the jet was estimated from the measured values of the spectrum extrapolated to zero frequency,

$$\tau = \frac{S(o)}{2\overline{u_i^2}} \tag{2.4.2}$$

The integral scale τ at centerline is around 0.08 sec.

As described in Chapter 5, the sampling rate in this experiment was determined by the rotation speed of the wing. The rotation speed of the wing was 1.1 cycles per second. This 1.1 samples per second is a lot slower than the maximum sampling rate constraint required to obtain independent samples which is $(2\tau)^{-1}$. Thus the variability in the mean can be estimated from

$$e = \frac{1}{\sqrt{N_{eff}}} \sqrt{\frac{\{\text{var } u_i\}}{u^2}} \tag{2.4.3}$$

The variability for the mean was 0.1%, while the rms was larger but of the same order.

2.5 Differentiation

The streamwise gradients of the velocity components were computed from Taylor's hypothesis using

$$\frac{\partial}{\partial x} = \frac{1}{U}\frac{\partial}{\partial t} \tag{2.5.1}$$

where U_c is the convection velocity usually taken as the local mean velocity. The applicability of this hypothesis to the jet is discussed in Chapter 4 and Appendix II.

The differentiation of the electronic signal was accomplished by utilizing the high-pass filter characteristics of the Dantec 55D26

signal conditioning unit. It is well-known that differentiation correspounds to +6 dB/octave frequency response function which is also the low frequency asymptote of a single-pole high pass filter. To ensure that the deviations from this asymptote near the breakpoint were negligible, the high pass cuttoff frequency was chosen about five times higher than the highest frequency of interest in the signal, that corresponding to the Kolmogrov microscale. For the moving probe experiment this correspounds to a high frequency cuttoff of 65 kHZ. The time derivative were computed from the output using the following relation which can be readily derived from linear system theory:

$$\frac{de_i}{dt} = 2\pi f_{HP} e_o \qquad (2.5.2)$$

where e_i is the voltage of the signal to be differentiated, e_o is the voltage of the differentiated signal and f_{HP} is the setting of the high pass filter. Because of the severe attenuation at the lowest frequencies by the high-pass filter, the amplifier gain was set at 100 to provide additional amplification.

The measurements of the spatial derivatives were done by measuring the velocity components at two points that are in close proximity to each other, and taking the difference to approximate the velocity gradient. Figure 2.5.1 shows two velocity signals from parallel wires at the centerline of the jet and the difference of these two signals. The noises in the difference signal are due to either quantization and electronic noise or to uncertainty in the calibration of the two wires. As dicussed in chapter 3 the voltage to velocity transformation is accurate to within 1%. The quantization error is of the order of 0.6 mv, and rms electronic noise is of the

Figure 2.5.1 Velocity Signals from Parallel Probes and Their Difference.

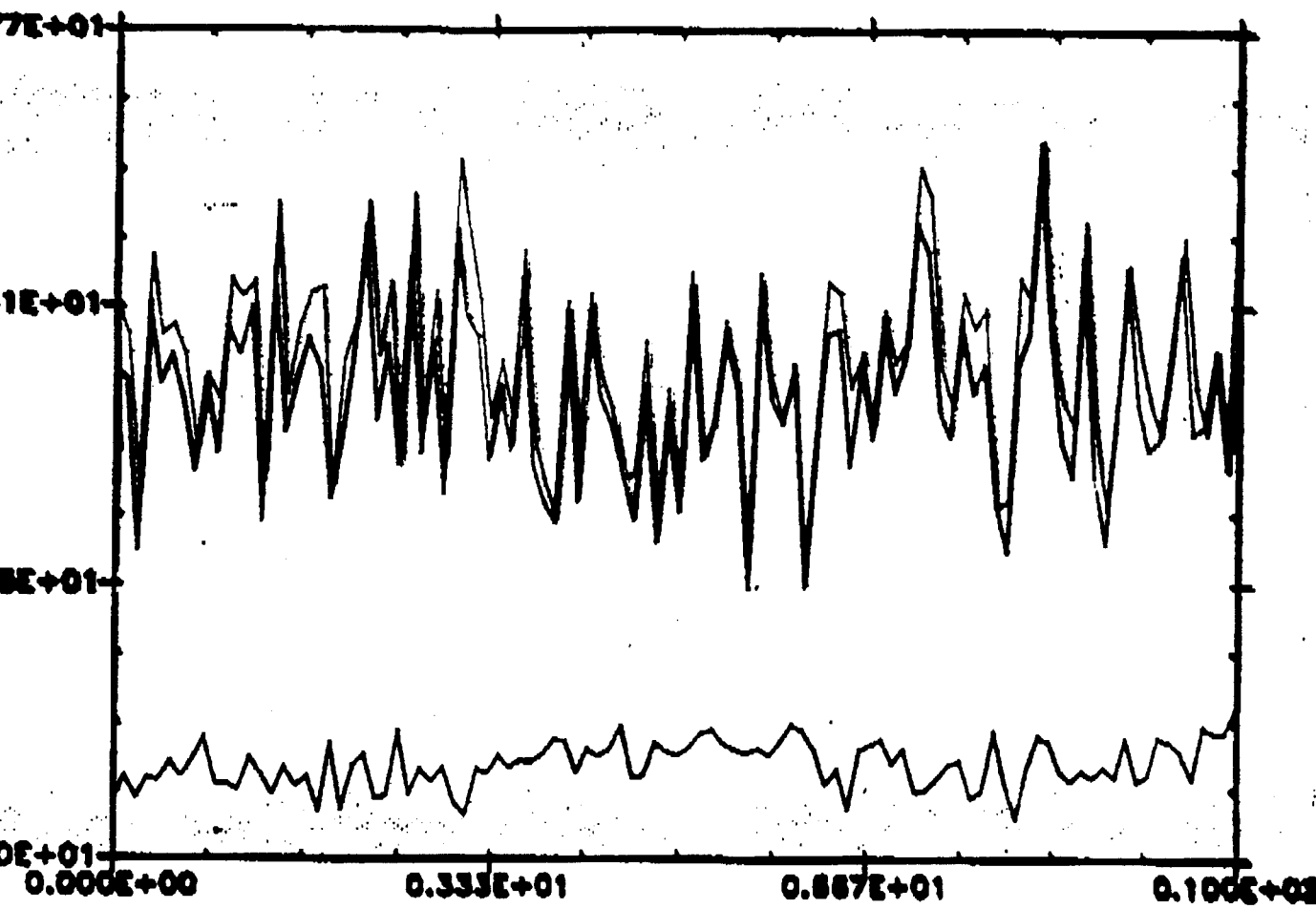

order of 3 mv. The measured difference can be written as:

$$\Delta u_m = \left[(U^{(1)} - U^{(2)})\right] + (n^{(1)} - n^{(2)}) + (\epsilon^{(1)} - \epsilon^{(2)}) \tag{2.5.3}$$

where n represents the random (electronic and quantization) noise and ϵ errors due to the calibration. Averaging the above equation:

$$\Delta U_m = U^{(1)} - U^{(2)} + \bar{\epsilon}^{(1)} - \bar{\epsilon}^{(2)} \tag{2.5.4}$$

since the average noise is zero. Thus only the calibration errors and the statistical errors affect the mean difference measurement.

For wires that are in close proximity the velocity gradient can be estimated using:

$$\frac{\Delta U_m}{\Delta y} = \left[\frac{dU}{dy}\right] \Delta y + \frac{1}{2} \left[\frac{d^2U}{dy^2}\right] \Delta y^2 + \ldots \tag{2.5.5}$$

or

$$\frac{\Delta U_m}{\Delta y} \cong \frac{dU}{dy} \left[1 + \frac{1}{2} \frac{\left[\frac{d^2U}{dy^2}\right]}{\left[\frac{dU}{dy}\right]} \Delta y\right] \tag{2.5.6}$$

where it is to be hoped that the last term is negligible

From the mean velocity profile $\frac{dU}{dy}$ and $\left[\frac{d^2U}{dy^2}\right]$ can be estimated as,

$$U = U_m \exp(-Dy^2/x^2) \tag{2.5.7}$$

$$\frac{dU}{dy} = - U_m \, 2D \frac{y}{x^2} \exp(-Dy^2/x^2) \tag{2.5.8}$$

$$\frac{d^2U}{dy^2} = - U_m \, 2D \frac{1}{x^2} \left[\exp(-Dy^2/x^2)\right] \left[1 - \frac{2Dy^2}{x^2}\right] \tag{2.5.9}$$

$$\frac{\left[\frac{d^2U}{dy^2}\right]}{\left[\frac{dU}{dy}\right]} = \frac{\left[1 - \frac{2Dy^2}{x^2}\right]}{y} \tag{2.5.10}$$

The above ratio blows up at y=0, which shows that the differencing method is not suitable for determining the mean velocity derivative since the higher order terms dominate over the core region of the jet.

Figure 2.5.2 shows the results of an attempt to measure the mean spatial derivative in the radial direction of the longitudinal velocity. The solid line is the result $\partial U/\partial y$ obtained by differentiating the mean velocity profile. The dotted line was determined from the parallel wire by differencing the two signals. As expected from the above, the derivative from the parallel wires fluctuates around the results from the mean velocity profiles. The amount of the fluctuation is a direct measure of the calibration errors, while the bias is a reflection of the second derivative contribution.

We now examine the use of parallel wires to estimate the fluctuating spatial derivatives. The mean square fluctuating difference is given by:

$$(\Delta\overline{u_m^2}) \cong \overline{\left[\frac{du}{dy}\right]^2} \Delta y^2 + \frac{1}{4} \overline{\left[\frac{d^2u}{dy^2}\right]^2} \Delta y^4 \qquad (2.5.11)$$

where the correlation between du/dy and d^2u/dy^2 has been assumed to be negligible (since they are determined by different scales of motion.) Thus,

$$\left[\frac{\Delta u_m}{\Delta y^2}\right]^2 \cong \overline{\left[\frac{du}{dy}\right]^2} \left[1 + \frac{1}{4} \frac{\overline{\left[\frac{d^2u}{dy^2}\right]^2}}{\overline{\left[\frac{du^2}{dy}\right]}} \Delta y^2\right] \qquad (2.5.12)$$

From Champagne (1978), $\dfrac{\overline{\left[\frac{\partial^2 u}{\partial x^2}\right]^2}}{\overline{\left[\frac{\partial u}{\partial x}\right]^2}}$ can be estimated as $\sim 0.1\eta^{-2}$ where η is

Figure 2.5.2 Derivative of the Mean Velocity in the Radial Direction

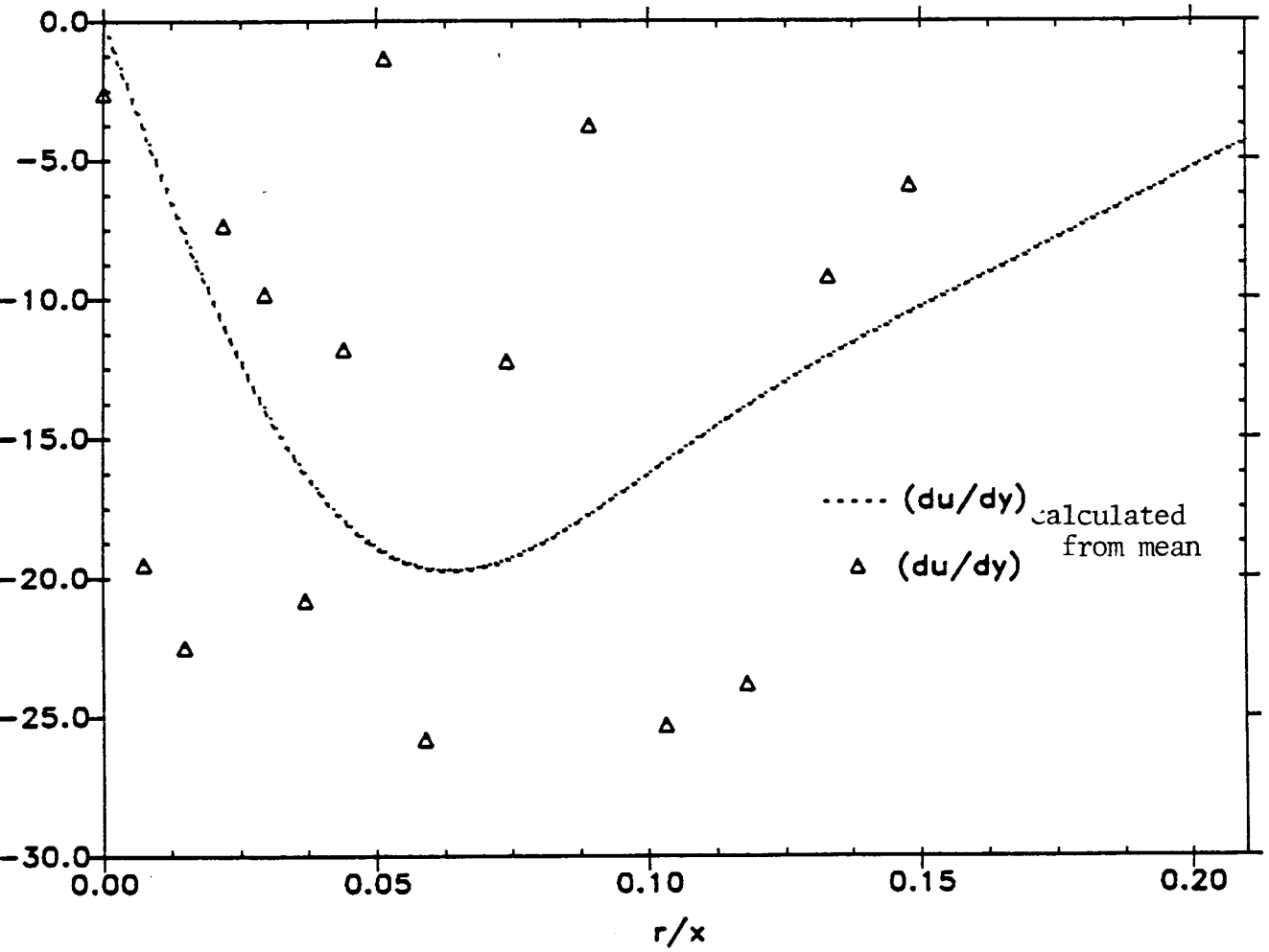

the Kolmogorov microscale. Therefore equation (2.5.13) can be written as

$$\overline{\left[\frac{\Delta u_m}{\Delta y^2}\right]^2} \cong \overline{\left[\frac{\partial u}{\partial y}\right]^2} \left\{1+0.1 \left[\frac{\Delta y}{\eta}\right]^2\right\} \qquad (2.5.13)$$

For this work the spacing between the wires is given by $\Delta y = \eta$. Therefore, the differencing method over-estimates the derivative by 10% which is within experimental error, and differencing is therefore an acceptable means of measuring the fluctuating velocity gradient.

The effect of calibration and noise (quantization and electronic) can also be estimated using equation (2.5.3) for the instantaneous differences. Assuming the noise and velocity to be uncorrelated

$$\overline{(\Delta u_m)^2} = \overline{\left[u_1^{(1)}-u^{(2)}\right]^2} + \overline{\left[n^{(1)}-n^{(2)}\right]^2} + \overline{\left[\epsilon^{(1)}-\epsilon^{(2)}\right]^2} \qquad (2.5.14)$$

The worst case is if the errors between the wires are uncorrelated with each other so that

$$\overline{[\Delta u_m]^2} = \overline{\left[u^{(1)}-u^{(2)}\right]^2} + 2\left[\sigma_n^2+\sigma_\epsilon^2\right] \qquad (2.5.15)$$

Thus the major concern is whether

$$2\left[\sigma_n^2 + \sigma_\epsilon^2\right] << \overline{\left[u^{(1)} - u^{(2)}\right]^2} \qquad (2.5.16)$$

so that measurement is not contaminated by noise and errors.

σ_n and σ_ϵ can be related to the rms voltages $\sigma_{ne}, \sigma_{\epsilon e}$ at the A/D in the following way

$$\sigma_n \cong \frac{dU}{dE}\,\sigma_{ne}$$

$$\sigma_\epsilon \cong \frac{dU}{dE}\,\sigma_{\epsilon e} \qquad (2.5.17)$$

In this experiment typical values were

$$\sigma_{ne} \simeq 2\times10^{-3}\ \text{v.}$$

$$\sigma_{\epsilon e} \simeq 0.6 \times 10^{-3} \text{ v.}$$

$$\left.\frac{dU}{dE}\right|_{4.8 \text{ m/s}} \simeq 12.8 \text{ m/s/volt}$$

so that

$$\sigma_n^2 + \sigma_e^2 \cong 6.5 \times 10^{-4} \text{ m}^2/\text{s}^2$$

The mean square velocity difference can be estimated using the isotropic relation for $\overline{(du/dy)^2}$ as

$$\overline{\left[u(1)-u2\right]^2} \cong \overline{\left[\frac{\partial u}{\partial y}\right]^2}\Delta^2 = \frac{2}{15}\left[\frac{\epsilon}{\nu}\right]^{1/2}(\Delta y^2) = \frac{2}{15}(\epsilon\nu)^{1/2} \quad (2.5.18)$$

since $\Delta y = \eta$ here. Using (Champagne 1978)

$$\epsilon = 0.22\, U_m^3/x$$

we obtain

$$\overline{\left[u(1)-u(2)\right]^2} \cong 1.4 \times 10^{-2} \text{ m}^2/\text{s}^2$$

Hence the inequality of equation (2.5.16) is marginally satisfied for the experiment here.

In view of the fact that σ_n is the major determinant, and that a significant portion of the noise <u>is</u> correlated between channels, the actual contamination is probably much less than the worst case estimate. Thus direct measurement of fluctuating velocity derivatives by spatial differencing is acceptable in this experiment.

CHAPTER 3

The Moving Probe

3.1 Difficulties in Measurements of High Turbulence Intensity Flow

The axisymmetric jet is a difficult environment for conventional hot-wire measuring techniques. The three major problems in measuring velocities in a high turbulence intensity flow such as the jet are, rectification, cross-flow and directional ambiguity. The turbulence intensity for the jet is 25% at the centerline and the local turbulence intensity increases with increasing radius as shown in Figure 3.1. Since the maximum acceptable intensity for a hot-wire is about 25%, the turbulence intensity in almost all the jet is above the range in which cross-flow and hot-wire rectification errors can be neglected.

The measurement of turbulence derivatives can be particularly difficult in flows of high turbulence intensity. Beuther(1980) noticed large excursions in derivative signals from cross-wires which he attributed to local flow reversal on one of the wires. Additional problems arise in the interpretation of spectral and derivative signals using Taylor's hypothesis in such flows. In the following sections the origin of these problems will be discussed in detail and the rationale for a moving probe will be established. Then the moving probe will be described in detail.

3.2 Cross-flow and Rectification Errors.

Unlike single wires in which rectification occurs when the flow reverses itself, cross-wires respond to rectification in a more subtle way. Figure 3.2.1 shows how even fluctuaions with a small magnitude

Figure 3.2.1 Rectification in Cross-wires

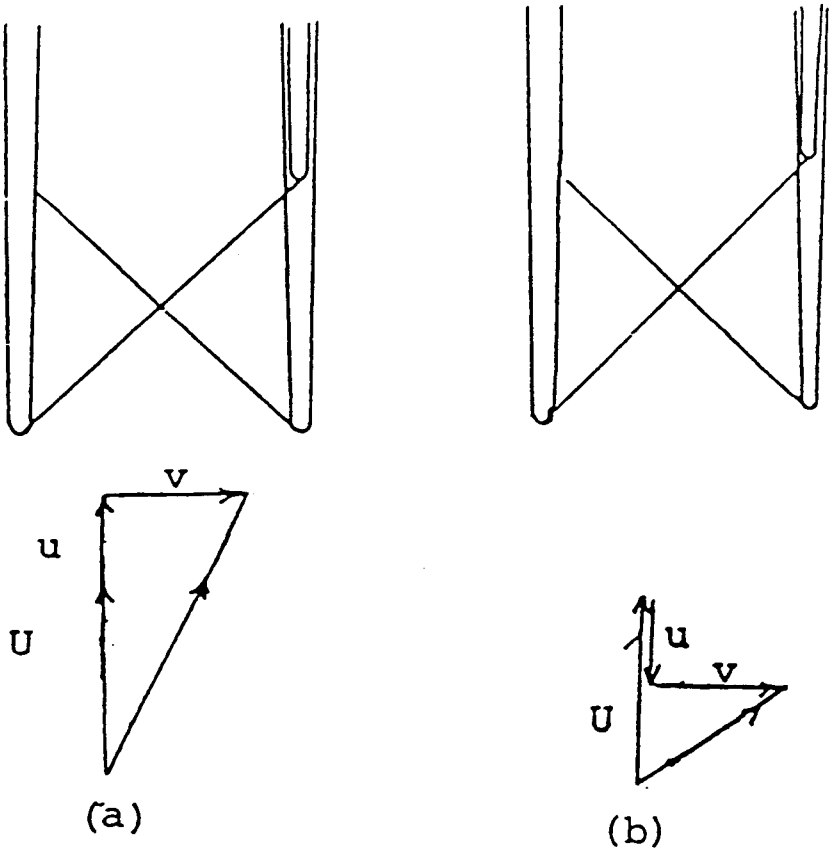

can cause a rectification problem for cross-wires. Figure 3.2.2 from Beuther (1980) shows a 2-D probability plot of u and v velocity components. The two slanted lines represent the cutoff of all velocity vectors exceeding 35^{o}. The vertical lines represent the lower limits of the hot-wire calibration. As can be seen, the lower left corner of the probability contour is dramatically compressed. This is due to the effects of low velocity beginning to be of importance. This resolution problem gets worse at larger distances from the center of the jet.

An additional effect of the rectification problem is the occurrence of voltage pairs which can not be resolved into velocity pairs from the angle calibration. The process of voltage to velocity transformation in a cross-wire is described in Section 3.6 of this chapter. Figure 3.2.3 shows the range of calibration outside which the instantaneous voltage pairs cannot be converted to the corresponding velocities. The three different methods shown on Figure 3.2.3 differ in their resolution of low velocities. As described in Beuther et al. (1987), at high velocities the all three methods perform adequately as long as the turbulence intensity is low enough.

Tutu and Chevray (1975) and Beuther et al. (1987) have shown that hot-wire errors can amount to significant values in high turbulence intensity flows. Here we will present equations containing the leading error terms obtained from binomial expansions for the measured velocity valid for vanishing turbulence intensity. These equations break down rapidly for turbulence intensities above 30-50%, and do not account for rectification effects. Thus they are at most an indication of when the problems begin. Note that here only, the lower case variables refer to the mean plus fluctuating parts.

Figure 3.2.2 2-D Probability Contours (from Beuther 1980)

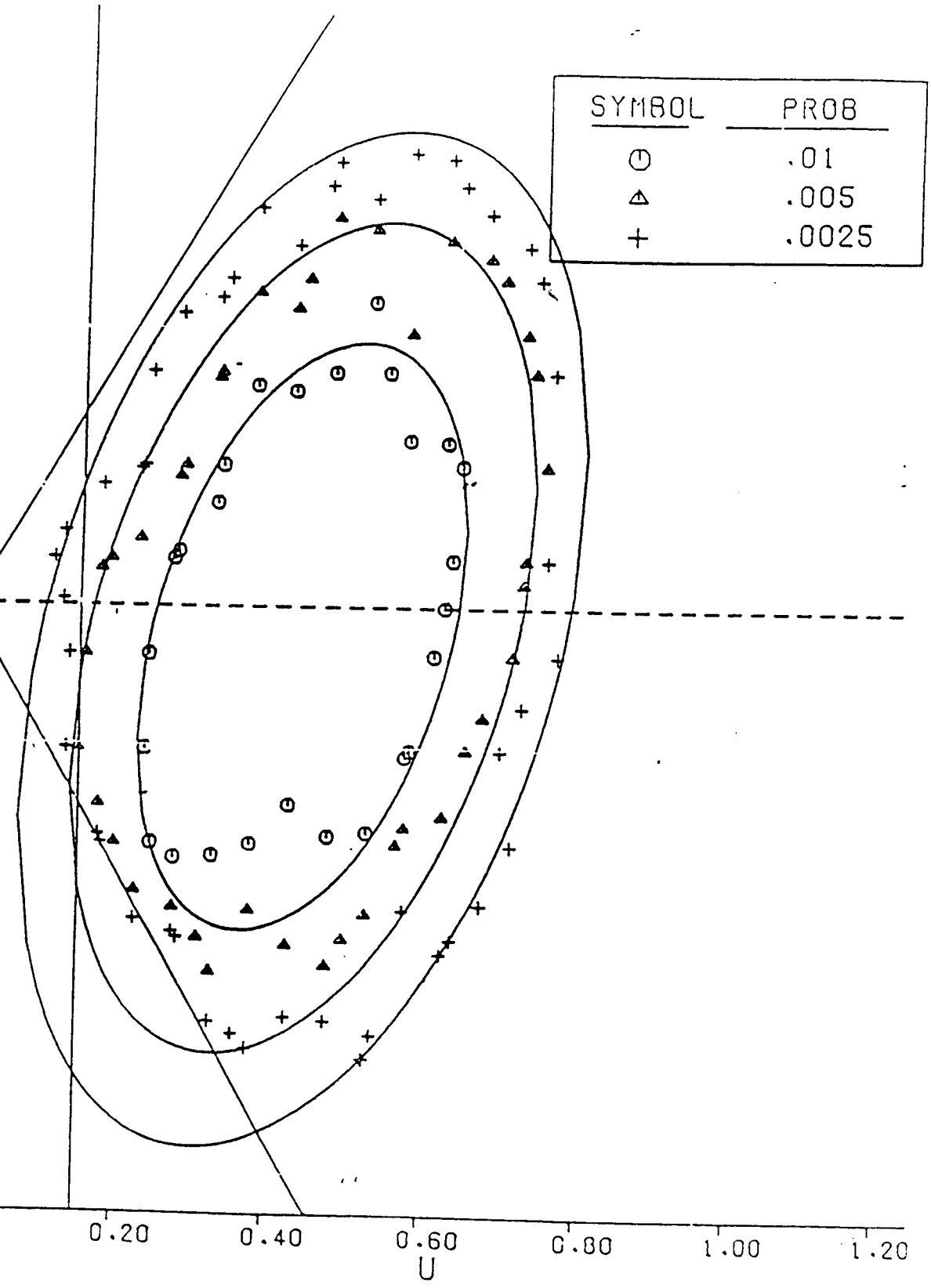

Figure 3.2.3 Angle Calibration for Cross-wires (from Beuther (1980)

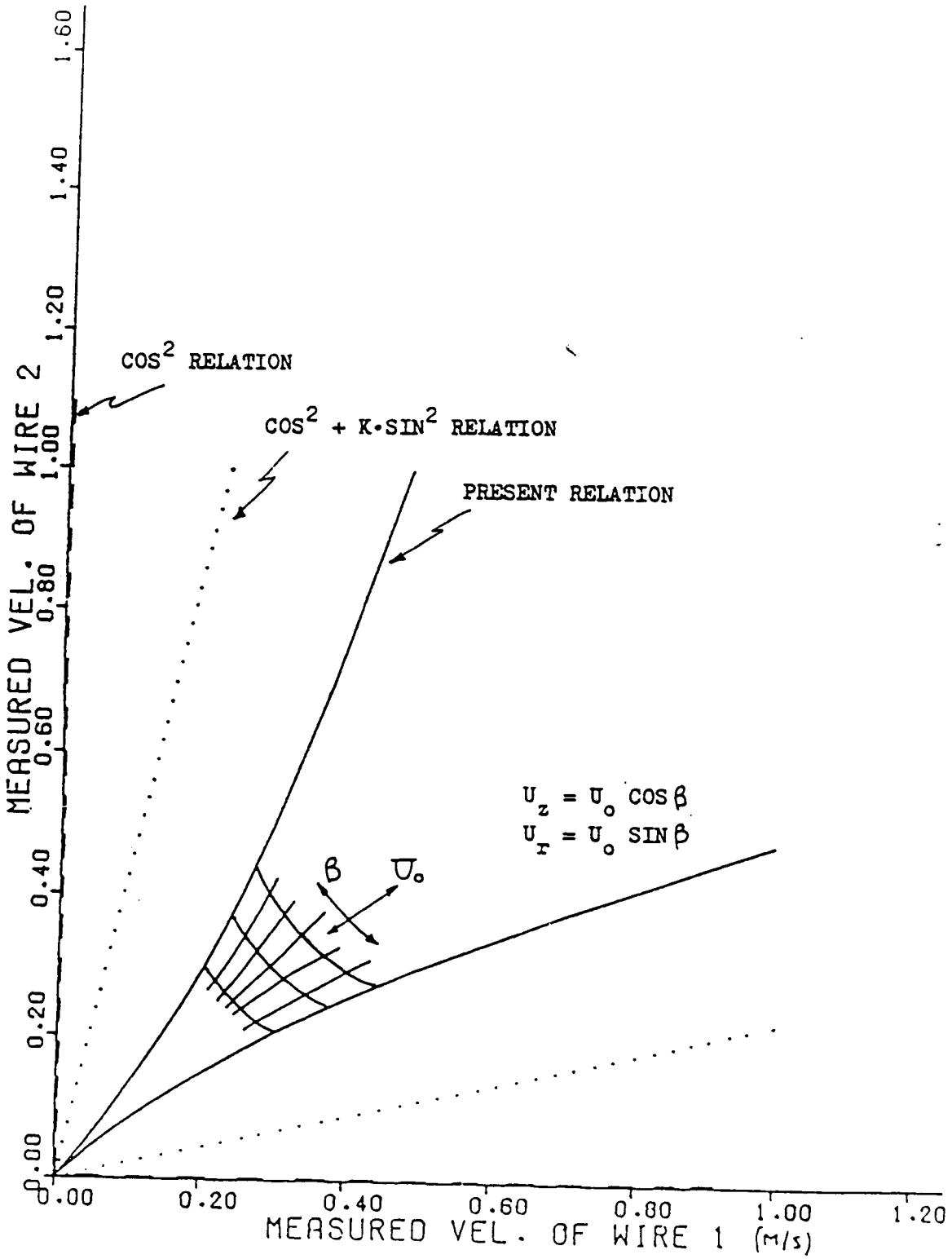

Mean:

Cross-wire

$$U_m = U\left\{1 + \frac{1}{(1+k^2)}\left[\frac{\overline{w^2}}{U^2} - \frac{\overline{uw^2}}{U^3} + \ldots\right]\right\} \tag{3.2.1}$$

Single-wire

$$U_m = U\left\{1 + \frac{1}{2}\left[\frac{\overline{w^2}}{U^2} - \frac{\overline{uw^2}}{U^3} + \ldots\right]\right\} \tag{3.2.2}$$

Second Moments:

Cross-wire

$$u_m^2 = \overline{u^2}\left\{1 + \frac{2}{(1+k^2)}\left[\frac{\overline{uw^2}}{u^2U} - \frac{\overline{u^2w^2}}{u^2U^2} \ldots\right]\right\} \tag{3.2.3}$$

Single-wire

$$u_m^2 = \overline{u^2}\left\{1 + \left[\frac{\overline{uw^2}}{u^2U} - \frac{\overline{u^2w^2}}{u^2U^2}\ldots\right]\right\} \tag{3.2.4}$$

Shear Stress:

$$\overline{u_m v_m} = \overline{uv} \tag{3.2.5}$$

It is interesting to note that the errors are larger for x-wires than for single wires. Also, of interest is that the contamination in a Reynolds stress measurement is entirely due to the decomposition of the velocity into mean and fluctuating parts.

3.3 Assessment of Taylor's Hypothesis

The analysis of hot wire errors in section 3.2 is limited to the measurements of the velocity and it's moments. In measuring the velocity derivatives there are other considerations which also present

difficulties in high turbulence intensity flows. It is common to measure the fluctuating gradients in the streamwise direction by invoking Taylor's frozen field hypothesis. Taylor's hypothesis assumes the measured temporal fluctuations are really spatial ones that are being convected past the measurement point. If the disturbance can be considered to not vary in time as it is convected (i.e. "frozen"), then it's streamwise derivative is related to the time derivative at the fixed point by

$$\frac{\partial}{\partial x} = \frac{1}{U_c} \frac{\partial}{\partial t} \tag{3.3.1}$$

where U_c is the rate at which a disturbance is convected past the probe.

The correct applicability of Taylor's hypothesis in a turbulent shear flows relys on numerous assumptions. Lumley (1965) outlines several criteria for the breakdown of the frozen field hypothesis:

1) Non-uniform convection velocity. Taylor's hypothesis assumes that the convection velocity U_c is a constant. It is reasonable to expect that the smaller scales are convected at different speeds than the larger ones. However the effect of these different convection velocities can be ignored if the non-uniformity is small compared to the convection velocity itself.

2) Spectral aliasing due to non-uniform convection velocity. The non-uniform convection velocity will have the effect of spectral broadening on the velocity spectra unless the following criterion is met:

$$\frac{2 \frac{d^2}{dk_1^2} (F_{11}) \pi^2 \left|\nabla U\right|^2}{3U^2 F_{11}} << 1 \tag{3.3.2}$$

where F_{11} is the one dimensional spectrum and k_1 is the wavenumber.

3) Temporal variation of the convected eddy. For the concept of a frozen field to be acceptable, the time scale of evolution of a disturbance must be much greater than the time it takes the disturbance to traverse the probe. This can be satisfied if

$$F_{11} <<< \frac{U^2}{k} \tag{3.3.3}$$

4) Unsteady convection velocity. In high intensity turbulent flow, the eddies are not being convected at a constant rate. The hypothesis is acceptable only if the fluctuation of the convection velocity is sufficiently small to avoid the leaking of energy at a particular wavenumber into a band of frequencies.

The small scales in the turbulent jet that are of interest in this work satisfy the first three criteria. Thus only the third criterion is of continuing concern in this work.

Lumley (1965) developed a model for the effects of the fluctuating convection velocity on the spectra and the derivatives. The model was derived by assuming that the turbulence had a Gaussian probability density, and by expanding about the state of zero turbulence intensity. The model was extended to higher turbulence intensities by Wyngaard and Clifford (1977) using a numerical integration. George and Beuther (1979) were able to show that Lumley's result for the derivative could be obtained without the Gaussian assumption. This analysis is repeated in Appendix II. The principal result is that the mean square spatial derivatives can be related to the temporal derivative by:

$$\overline{\left(\frac{\partial u}{\partial t}\right)^2} = U^2 \overline{\left(\frac{\partial u}{\partial x}\right)^2} \left[1 + \frac{\overline{u^2}}{U^2} + 2\left(\frac{\overline{v^2}+\overline{w^2}}{U^2}\right)\right] \qquad (3.3.4)$$

Thus Taylor's hypothesis becomes progressively less valid as the turbulence intensity is increased. One of the objectives of the work reported here was to test (for the first time) experimentally the validity of equation (3.3.4).

3.4 Rationale for the Moving Probe

The numerous problems described in Sections 3.2 and 3.3 associated with hot-wire measurements are a result of the high level of the turbulence intensity. The errors due to cross-flow and the effect of the fluctuating convection velocity on the measured derivative both scale with $\overline{u^2}/U^2$. These hot-wire errors can be avoided by reducing the effective turbulence intensity. This is accomplished in this work by moving the hot-wires through the flow so that the effective mean velocity seen by the probe is that of the flow plus that of the wire, thereby reducing the effective turbulence intensity.

Flying hot wires in turbulent flows were used in the past by various investigators. Uberoi (1985) used a flying wire in his study of entrainment in shear flows. Cantwell & Coles (1983), Watmuff et al. (1983), Panchapakesan and Lumley (1987) are other investigators that applied the moving wire techniques in a wind-tunnel, wake and a heated jet respectively. There are various reasons why the moving wires were used. In this work the object is two-fold; to decrease the errors due to cross-flow and rectification, and to enable a correct implementaion of Taylor's hypothesis. These particular advantages of a moving probe appear to have first been noted by George and Beuther (1979).

3.5 Description of the Moving Probe

The moving wire experiments were performed with an array of multiple wires described in Chapter 2. Figure 3.5.1 shows the mechanism on which the probes were mounted. The superimposed velocity was attained by whirling the probes about an axis perpendicular to the axis of the jet. To decrease the interference of the supporting arm, the probes were mounted on a one meter long, low drag symmetric NACA 0010 airfoil. A one horse-power motor was used in combination with a set of reduction gears and counter weights to obtain a smooth rotation of the wing. The entire mechanism was mounted on a one dimensional manual traversing system which was used to traverse the probes across the jet.

The effect of the wing on the flow was carefully studied. The wing had a low coefficient of drag C_d of 0.0045 and a Reynolds number of 1700 at 1 m/s. The large scale characteristics of the flow around the moving wing were observed with smoke wires. The results showed minimal amounts of flow disturbances on the jet as the wing rotated through it.

The best way to understand the effect of the wing on the small scales is to compare the time scales of turbulence to the time scale of the rotating wing. Another way of addressing this issue is to ask if the disturbances from the wing get convected downstream fast enough so as not to contaminate the next sample collected when the wing sweeps back to the vertical location. We have confidence that this is the case since the largest time scales of turbulence range from about 0.07 to 0.15 seconds as compared to the one second time scale of the wing.

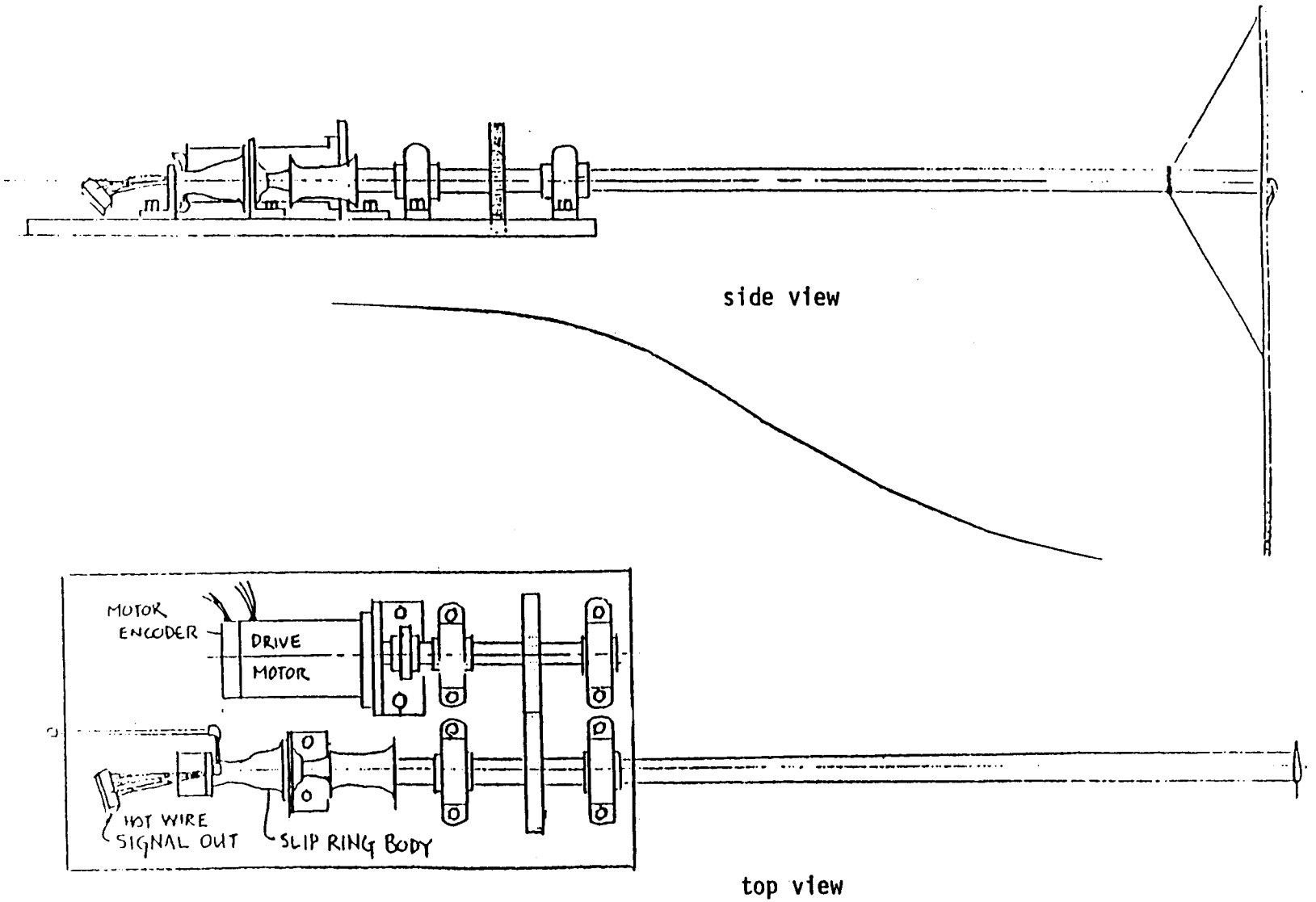

Figure 3.5.1 Mechanism for Flying Hotwire Probe

Since we measured the velocity time derivative in a moving frame of reference, we were interested in knowing the effect the moving frame had on the measured derivative. The equations relating the velocity and velocity derivative for the moving and stationary frame of references shown on Figure 3.5.2 give for $\theta = \pi/2$,

$$u_1 = - u_2' + x_2'\dot{\theta}$$
$$u_2 = v_1' - x_2'\dot{\theta} \qquad (3.5.1)$$

$$\dot{u}_1 = - \dot{u}_2' - 2u_2'\dot{\theta} + [2\, x_2']\dot{\theta}^2$$
$$\dot{u}_1 = \dot{u}_1' - 2u_2'\dot{\theta} + [2x_2' + x_1']\dot{\theta}^2 \qquad (3.5.2)$$

The primes denote the stationary frame of reference, the dots denote derivatives with respect to time, r is the distance of the probe from the center of rotation and θ is the angle of rotation measured from the x-axis. The last term on the right hand side of equation (3.5.2) is the acceleration due to the rotating frame of reference and makes no contribution to the unsteady signal of $\dot{\theta}$ = constant. In equations (3.5.1) and (3.5.2) the u_1', u_2', $\dot{u}_1'$ and $\dot{u}_2$ are the measured quantities, and $\dot{\theta}$, x_1' and x_2' are known quantities. Equations (3.5.1) and (3.5.2) can be combined to yield the unsteady derivative as,

$$\dot{u}_1 = - \dot{u}_2' - u_2\dot{\theta}$$

$$\dot{u}_2' = - \dot{u}_1' + 2\dot{\theta}u_1' + 2(\dot{\theta})^2 r \qquad (3.5.3)$$

Thus both components of velocity are needed to determine either $\dot{u}_1$ or $\dot{u}_1$ due to the Coriolis effect.

The orders of magnitude at the centerline of the jet of the

Figure 3.5.2 Reference Frame for the Moving Wire

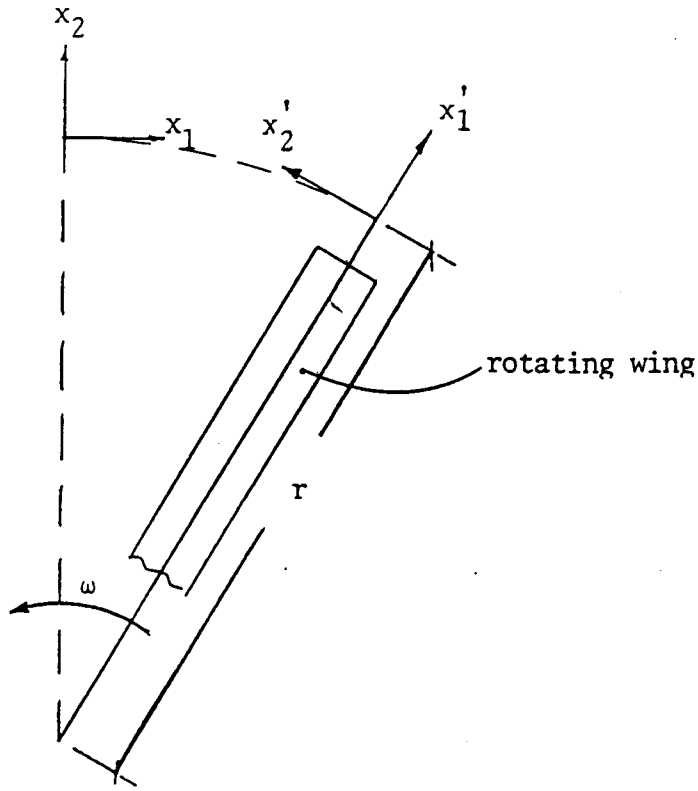

various terms in the equation above can give insight on the effect of the rotating frame on the measured quantities. The rotation speed of the wing was equal to 1.1 cycles per second, giving $\dot{\theta}r$ to be 1.46 times the centerline velocity of 4.8 m/s.

$$2\dot{\theta}u_1 = (2.9U_o^2)/r \tag{3.5.4}$$

$$2(\dot{\theta})^2 r = (4.26\ U_o^2)/r \tag{3.5.5}$$

Assuming isotropic flow to estimate the order of magnitude:

$$\overline{\dot{u}_1^2} = U_o^2\overline{\left[\frac{du}{dx}\right]^2} = U_o^2\left[\frac{\epsilon}{15\nu}\right] \tag{3.5.6}$$

The dissipation scales like the velocity cubed divided by the distance downstream x from the jet exit, thus:

$$\overline{\dot{u}_1^2} = U_o^5/(15x\nu) \tag{3.5.7}$$

Comparing the above three terms, the unsteady term is seen to be several order of magnitudes larger than the other two terms, therefore the effect of the moving frame on the measured derivatives is negligible, except for the increased convection velocity.

3.6 Data Acquisition From the Moving Probe

The data was collected only when the probe was parallel to the axis of the jet. This was accomplished by using an encoder pulse that triggered the A/D converter to start collecting data. The short charging time of the sample and hold of the A/D (nanoseconds) insured that the measurement was effectively taken at a point. One data sample was collected for each revolution and 4800 samples were taken at each radial position.

The hot-wire signal was transmitted from the probes to the anemometers using low noise slip-rings. The slip-rings were enclosed in a grounded aluminium housing so as to avoid stray electromagnatic noise. The coaxial cables connecting the slip-rings to the anemometers were also shielded. The noise due to the slip-rings was estimated to be of the order of 1 mV.

Signals from the anemometers were differentiated as described in chapter 2. Both the original velocity signal and it's time derivative were recorded for each of the wires. The signals were digitized using a 15 bit, 16 channel A/D converter. The +10 to -10 volt range of the A/D converter results in a quantization error of 0.6 mV. The A/D converter was interfaced with a DEC PDP 11/84 computer using a DEC DR11-W interface module.

3.7 Calibration

The hot-wires were calibrated in a low turbulence intensity calibration tunnel. The calibration was done against a linear pressure transducer which was in turn monitored with a manometer. A pressure tap at the settling chamber of the calibration tunnel was used for determining the velocity at exit of tunnel. The wire was held at the exit of the tunnel during the calibration process. The calibration data and the pressure transducer output were digitized with an A/D converter. The calibration system, from the wires through the slip-rings and to the A/D converter including cables, grounding, etc., was the same used in the actual experiment. The voltage to velocity data linearization was done digitally. A fourth order polynomial as described in George et al. (1987) was used, i.e,

$$U = A_0 + A_1 E + A_2 E^2 + A_3 E^3 + A_4 E^4 \qquad (3.7.1)$$

A least square technique was used to determine the coefficients in the calibration curve. The error in predicting the measured velocity from measured voltages was typically less then 0.1% over the entire range. Once the coefficients were found, they were used for the determination of instantaneous velocity from the instantaneous voltages sampled by the A/D. The calibration data was verified at the end of each experiment to insure that the calibration did not shift during the course of the experiment.

To calibrate the wires for angle dependence the cross-wires were mounted on a holder with marked degree graduations. The wires were rotated 5^0 at a time to an angle of 50^0. The calibration data for both wires were recorded for every 5^0. This was repeated for four different freestream velocities to obtain the angle dependence of the wires for the entire velocity range in the experiment. The angle calibration for the cross-wires was done using a modified cosine law, Beuther et al. (1987).

$$U_{eff}/U_o = \left[\cos^2\phi + k^2\sin^2\phi \right]^{1/2} \qquad (3.7.2)$$

where k is dependent on the total velocity U_o. In this experiment a k-factor between 0.1 to 0.3 was common for hot-wires which makes the contribution of k significant. We expressed k as polynomial

$$k^2 = B_o + B_1 U_o^{1/2} + B_2 U_o^{3/2} \qquad (3.7.3)$$

Due to the velocity dependence of k, the solution of equation (3.6.3) required an iterative procedure.

3.8 Probe Response

In the measurement of small scales of turbulence, a good spatial and temporal resolution of the probes was necessary. As described in

Chapter 2, multiple components of the velocity signal, the time derivative in the streamwise direction and various spatial derivatives were measured. This required an analysis of the effects of thermal lag, finite wire length and the separation of the probes. The probe spatial response determines the highest frequency signal which can be resolved by the sensor. The frequency response, which is dependent on the heat transfer characteristics of the sensor, determines the size of the velocity flucutations that can be correctly measured by the probe.

3.8.1 Thermal Response

The temporal response of hot wires is determined by the instantaneous energy balance equation for the hot wire:

$$dH/dt = RI^2 - \Phi \qquad (3.8.1)$$

Where H is the heat content of the wire, RI^2 is the Joule heating and Φ is the heat convected from the sensor by the fluid. It takes a finite amount of time for the fluid around wire to transfer information to the wire. This is the cause of the thermal lag in wire response to a fluctuating medium. An ideal wire would exhibit a zero time response, i.e dH/dt would be equal to zero. For this experiment it was ensured that the thermal lag was small enough to provide an acceptable frequency response. The frequency responses of the wires were determined from a known input signal. This was accomplished by simulating a sudden change in the flow around the wire. The wire was exposed to a constant flow and a square wave signal was fed into the bridge. The bridge was aligned to produce an output with the shortest possible impulse response from the square wave input resulting in a frequency response of 120 kHz.

3.8.2 Spatial Resolution

For this experiment the scales of turbulence dissipation were of interest and they put a constraint on the size of the wires that were used. It is well known that wires cannot resolve scales that are much smaller than the length of the wire. Wyngaard (1968) studied the effect of finite wire length on the measured spectra. In addition to the wire length constraints, the separation between the multiple wires determines the resolution to which spatial derivatives can be measured. This problem is considered in more detail in Section 5.2.

3.9 Evaluation of the Fluctuating Convection Velocity Effect

Equation (3.3.4) gives a model for the effect of the fluctuating convection velocity on the measured time derivatives. The moving probe decreases the effective turbulence intensity, and therefore the correction terms $\overline{u^2}/U^2$ and $2[\overline{v^2}+\overline{w^2}/U^2]$ become smaller as the effective mean velocity increases. By comparing the time derivative obtained with the moving probe to that obtained with a stationary probe this model can be evaluated. Note that Champagne (1978) used this correction for his derivative measurements only at the centerline of the jet.

Since the turbulence intensity varies with radial position, the best way to do this evaluation is to compare the theoretical correction of the time derivative to that found experimentally from the two experiments (i.e. the moving wire experiment and the stationary wire experiment). The stationary wire results in this work at the centerline are consistent with those of Champagne. The error term,

$$\frac{\overline{u^2}}{U^2} + 2\,\frac{\overline{v^2}+\overline{w^2}}{U^2}$$

is shown on Figure 3.9.1. The dashed line is computed from the measured Reynolds stresses $\overline{u^2}$, $\overline{v^2}$ and $\overline{w^2}$. The triangles are the experimental data obtained by assuming that the moving probe results of the time derivative have negligible correction terms. These results are plotted against the turbulence intensity. The theory is in remarkable agreement with the experimental data.

Figure 3.9.1 Effect of Fluctuating Convection Velocity

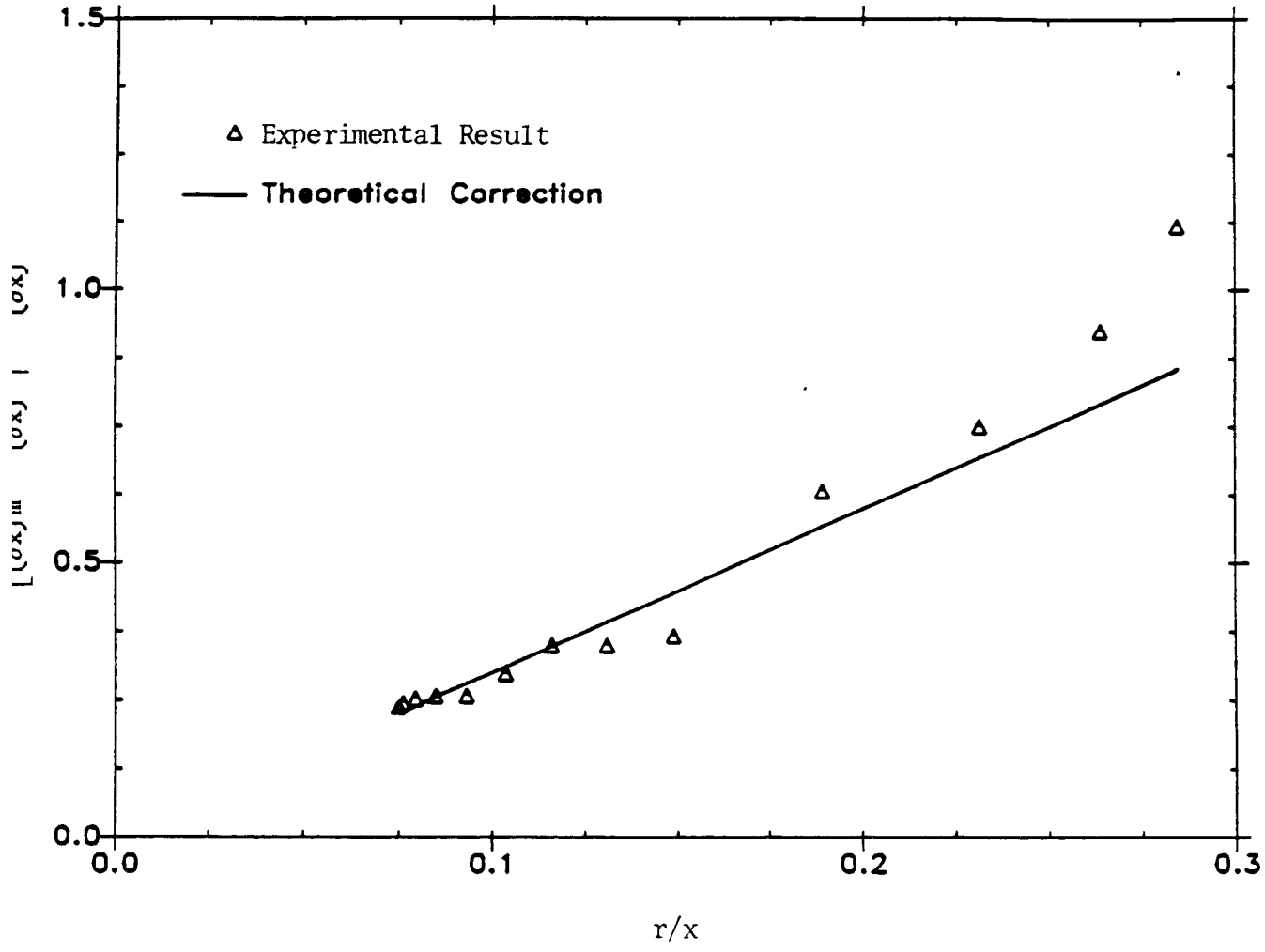

CHAPTER 4

The Measured Velocity Moments

4.1 First and Second Moments of the Velocity Field.

Discrepancies in the mean velocity profile of the jet between LDA measurements by Capp (1983) and earlier stationary hot wire measurements by Wygnansi and Fiedler (1969) could not be accounted for by the effect of hot-wire errors. Eguations (3.2.1) to (3.2.4) give the effect of these errors which are due to cross-flow and rectification. These equations show the mean velocity profile measured with a stationary hot-wire to be overestimated as found by Capp (1983), contrary to the results of Wygnanski and Fiedler (1969). This difference was attributed to facility problems in Wygnanski's experiment since his data could be shown to not conserve momentum at the largest streamwise distances (See Capp 1983).

In this work the problem of hot wire response in high turbulence intensity flow was addressed by doing two experiments with hot wires, one stationary and one moving, and comparing the results with the LDA experiments of Capp (1983) and Capp et al. (1988). As described in Chapter 3, the superimposed velocity on the wire reduces the cross-flow and rectification errors that are due to the high turbulence intensity. All three experiments (including Capp et al. 1988) were carried out in the momentum conserving jet described in Chapter 2. For the rest of this chapter reference to the stationary and moving wire experiments refers to the results of this work, and while reference to the LDA refers to the experiments performed in the same facility by Capp (1983) and Capp et al. (1988).

Figure 4.1.1 shows the variation of the centerline mean velocity with the distance from the jet exit. Both the stationary and moving wire results are in excellent agreement with those measured by Capp using the LDA and those obtained earlier by Peng (1985) in the same facility using stationary hot-wires. This is, of course, the expected result since the turbulence intensity is a minimum at the centerline and the hot-wire cross-flow errors are less than a few percent of the mean value there. Also shown for comparison is the centerline data of Wygnanski and Fiedler (1968). These have been discussed in detail by Capp (1985) who attributed the difference to problems in their facility.

The data for x/D > 30 are described to within the experimental error by the similarity relationship

$$\frac{U_c}{U} = \frac{1}{5.9}\left[\frac{x}{D} - 2.7\right] \qquad (4.1.1)$$

or

$$U = 6.7\sqrt{M_o}\,(x-2.7D)^{-1} \qquad (4.1.2)$$

The virtual origin is 2.7 diameters and is consistent with that determined by the Capp 1983 experiment. The Wygnanski and Fiedler data have been discussed in detail by Capp (1983), and the differences attributed to facility-related problems - in particular, backflow.

The mean axial velocity normalized by the centerline velocity, U/U_c, is plotted versus the nondimensional radial coordinate, η=r/x, in Figure 4.1.2. (Note that x is measured from the virtual origin established above.) To avoid clutter, the data of Wygnanski and Fiedler (1969) has been plotted only as a smooth line. The mean profiles of the current facility collapse by 30 diameters with a

Figure 4.1.1 Centerline Decay

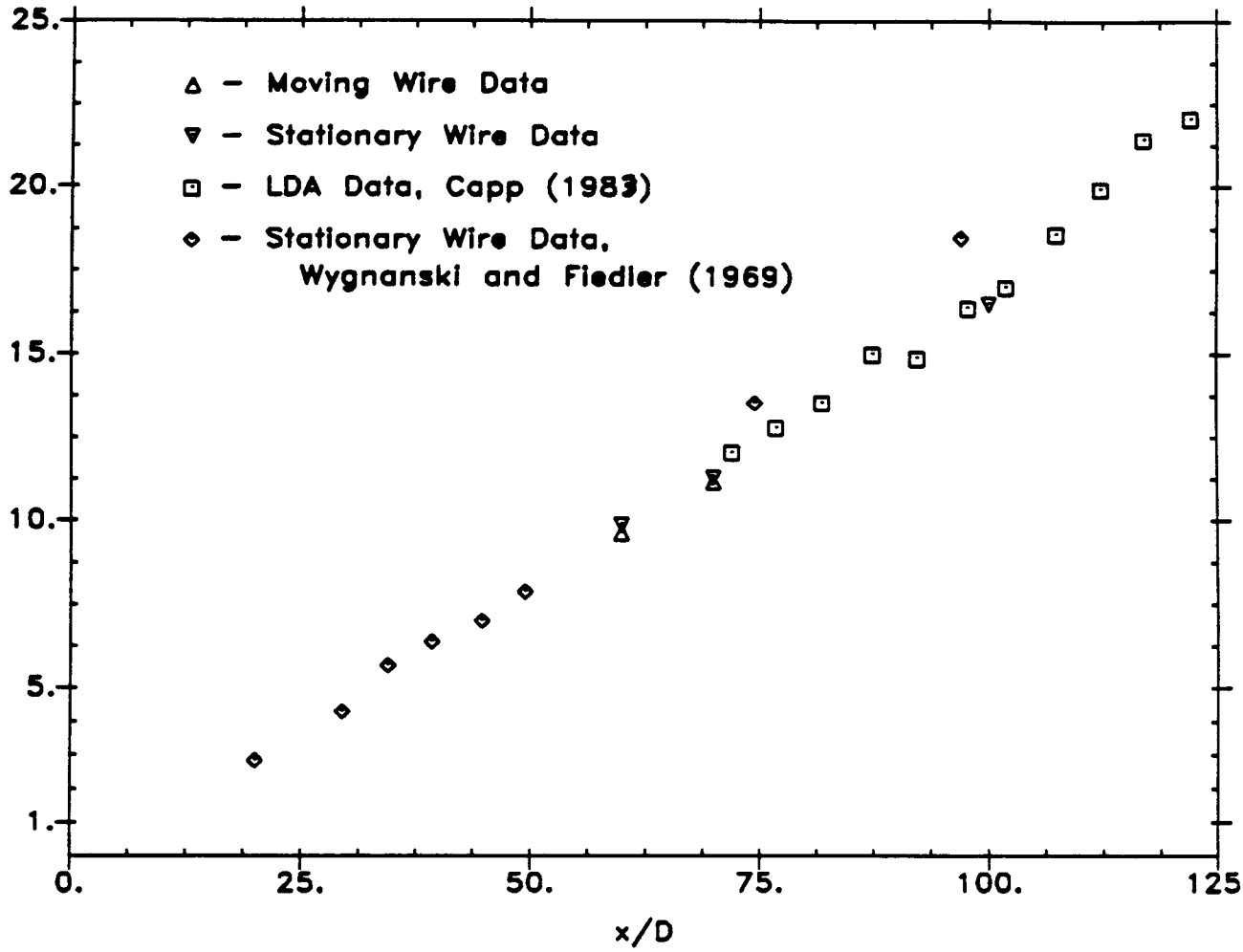

Figure 4.1.2 Mean Velocity Profile

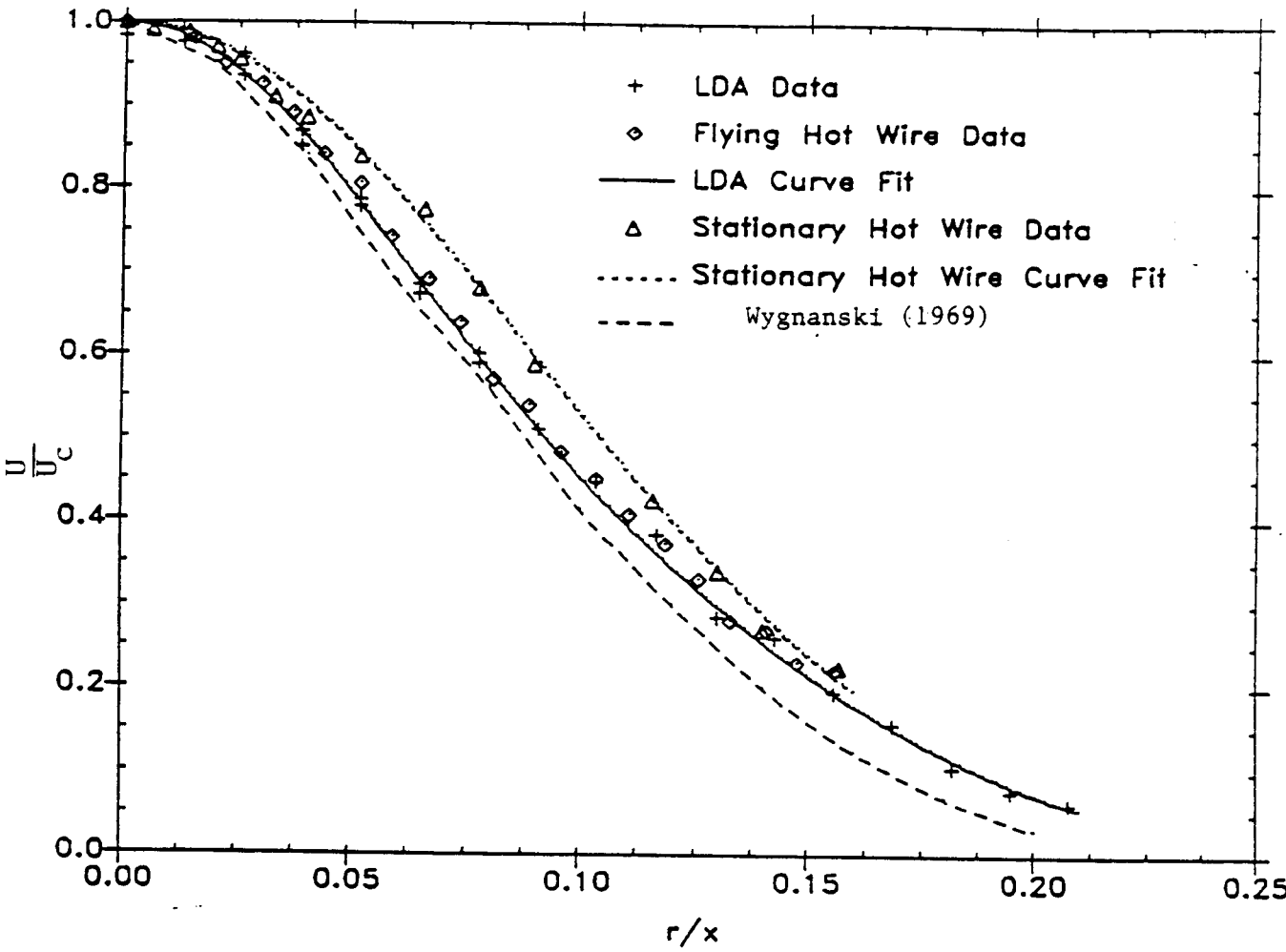

virtual origin of 3 times the diameter of the jet, a value consistent with that obtained from the centerline mean velocity decay. The stationary wire profile gives a half width of 0.102 which is wider than the 0.094 obtained with the LDA (Capp 1983), 0.094. The moving wire results for the mean velocity reproduce the LDA results as shown on Figure 4.1.2. This behavior pattern is expected, since a binomial expansion of the error due to cross-flow effects reveals the leading error term is positive as shown on equations (3.2.1) and (3.2.2). Because of these errors, the LDA and moving probe results are preferred.

4.2 The Second Order Moments

The Reynold's stress terms that are non-zero in this axisymmetric jet are $\overline{u^2}$, $\overline{v^2}$, $\overline{w^2}$ and $\overline{uv}$. These terms are plotted in Figures 4.1.3 to through 4.1.6 respectively. In all the plots, the Reynold's stress measurements are nondimensionalized by the square of the centerline velocity. The centerline values for the normal stresses in the axial, radial and the azimuthal directions measured by the LDA are 0.075, 0.045 and 0.047 respectively. The stationary hot-wire measured a centerline value of 0.078 for the axial stress, only 4% higher than the LDA. The moving hot wire measured a centerline value of 0.077. All of these are within the experimental error, consistent with the negligibility of the stationary hot-wire errors near the center. Note that since these results have been normalized by the corresponding mean velocity, they also contain the effect of the error terms on the mean.

The normalized stationary wire centerline values for the radial and azimuthal normal stresses have the same value of 0.057 and

significantly overshoot the LDA values by 24%. The results obtained with the moving probe are closer to the stationary wire values than those of the LDA as shown in Figures 4.1.4 and 4.1.5. These differences between moving wires and the LDA have not yet been explained, but cannot be attributed to the cross-flow errors on the wires.

The profile of the axial normal stress measured with the stationary hot-wire fails to detect the distinct off-axis peak detected by the LDA. This peak is consistent with turbulence model calculations, and is due to the strong off-axis peak in the production of turbulent energy by the Reynolds stress working against the mean shear. This peak in the normal stresss occurs at a an $\eta = 0.024$. The moving wire also shows this off-axis peak although it is not as distinct as the LDA results.

The largest discrepancies between moving and stationary wire results occur off-axis at higher turbulence intensities. Here the hot-wire profiles decrease much more rapidly with radius and pass under the curve obtained with the moving wire. At $\eta = 0.1$ (near the jet half width) the local turbulence intensity from the moving wire is approximately 55% while normalized stationary hot-wire values are roughly 25% less than those obtained with the moving wire. The relatively good agreement between the moving wire and LDA results confirms Capp's earlier LDA results and lends considerable confidence to his LDA bias correction procedures.

For the $\overline{uv}$ profile the LDA, moving and stationary hot-wires give very close results as shown on Figure 4.1.6. Equation (3.2.5), shows the contamination of the shear stress arise entirely from errors in

Figure 4.1.3 Axial Component of Reynolds Stress

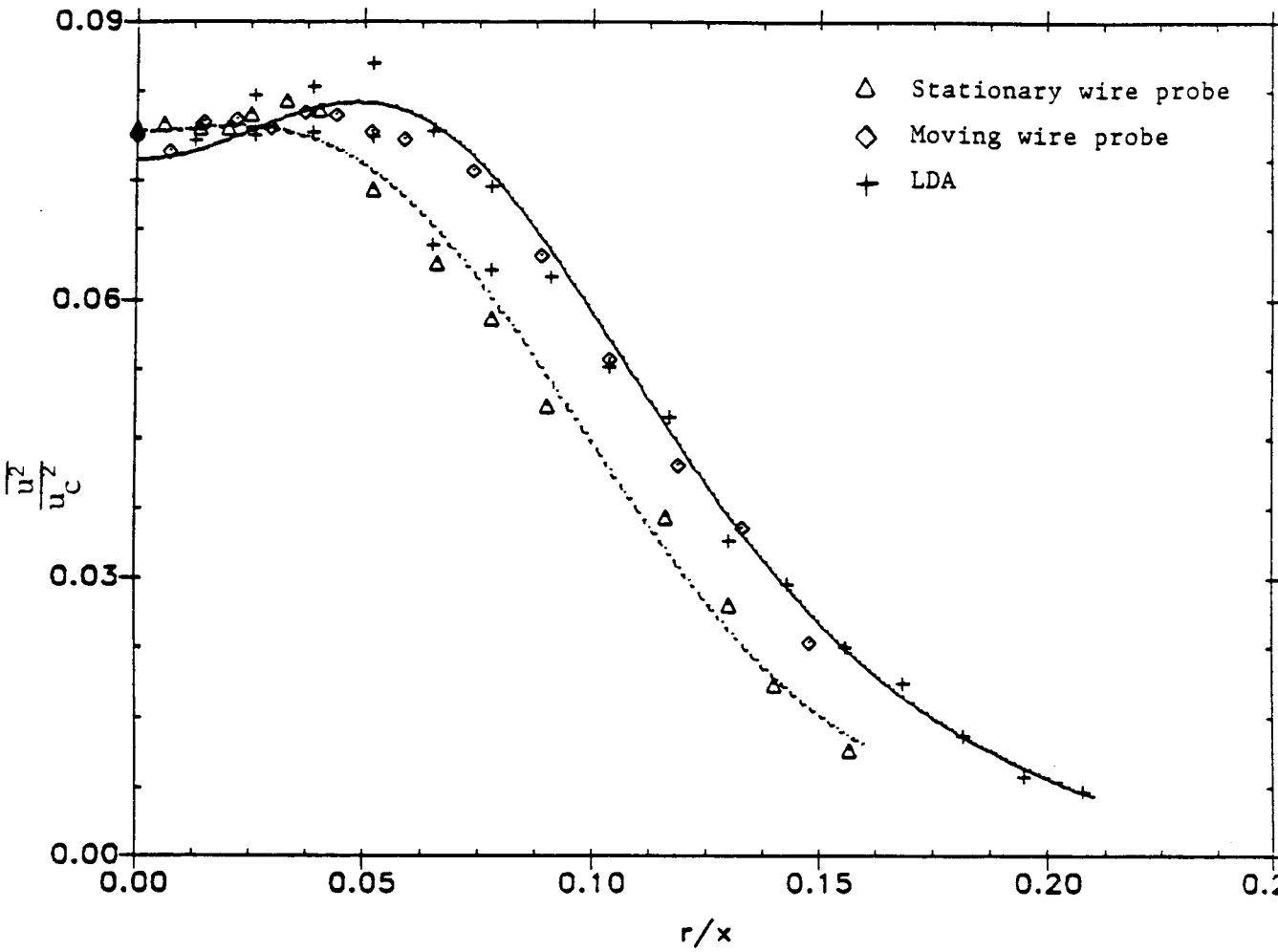

Figure 4.1.4 Radial Component of the Reynolds Stress

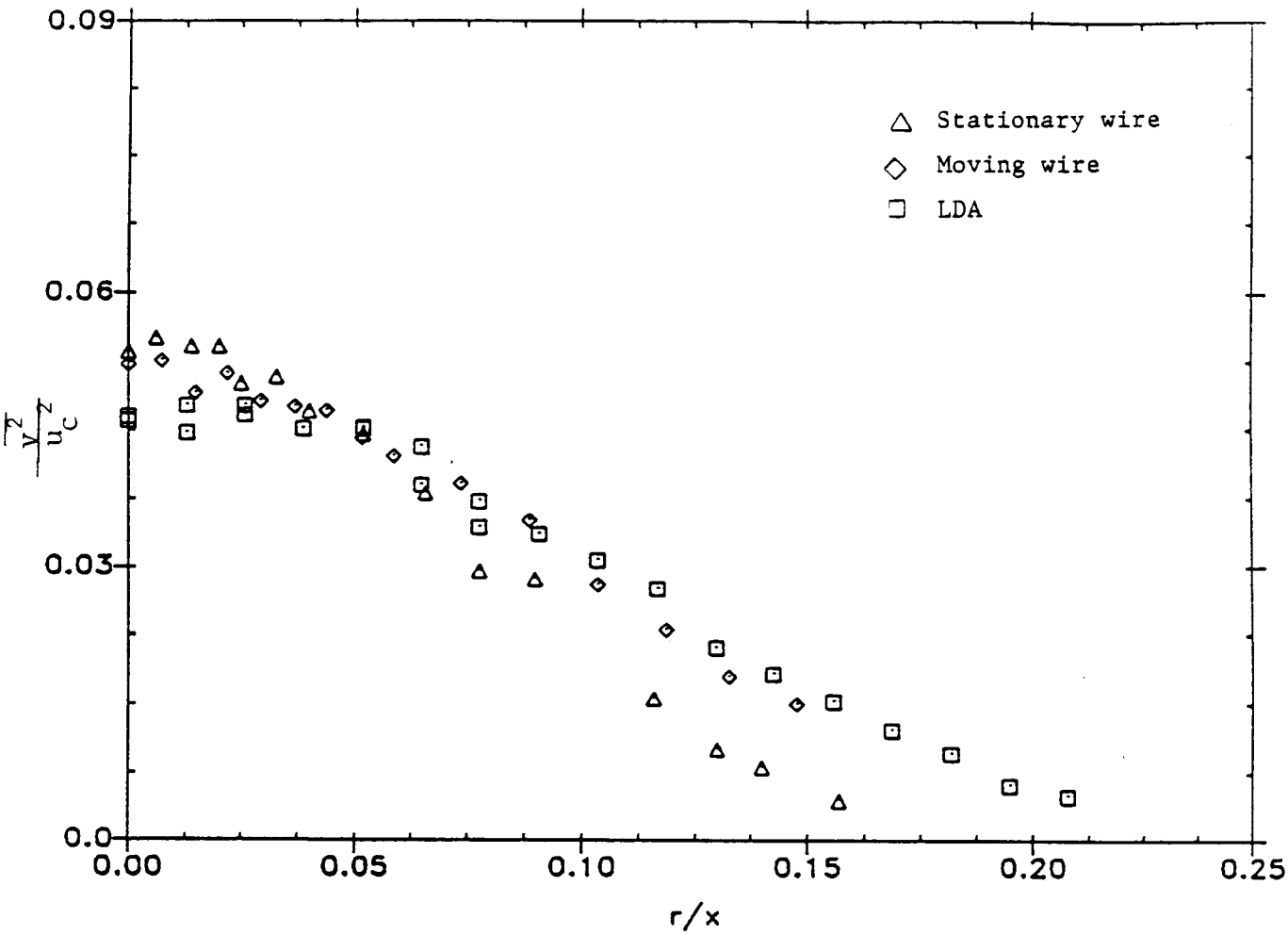

Figure 4.1.5 Azimuthal Component of the Reynolds Stress

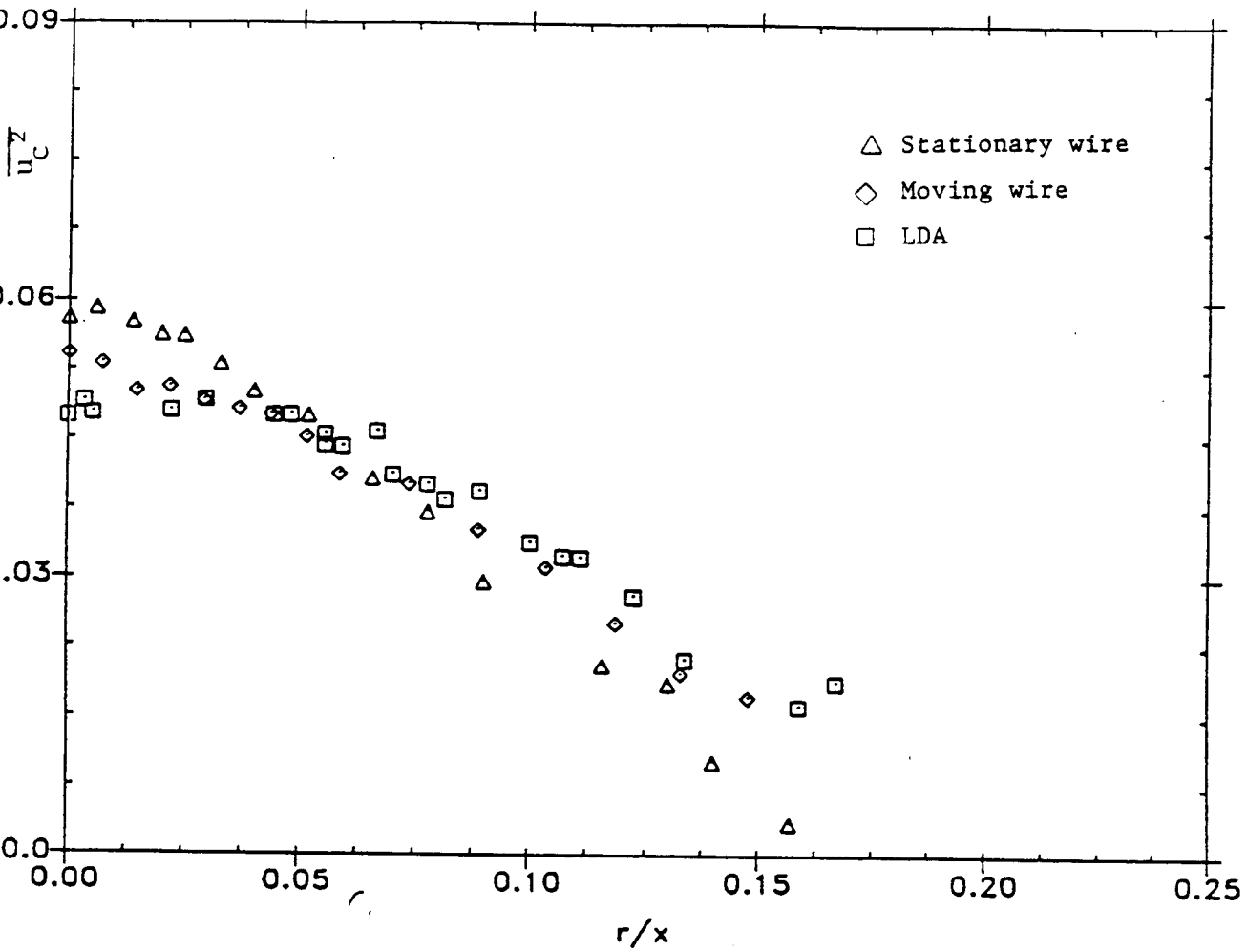

Figure 4.1.6 Reynolds Shear Stress

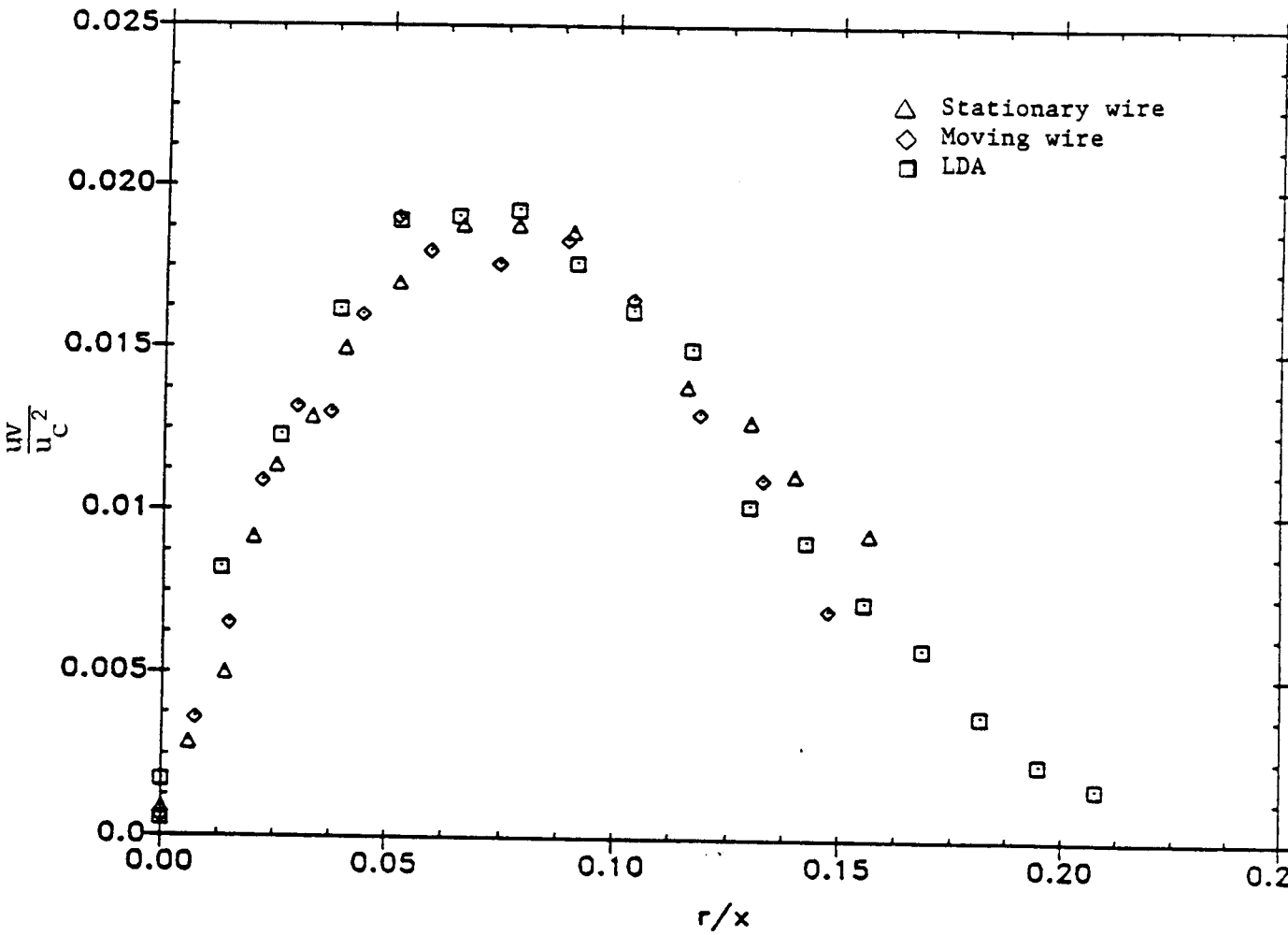

determining the mean velocity. This enables the stationary wire to give good shear stress results as compared to it's measurement of the normal, radial and azimuthal results. This agreement confirms the dramatic effect of the facility on the shear stress alleged by Capp (1983) since there have been large variations in the peak $\overline{uv}$ reported in the past. These clearly cannot be attributed to the use of different measuring technique, but must be attributed to the facility.

The behavior discussed above is consistent with the equations developed for stationary wire cross-flow errors in Chapter 3. Errors for the second-order moments enter at the third order, are therefore only one level higher than the measured quantity, and so are subject to greater contamination than the estimates for mean values. When measuring an unknown flow, it is tempting to use this expansion to correct the second order measurements. However, even though one might model the higher order terms using a Gaussian approximation, no convenient approximation is apparent for the third order values. Flow reversal and prong inteference errors are not accounted for in this analysis and higher order terms have been observed to drop off very slowly. As a consequence of these features, it does not appear practical to attempt to correct the stationary hot-wire measurements, at least for turbulence intensities as high as those reported here.

4.3 Verification of the First and Second Moment Data Using Governing Equations for a Free Jet

An entirely separate question from that of measurement accuracy is whether or not the experimental flow is a reasonable model of an axisymmetric jet in a free environment as hypothesized. This evaluation can be made only by substituting the measured values into the governing equations for the assumed flow. As George (1988a) has

pointed out, for the experimentalist the solution to the equations is known from the measurements, only the equations which determine it are not. Note that it was failure to satisfy the governing equations for a free jet which had Baker (1980) and Capp (1983) to disregard the Wygnanski and Fiedler (1969) data, and not questions about the hot-wire technique as were raised above.

To evaluate the accuracy of the measured data two forms of the momentum equation can be used. The first form enables a verification of the inter-consistency of the data. This form described in Taulbee (1987) is a similarity form of the momentum equation. An expression for the shear stress in terms of the mean velocity, the axial, radial and azimuthal components of the Reynold's stress can be obtained by integrating the reduced momentum equation. This expression given in Taulbee et al (1987) is,

$$\frac{\overline{uv}}{U_c^2} = \frac{1}{\eta} f \int_0^{\eta} f\eta d\eta + \eta \frac{\overline{u^2} - \overline{v^2}}{U_c^2} + \eta \int_{\eta}^{\infty} \frac{\overline{v^2} + \overline{w^2}}{\eta U_c^2} d\eta \qquad (4.3.1)$$

The data evaluation is done by substituting the experimental results of U, $\overline{u^2}$, $\overline{v^2}$ an $\overline{w^2}$ into the right hand side of equation 4.3.1 and comparing the results with the directly measured non-dimensional form of the shear stress. The results of this comparison for all three experiments (LDA, moving and stationary wire experiments) are given in Figures 4.1.7, 4.1.8 and 4.1.9. The stationary wire results shown on Figure 4.1.7 show that the component from the mean value contribution which is the first term on the right hand side of equation (4.3.1) to be higher then the measured shear stress. Since the sum of the other two terms are positive, they make the momentum balance even worse. The over–all balance of the momentum equation for this data gives a value

that is 23% higher than the measured shear stress at the peak. This is due to the over-estimation of the mean value by the stationary hot wire (see Section 4.1).

The LDA and moving wire results are shown on Figures 4.1.8 and 4.1.9 respectively. Both sets of data show a much better balance of equation (4.3.1). The values from only the mean contribution are smaller than the measured shear stress, and the contributions from the Reynolds stress bring the balance to a very good agreement with the measured shear stress.

The second form of the momentum equation that can be used to evaluate the acuracy of the data is the momentum integral given by equation (1.3.5). The constancy of this momentum integral is required for the equations of motion to be satisfied, Capp (1983). The integral momentum constraint in equation (1.3.5) is written for an axisymmetric turbulent jet in an infinite environment. The terms U, $\overline{u^2}$, $\overline{v^2}$ and $\overline{w^2}$ which have all been measured were used to calculate the integral for each of the three experiments. The results given in Table 4.1.1 show that the stationary wire data overestimates the momentum balance by 20%. This result is consistent with the expectation that the stationary wire overestimates the mean velocity, and stands in contrast to the earlier hot-wire measurements of Wygnanski and Fiedler (1969), Rodi (1975) and others for which the integral is substantially less than unity (see Baker 1980 and Capp 1983). Table 4.1.1 also shows that LDA results underestimate the momentum balance only by 6%, and the moving wire results conserve momentum to within 5%. This fact, together with the confidence in the techniques, lends strong support to belief that the experiment is a reasonable model of an axisymmetric

Figure 4.1.7 Reynolds Shear Stress - HW

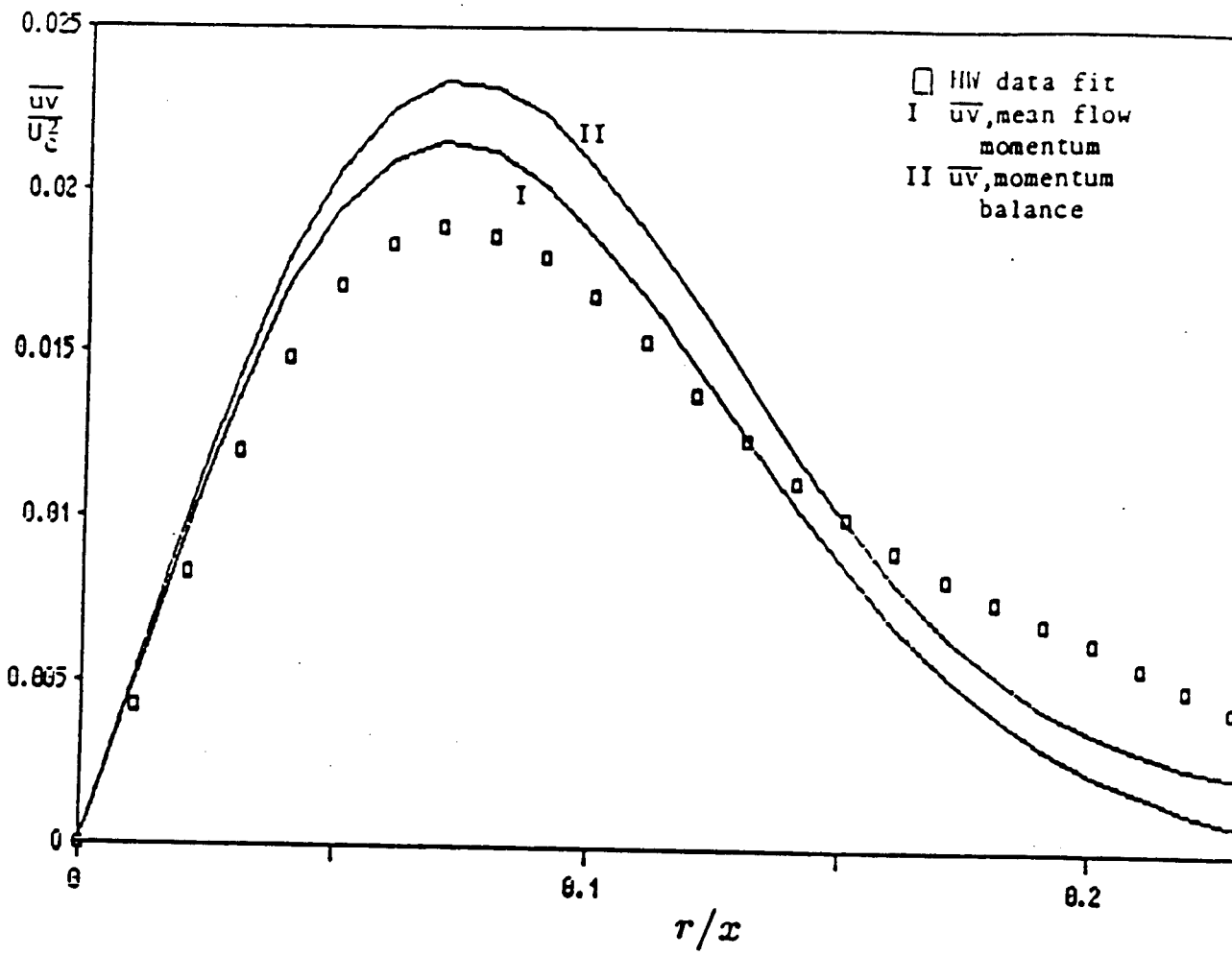

$$\frac{\overline{uv}}{U_c^2} = \frac{1}{\eta} f \int_0^{\eta} f \eta d\eta + \eta \frac{\overline{u^2} - \overline{v^2}}{U_c^2} + \eta \int_{\eta}^{\infty} \frac{\overline{v^2} - \overline{w^2}}{\eta U_c^2} d\eta$$

Figure 4.1.8 Reynolds [illegible] (Tsuge et al. 1988)

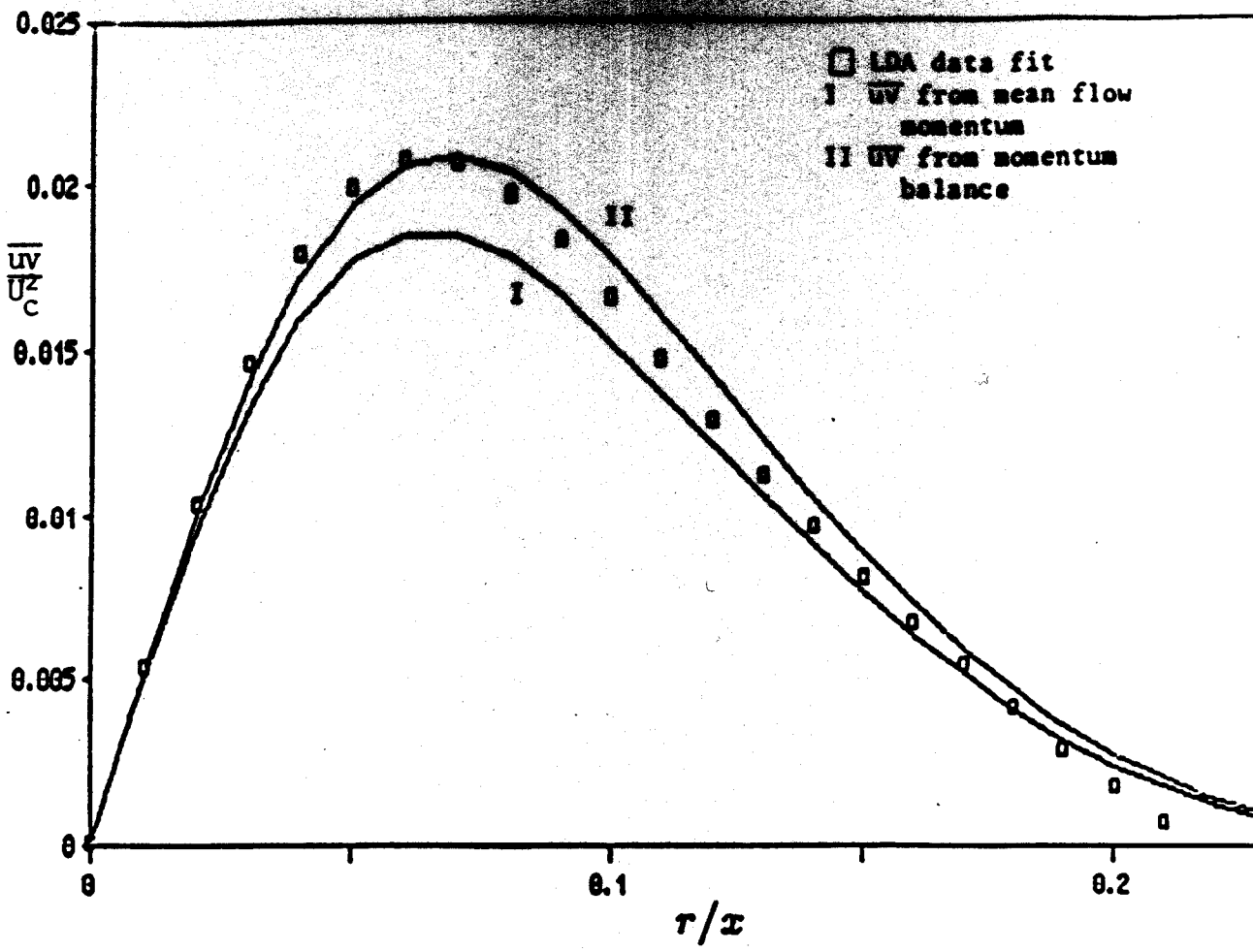

$$\frac{\overline{uv}}{U_c^2} = \frac{1}{\eta} f \int_0^{\eta} f \eta d\eta + \eta \frac{\overline{u^2} - \overline{v^2}}{U_c^2} + \eta \int_{\eta}^{\infty} \frac{\overline{v^2} - \overline{w^2}}{\eta U_c^2} d\eta$$

Figure 4.1.9 Reynolds Shear Stress - Moving HW

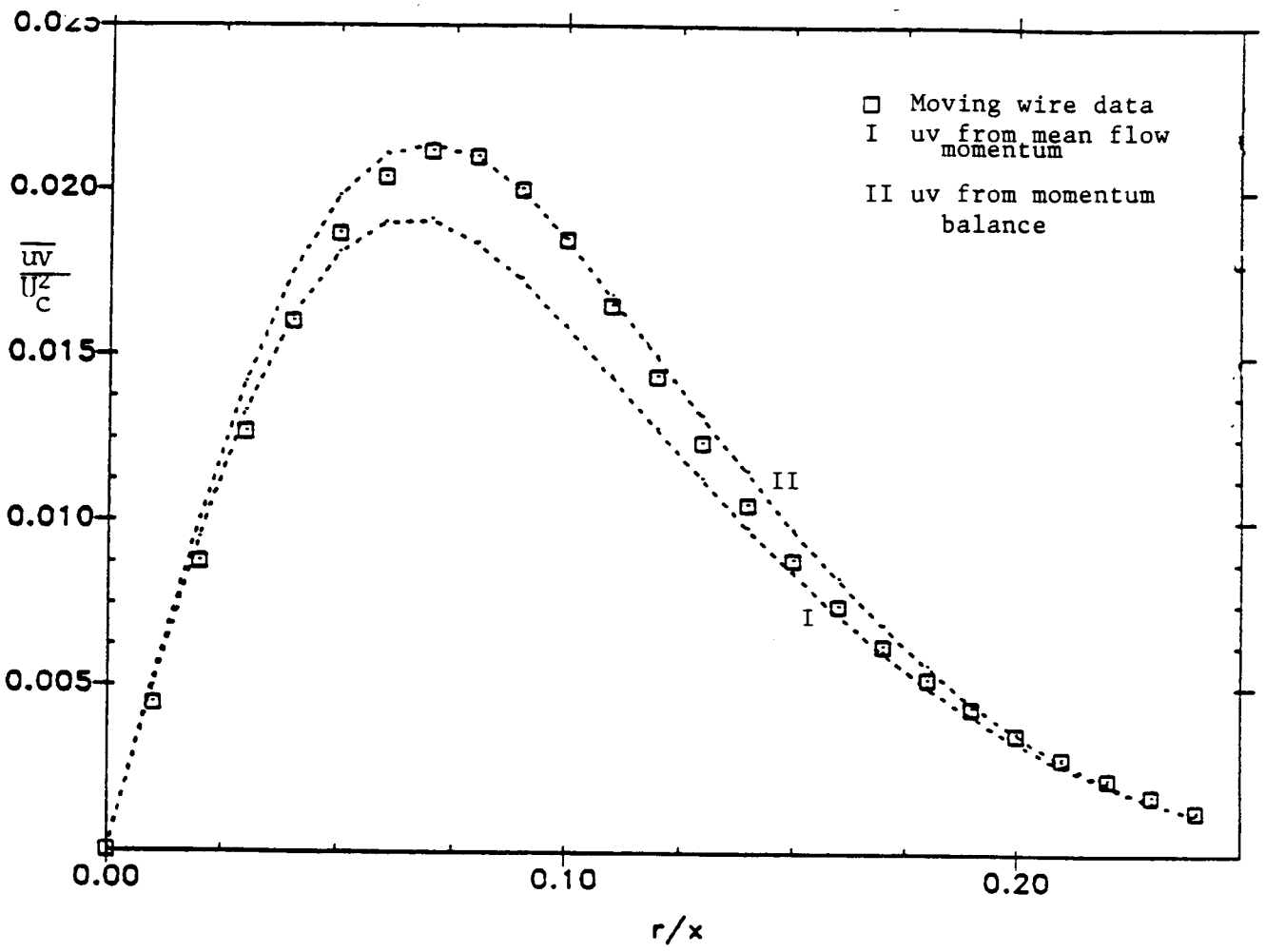

$$\frac{\overline{uv}}{U_c^2} = \frac{1}{\eta} f \int_0^{\eta} f \eta d\eta + \eta \frac{\overline{u^2} - \overline{v^2}}{U_c^2} + \eta \int_{\eta}^{\infty} \frac{\overline{v^2} - \overline{w^2}}{\eta U_c^2} d\eta$$

jet in a free environment. It also supports Baker's and Capp's arguments that the earlier experiments were not acceptable models of a jet in a free environment.

TABLE 4.1.1

	U**2	u**2	-u**2/2	-w**2/2	Sum
LDA	0.873	0.204	-0.063	-0.074	0.940
SHW	1.022	0.143	-0.036	-0.027	1.102
FHW	0.914	0.193	-0.044	-0.058	1.005

4.4 Evaluation of Hot wire Errors

Standard measuring tools such as stationary hot wires give poor results in high turbulence intensity environments. The turbulence intensity of the axisymmetric jet, calculated from the local mean velocity gives a turbulence intensity of 25% at the centerline which increases to 100% at the outer edge of the jet. This turbulence intensity is too large for the cross-flow and the rectification errors to be negligible. Equations (3.2.1) to (3.2.5) show the leading cross-flow error terms obtained by a binomial expansion of the hot wire response equation. The above mentioned equations do not provide a quantitative handle on the hot wire errors since they break down at intensities between 30-50% and they do not include the rectification errors. Thus the equations provide at most a basis for predicting the onset and the initial sign of the errors.

In Sections 4.1 and 4.2, comparisons of velocity moments between stationary wire, moving wire and Capp's LDA results show a considerable difference which gets worse for higher moments. The

advantages for moving the hot wire in the flow field are discussed in detail in Section 3.4 where it is pointed out that the superimposed velocity decreases the effective turbulence intensity and hence reduces the cross-flow and rectification errors. A comparative set of experiments to document these advantages in a flow with such a high intensity has never been performed in the past. Experiments reported here, in addition to Capp's LDA results in the same flow facility provide a unique opportunity to asses these errors in detail.

The results of Sections 4.1 and 4.2 show that the LDA data is reproduced by the moving probe to within experimental error. This means that with the moving probe one is able to reduce both the effects of rectification and cross-flow on the hot wire probes to an acceptable level. Also the constraints imposed by the equations of motion were shown to be satisfied by both the moving wire and the LDA. Therefore the stationary and moving wire results provide an acceptable data set that enables the evaluation of how these errors change across the jet as the turbulence intensity varies to a maximum value at the outer edge of the jet.

The notation used for the normalized difference between the moments obtained with the stationary wire and those from moving wire is ϵ with a subscript denoting the specific moment. For the mean value the error term is defined as:

$$\epsilon_U = \frac{U_{sta} - U_{mov}}{U_{mov}} \qquad (4.4.1)$$

For all the moments the values used in the error analysis is done using relations similar to equation (4.4.1), except that for convenience the denominator was taken as the mean velocity squared.

Figure 4.4.1 shows the results of the error analysis for the mean velocity. The results for the mean values obtained from the moving and stationary wires are very close at the centerline of the jet, where the turbulence intensity has the smallest value. Therefore the figure shows the error term ϵ_U is zero at the centerline of the jet and increases away towards the edge of the jet as expected. The stationary wire result for the mean value at every radial location is larger than the correspounding moving wire result, which makes ϵ_U positive across the entire jet. This is consistent with the predictions of equations (3.2.1) and (3.2.2) in which the leading error terms for stationary wire due to cross-flow errors are positive for the mean velocity. The last few points are misleading in that they seem to indicate that the error is decreasing which is contrary to our expectations. While this may indicate the increasing importance of the higher order error terms, it is probably due to the drop-out" phenomenon first reported by Beuther (1980) (see also Beuther et al. 1987). "Drop-out" occurs because the digital x-wire analysis cannot resolve the two components of velocity for the voltages measured due to local flow reversal on one of the wires, prong effects, etc. These effects became substantial at the outer edge of the flow so that as much as 40% of the data must be discarded for the stationary probe.

The results for the error analysis of the Reynolds stress component in the streamwise direction are shown on Figure 4.4.2. The equations (3.2.3) and (3.2.4) show the leading cross-flow error terms to be negative for these measurements. This error term is shown on the figure to be consistent with the predictions of the equations, since the error term is negative almost across the entire jet. The

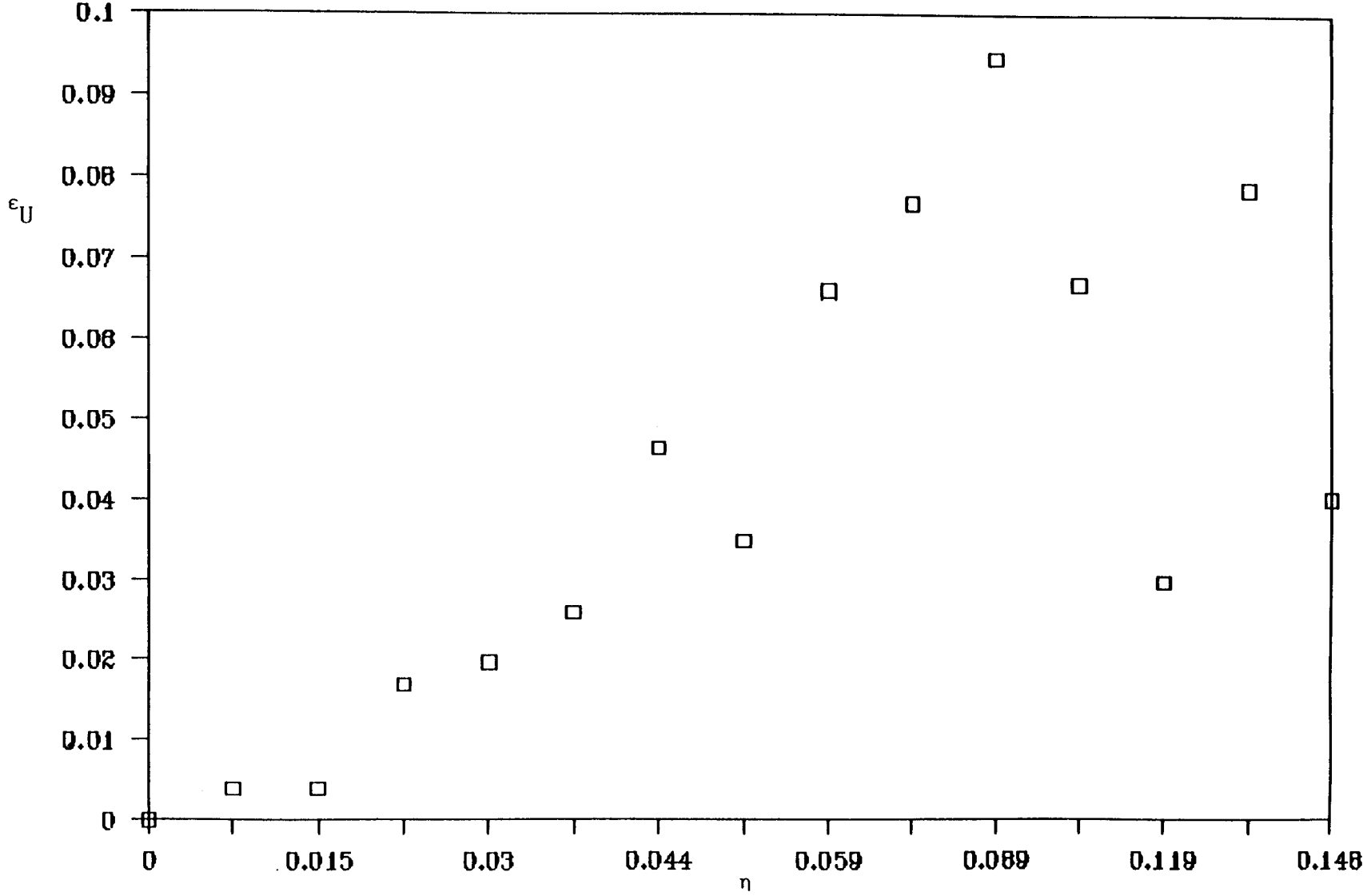

Figure 4.4.1 Hot-Wire Error Analysis for the Mean Velocity

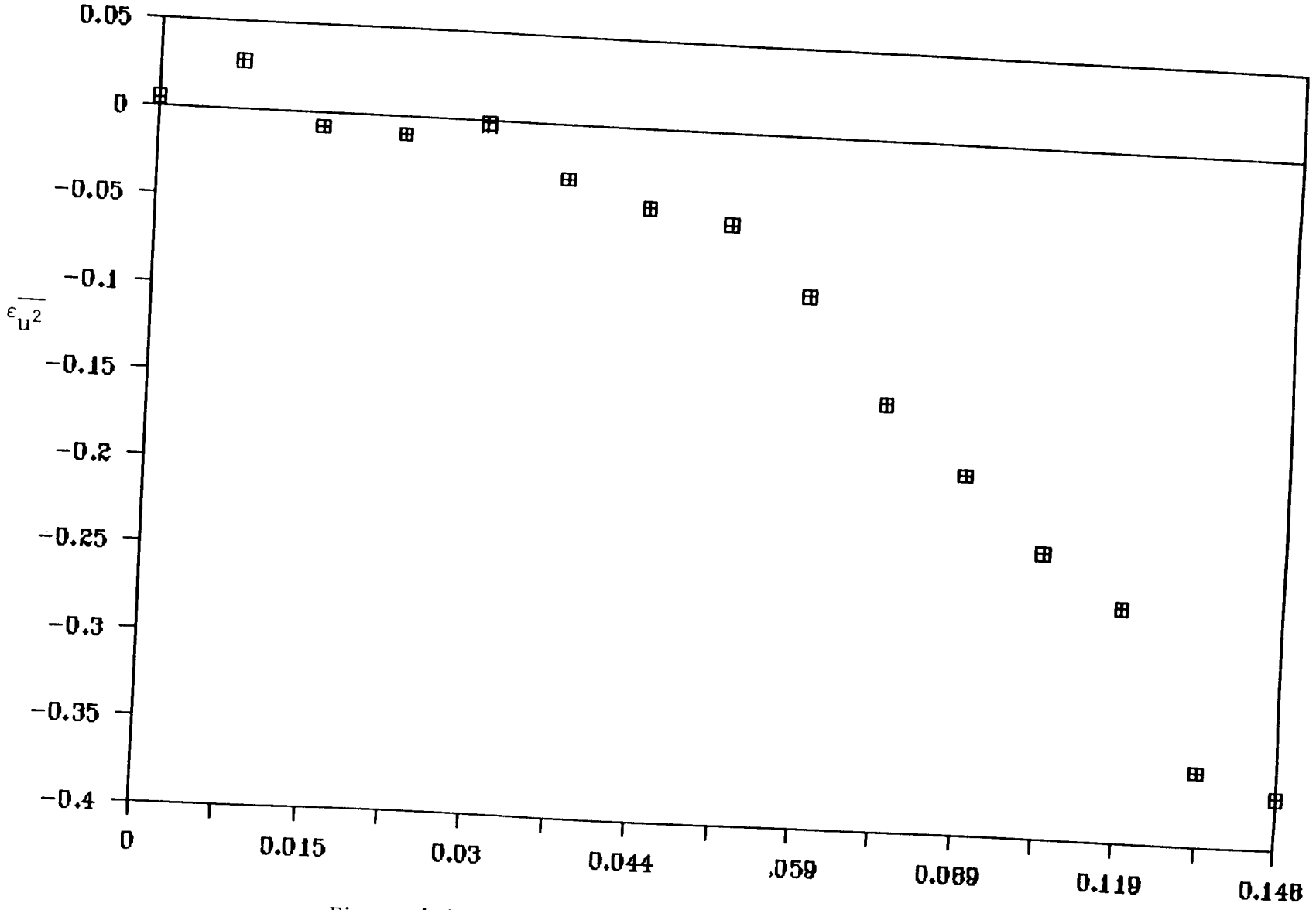

Figure 4.4.2 Hot-Wire Error Analysis for the Longitudinal Component of the Reynolds Stress

error term at the centerline of the jet is shown on the figure to be zero, consistent with the fact that the leading error terms are minimum at the centerline of the jet and the error increases off-axis.

Figure 4.4.3 shows the error analysis for the azimuthal and radial components of the Reynolds stress. The two error terms exhibit the same behavior except for the fact that the error terms start out to be positive before becoming negative at an ϵ of about 0.05. This behavior cannot readily be predicted from the equations for cross-flow errors.

The errors in the shear stress are shown in Figure 4.4.4. Equation (3.2.5) shows that the cross-flow error on this term stem only from the errors in determining the mean. As a consequence, the stationary wire results should give better results of this term as compared to the other second moments. This is consistent with the error analysis data of ϵ_{uv} shown in the figure, for which the ϵ_{uv} is small and so does not increase with increasing radial location (i.e. higher turbulence intensities).

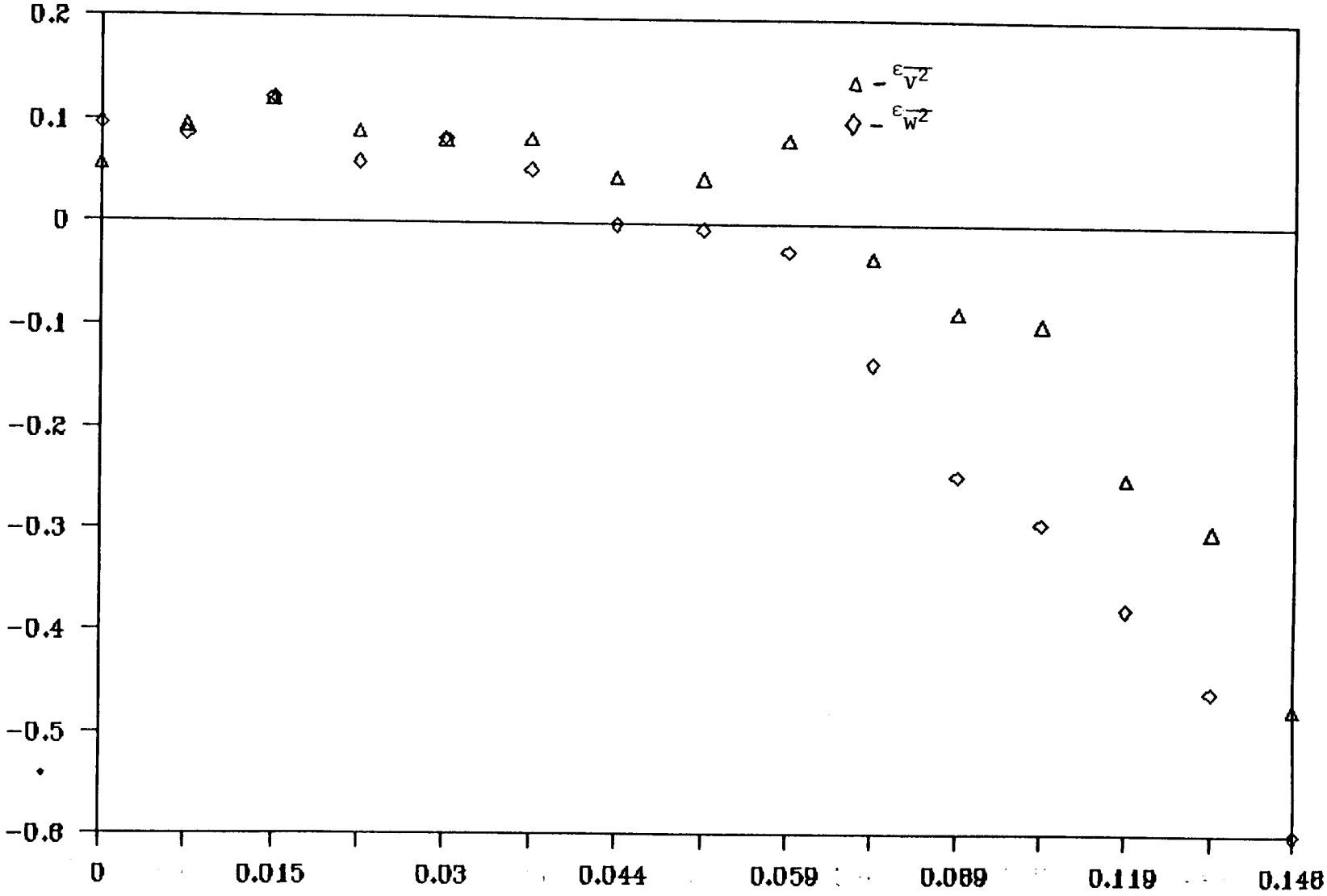

Figure 4.4.3 Hot-Wire Error Analysis for the Radial and Azimuthal Components of the Reynolds Stress

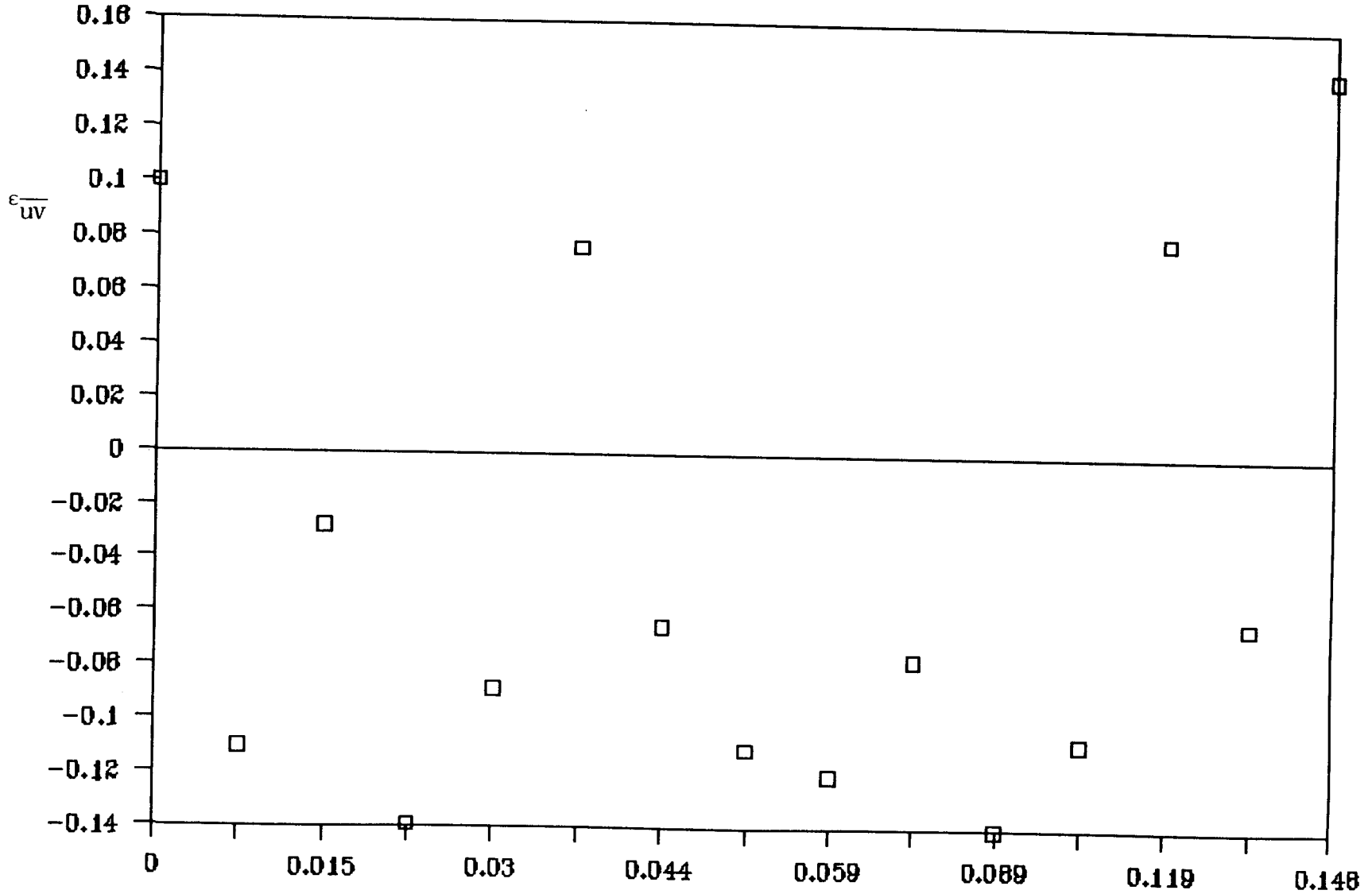

Figure 4.4.4 Hot-Wire Error Analysis for Reynolds Shear Stress

CHAPTER 5

Measurements of Dissipation and Mean square Vorticity

5.1 Locally Axisymmetric Homogeneous Turbulence

It has been of considerable interest to turbulence modelers and theoreticians to obtain measurements of the rate of dissipation of turbulence kinetic energy, ϵ, and mean square fluctuating vorticity, $\overline{\omega^2}$.

The average dissipation is given by (Hinze 1975):

$$\epsilon = 2\nu\left\{\left[\overline{\left(\frac{\partial u}{\partial x}\right)^2}+\overline{\left(\frac{\partial v}{\partial y}\right)^2}+\overline{\left(\frac{\partial w}{\partial z}\right)^2}\right] + \frac{1}{2}\left[\overline{\left(\frac{\partial u}{\partial y}\right)^2}+\overline{\left(\frac{\partial u}{\partial z}\right)^2}+\overline{\left(\frac{\partial v}{\partial x}\right)^2}\right.\right.$$
$$\left.\left. + \overline{\left(\frac{\partial v}{\partial z}\right)^2}+\overline{\left(\frac{\partial w}{\partial x}\right)^2}+\overline{\left(\frac{\partial w}{\partial y}\right)^2}\right] + \left[\overline{\left(\frac{\partial v}{\partial x}\right)\left(\frac{\partial u}{\partial y}\right)}+\overline{\left(\frac{\partial w}{\partial x}\right)\left(\frac{\partial u}{\partial z}\right)}+\overline{\left(\frac{\partial w}{\partial y}\right)\left(\frac{\partial v}{\partial z}\right)}\right]\right\} \quad (5.1.1)$$

and the mean square vorticity $\overline{\omega_i \omega_i}$ is given by (Hinze 1975):

$$\overline{\omega_i \omega_i} = \left[\overline{\left(\frac{\partial u}{\partial y}\right)^2}+\overline{\left(\frac{\partial u}{\partial z}\right)^2}\right] + \left[\overline{\left(\frac{\partial v}{\partial x}\right)^2}+\overline{\left(\frac{\partial v}{\partial z}\right)^2}\right] + \left[\overline{\left(\frac{\partial w}{\partial y}\right)^2}+\overline{\left(\frac{\partial w}{\partial x}\right)^2}\right]$$
$$- 2\left\{\left[\overline{\left(\frac{\partial u}{\partial y}\right)\left(\frac{\partial v}{\partial x}\right)} + \overline{\left(\frac{\partial u}{\partial z}\right)\left(\frac{\partial w}{\partial x}\right)} + \overline{\left(\frac{\partial v}{\partial z}\right)\left(\frac{\partial w}{\partial y}\right)}\right]\right\} \quad (5.1.2)$$

(Note that homogeneity requires that $\overline{\omega_i \omega_i} = 2\overline{e_{ij} e_{ij}}$.)

The direct measurement of the average dissipation and mean square vorticity clearly requires measurements of various components of the spatial derivatives. Because of the near impossibility of this in practice, investigators have usually relied on the assumption of local isotropy and Taylor's frozen field hypothesis in determining the dissipation.

For isotropic turbulence (Hinze 1975):

$$2\overline{\left[\frac{\partial u}{\partial x}\right]^2} = \overline{\left[\frac{\partial u}{\partial y}\right]^2} = \overline{\left[\frac{\partial u}{\partial z}\right]^2} = \overline{\left[\frac{\partial v}{\partial x}\right]^2} = \overline{\left[\frac{\partial v}{\partial z}\right]^2} = \overline{\left[\frac{\partial w}{\partial x}\right]^2} = \overline{\left[\frac{\partial w}{\partial y}\right]^2}$$

$$\overline{\left[\frac{\partial u}{\partial x}\right]^2} = \overline{\left[\frac{\partial w}{\partial z}\right]^2} = \overline{\left[\frac{\partial v}{\partial y}\right]^2}$$

$$\overline{\left[\frac{\partial u}{\partial y}\right]\left[\frac{\partial v}{\partial x}\right]} = \overline{\left[\frac{\partial u}{\partial z}\right]\left[\frac{\partial w}{\partial x}\right]} = \overline{\left[\frac{\partial v}{\partial z}\right]\left[\frac{\partial w}{\partial y}\right]} = -\frac{1}{2}\overline{\left[\frac{\partial u}{\partial x}\right]^2} \qquad (5.1.3)$$

Thus only measurement of $\overline{(\partial u/\partial x)^2}$ is necessary. This has been usually accomplished by measuring only the temporal derivative of the longitudinal components of the velocity and using Taylor's frozen field hypothesis to obtain

$$\overline{\left[\frac{\partial u}{\partial x}\right]^2} = U^{-2}\overline{\left[\frac{\partial u}{\partial t}\right]^2} \qquad (5.1.4)$$

where U is the local convection velocity usually taken as the local mean velocity.

The assumption of local isotropy simplified the experiments significantly but the accuracy of the results were impaired by the fact that shear flows such as the jet did not usually satisfy the relations for local isotropy. For the jet, this anisotropy of the small scales becomes more pronounced the farther one gets from the centerline. In this work we were interested in direct measurements of <u>all</u> the terms necessary to determine the dissipation and the mean square vorticity.

As will be described in detail later, it was only possible to measure seven of the terms of equations (5.1.1) and (5.1.2) in this experiment. It will be seen that these derivative measurements did not satisfy the conditions for local isotropy. However, they were

found to satisfy the conditions for axisymmetric homogeneous turbulence to within the experimental error. Thus it is appropriate to introduce the concept of locally axisymmetric turbulence for which all of the derivatives can be described in terms of four invariants α_{02}, α_{22}, β_{02}, and β_{22} (see also Appendix I). From equations (A.I.18)-(A.I.21), these can in turn be determined as:

$$\alpha_{02} = \left[\frac{1}{8}\right] \overline{\left[\frac{\partial u}{\partial y}\right]^2} \tag{5.1.5}$$

$$\alpha_{22} = \left[\frac{1}{4}\right] \left[\overline{\left[\frac{\partial u}{\partial x}\right]^2} - \frac{1}{2} \overline{\left[\frac{\partial u}{\partial z}\right]^2} \right] \tag{5.1.6}$$

$$\beta_{02} = \left[\frac{1}{6}\right] \left[\overline{\left[\frac{\partial v}{\partial z}\right]^2} + \overline{\left[\frac{\partial u}{\partial x}\right]^2} - \left[\frac{3}{2}\right] \overline{\left[\frac{\partial u}{\partial z}\right]^2} \right] \tag{5.1.7}$$

$$\beta_{22} = \left[\frac{1}{2}\right] \left[\overline{\left[\frac{\partial v}{\partial x}\right]^2} + \overline{\left[\frac{\partial u}{\partial z}\right]^2} - \left[\frac{10}{3}\right] \overline{\left[\frac{\partial u}{\partial x}\right]^2} - \left[\frac{1}{3}\right] \overline{\left[\frac{\partial v}{\partial z}\right]^2} \right] \tag{5.1.8}$$

Other correlations can also be used to determine above invariants.

From these, and the relations for axisymmetric turbulence of Appendix I, the dissipation and mean square vorticity can be determined as

$$\epsilon = \nu \left[60\, \alpha_{02} + 20\, \alpha_{22} + 20\, \beta_{02} + 4\beta_{22}\right] \tag{5.1.9}$$

and

$$\overline{\omega_i \omega_i} = 60\, \alpha_{02} + 20\, \alpha_{22} + 20\, \beta_{02} + 4\, \beta_{22} \tag{5.1.10}$$

The dissipation can be expressed directly in terms of the four measured derivative moments by substituting equations (5.1.5)-(5.1.8)

into equation (5.1.9). Alternatively, the appropriate relationships between derivative moments can be substituted directly into the definition of ϵ. From Appendix I, equations (A.I.18)–(A.I.24), it follows that for axisymmetric turbulence,

$$\overline{\left(\frac{\partial u}{\partial y}\right)^2} = \overline{\left(\frac{\partial u}{\partial z}\right)^2} \tag{5.1.11a}$$

$$\overline{\left(\frac{\partial v}{\partial x}\right)^2} = \overline{\left(\frac{\partial w}{\partial x}\right)^2} \tag{5.11.1b}$$

$$\overline{\left(\frac{\partial v}{\partial y}\right)^2} = \overline{\left(\frac{\partial w}{\partial z}\right)^2} \tag{5.1.11c}$$

$$\overline{\left(\frac{\partial v}{\partial z}\right)^2} = \overline{\left(\frac{\partial w}{\partial y}\right)^2} \tag{5.1.11d}$$

$$\overline{\left(\frac{\partial v}{\partial y}\right)^2} = \frac{1}{3}\overline{\left(\frac{\partial u}{\partial x}\right)^2} + \frac{1}{3}\overline{\left(\frac{\partial v}{\partial z}\right)^2} \tag{5.1.11e}$$

$$\overline{\frac{\partial u}{\partial y}\frac{\partial v}{\partial x}} = \overline{\frac{\partial u}{\partial z}\frac{\partial w}{\partial x}} = -\frac{1}{2}\overline{\left(\frac{\partial u}{\partial x}\right)^2} \tag{5.1.11f}$$

$$\overline{\frac{\partial v}{\partial z}\frac{\partial w}{\partial y}} = \frac{1}{6}\overline{\left(\frac{\partial u}{\partial x}\right)^2} - \frac{1}{3}\overline{\left(\frac{\partial v}{\partial z}\right)^2} \tag{5.1.11g}$$

From equation (5.1.1) it follows immediately that

$$\epsilon = \nu\left[\frac{5}{3}\overline{\left(\frac{\partial u}{\partial x}\right)^2} + 2\overline{\left(\frac{\partial u}{\partial z}\right)^2} + 2\overline{\left(\frac{\partial v}{\partial x}\right)^2} + \frac{8}{3}\overline{\left(\frac{\partial v}{\partial z}\right)^2}\right] \tag{5.1.12}$$

For isotropic turbulence,

$$\overline{\left(\partial u/\partial z\right)^2} = \overline{\left(\partial v/\partial x\right)^2} = \overline{\left(\partial v/\partial z\right)^2} = 2\overline{\left(\partial u/\partial x\right)^2},$$

thus the familiar isotropic result $\epsilon = 15\nu\,\overline{(\partial u/\partial x)^2}$ can be recovered.

Two methods were used for derivative determination: 1) the use of time derivatives together with Taylor's hypothesis; and 2) the use of

direct measurements of the difference between the velocity sensed by adjacent sensors. Both parallel wire and AXI-wire configurations were utilized. In the following sections, the effect of spatial averaging for the probe length and separation is analyzed, the use of the axisymmetric relations is verified from the measurements, and the results are presented.

5.2 Evaluation of Wire Length and Probe Separation Effects on the Derivative Measurements

The measurements of spatial derivatives requires special attention to the spatial resolution of the probes. It is well-known that the smallest scales of the turbulence are strongly affected by the line averaging due to the finite wire length (Kovasnay and Uberoi 1953, Wyngaard 1968). However, the filtering imposed on multiple wire probes by the probe separation seems to be less well known. Since a direct measurement of the dissipation is of interest here, the dissipative scales of turbulence are the determining factor in choosing the size of the probe. In this section the finite wire length analysis of Wyngaard (1968) will be reviewed, and the results applied to the experiment reported herein. Then, a new analysis for the spatial filtering arising from the separation of the individual wires of multiple wire probes will be presented. Finally, the combined effects of wire length and separation will be analyzed, and criteria for the direct measurement of velocity derivatives will be established.

5.2.1 Effect of Finite Wire Length

Hot-wires with lengths that are not negligible compared to the scales of interest have a spatial resolution problem. Figure 5.2.1

Figure 5.2.1 Illustration of Measurement of Signals Using Wires with Finite Lengths

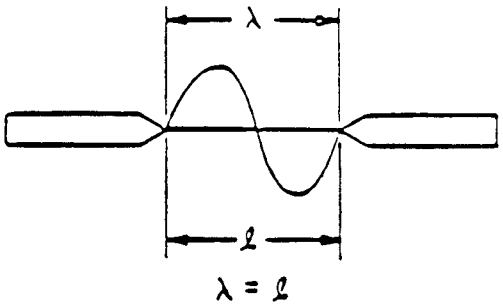

(a) - Non-resolvable Signal

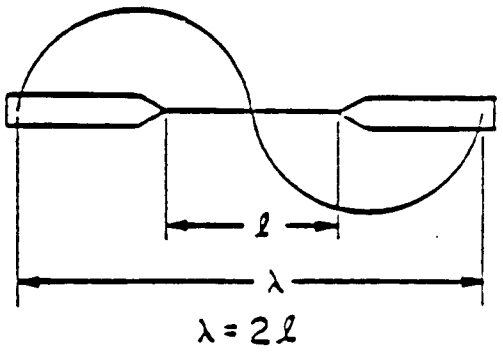

(b) Resolvable Signal

illustrates this problem by showing two wires with the same length responding to two different signals. The signal in Figure 5.2.1a cannot be resolved by the wire because the wire filters the Fourier components whose wavenumber along the wire direction is greater than π/ℓ. The phenomenon is complicated by the fact that turbulence has Fourier components in all three directions.

Wyngaard (1968) investigated the effect of line averaging on measured velocity. For a single wire responding only to the normal component of the velocity field, the velocity is averaged over the length of the wire. This can be represented as

$$\underset{\sim}{u}(\underset{\sim}{x},\ell) = \frac{1}{\ell}\int_{-\ell/2}^{\ell/2} \underset{\sim}{u}(\underset{\sim}{x}+\underset{\sim}{s})\, d\underset{\sim}{s} \tag{5.2.1}$$

where $\underset{\sim}{s}$ is the coordinate along the wire.

For a homogeneous random field, the velocity can be represented as (Lumley 1970):

$$\underset{\sim}{u}(\underset{\sim}{x}) = \int e^{i\underset{\sim}{k}\cdot\underset{\sim}{x}}\, \hat{\underset{\sim}{u}}\,(\underset{\sim}{k})d\underset{\sim}{k} \tag{5.2.2}$$

where $\underset{\sim}{k}$ represents the wavenumber vector and $\underset{\sim}{u}$ is the Fourier transform of the velocity vector. Unless otherwise denoted the integration is from $-\infty$ to $+\infty$.

Inserting equation (5.2.2) into equation (5.2.1)

$$\underset{\sim}{u}(\underset{\sim}{x},\ell) = \frac{1}{\ell}\int e^{i\underset{\sim}{k}\cdot\underset{\sim}{x}} \int_{-\ell/2}^{\ell/2} \underset{\sim}{u}(\underset{\sim}{x}+\underset{\sim}{s})d\underset{\sim}{s}\, d\underset{\sim}{k} \tag{5.2.3}$$

$$= \int \left[\frac{1}{\ell}\int_{-\ell/2}^{\ell/2} e^{i\underset{\sim}{k}\cdot\underset{\sim}{s}} d\underset{\sim}{s}\right] e^{i\underset{\sim}{k}\cdot\underset{\sim}{x}}\, \hat{\underset{\sim}{u}}(\underset{\sim}{k})d\underset{\sim}{k} \tag{5.2.4}$$

Carrying out the integral in brackets yields

$$u(\underset{\sim}{x},\ell) = \int \left[\frac{\sin(\underset{\sim}{k}\cdot\ell/2)}{(\underset{\sim}{k}\cdot\ell/2)}\right] e^{i\underset{\sim}{k}\cdot\underset{\sim}{x}}\, \hat{\underset{\sim}{u}}(\underset{\sim}{k})d\underset{\sim}{k} \tag{5.2.5}$$

The above equation differs from equation (5.2.2) because of the transfer function due to the line averaging. Wyngaard (1968) computed the effect of this line averaging on the measurements of the dissipative scales of turbulence. The results show that the line averaging attenuates the Fourier components with the largest wavenumbers. He concluded that an acceptable spatial resolution of the hot-wire to obtain 98% of the dissipation requires the ratio of the wire length ℓ to the Kolmogorov length scale η to be smaller than 2, i.e. $\ell_w < 2\eta$.

In this work the Kolmogorov scales were estimated to be about 0.16 mm at 70 diameters downstream from the exit of the jet where the experiments were performed. The length of the sensing element of the hot-wire probe was 0.2 mm. This length satisfied Wyngaard's criterion for an acceptable spatial resolution.

5.2.2 Effect of Spatial Difference

In measuring the spatial derivatives, the difference method described in Chapter 2 was used. The spatial difference between the wires acts as a filter which attenuates wavenumber contributions smaller than the spacing between the wires. The effect of this spatial averaging will be analyzed for parallel wires assuming the wires to be a point, i.e, the line averaging is neglected.

The velocity can be represented as before, i.e.,

$$\underset{\sim}{u}(\underset{\sim}{x}) = \int e^{i\underset{\sim}{k}\cdot\underset{\sim}{x}}\, \hat{\underset{\sim}{u}}(\underset{\sim}{k})d\underset{\sim}{k} \qquad (5.2.6)$$

We consider only the streamwise velocity component, $u(\underset{\sim}{x})$, and evaluate it at two different positions $\underset{\sim}{x}_1$ and $\underset{\sim}{x}_2$ which differ only in the y-coordinate, i.e.

$$\underset{\sim}{x}_1 = (x, y_1, z) \qquad (5.2.7)$$

and

$$x_2 = (x, y_2, z) \tag{5.2.8}$$

Suppressing for now the dependence on x and z we can write

$$u(y_1) = \int e^{-i\underset{\sim}{k}\cdot\underset{\sim}{x}_1}\, \hat{u}(\underset{\sim}{k})\, d\underset{\sim}{k} \tag{5.2.9}$$

$$u(y_2) = \int e^{-i\underset{\sim}{k}\cdot\underset{\sim}{x}_2}\, \hat{u}(\underset{\sim}{k})\, d\underset{\sim}{k} \tag{5.2.10}$$

The measured signal of the two wires can be differenced to obtain

$$\left[u(y_1) - u(y_2)\right] = \int d\underset{\sim}{k}\, \hat{u}(\underset{\sim}{k})\left[e^{-i\underset{\sim}{k}\cdot\underset{\sim}{x}_1} - e^{-i\underset{\sim}{k}\cdot\underset{\sim}{x}_2}\right] \tag{5.2.11}$$

It follows that the mean squared velocity difference is given by,

$$\overline{\left[u(y_1) - u(y_2)\right]^2} = \int d\underset{\sim}{k} d\underset{\sim}{k}'\, \overline{\hat{u}(\underset{\sim}{k})\hat{u}^*(\underset{\sim}{k})}\left[e^{-i\underset{\sim}{k}\cdot\underset{\sim}{x}_1} - e^{-i\underset{\sim}{k}'\cdot\underset{\sim}{x}_2}\right]$$

$$\left[e^{+i\underset{\sim}{k}\cdot\underset{\sim}{x}_1} - e^{+i\underset{\sim}{k}'\cdot\underset{\sim}{x}_2}\right] \tag{5.2.12}$$

For a homogeneous random field (Monin and Yaglom 1971)

$$\overline{\hat{u}_i(\underset{\sim}{k})\hat{u}_j^*(\underset{\sim}{k}')}\, d\underset{\sim}{k} d\underset{\sim}{k}' = F_{ij}(\underset{\sim}{k})\, \delta(\underset{\sim}{k}' - \underset{\sim}{k})\, d\underset{\sim}{k} d\underset{\sim}{k}' \tag{5.2.13}$$

where F_{ij} is the three-dimensional velocity spectrum. Therefore

$$\overline{\left[u(y_1) - u(y_2)\right]^2} = \int d\underset{\sim}{k}\, F_{11}(\underset{\sim}{k})\, \left[2 - e^{i\underset{\sim}{k}\cdot(\underset{\sim}{x}_1 - \underset{\sim}{x}_2)}\right.$$

$$\left. - e^{i\underset{\sim}{k}\cdot(\underset{\sim}{x}_1 - \underset{\sim}{x}_2)}\right]$$

$$= \int d\underset{\sim}{k}\, F_{11}(\underset{\sim}{k})\, 2\left[1 - \cos\, \underset{\sim}{k}\cdot(\underset{\sim}{x}_1 - \underset{\sim}{x}_2)\right] \tag{5.2.14}$$

If the wires are separated by a distance Δ in the 2-direction only, the measured difference spectra for a homogeneous field can be obtained in terms of the one dimensional spectra as:

$$F_\Delta(k_1) = \int\!\!\int_{-\infty}^{\infty} 2\left[1 - \cos\, k_2\Delta\right]\, F_{11}(k)\, dk_1 dk_3 \tag{5.2.15}$$

Figure 5.2.2a Comparison of Leading Terms for the Difference Spectra

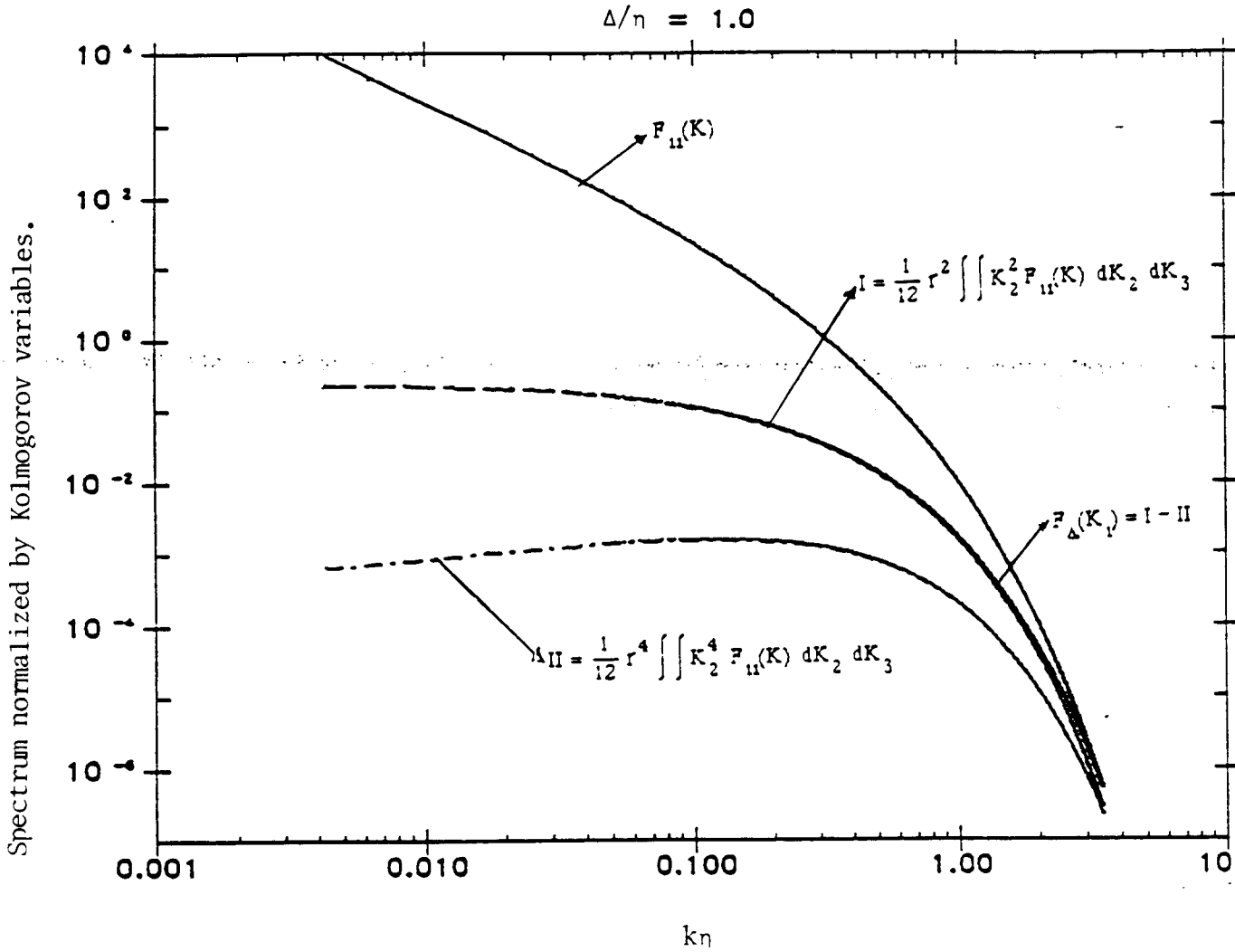

Figure 5.2.2b Comparison of Leading Terms for the Difference Spectra

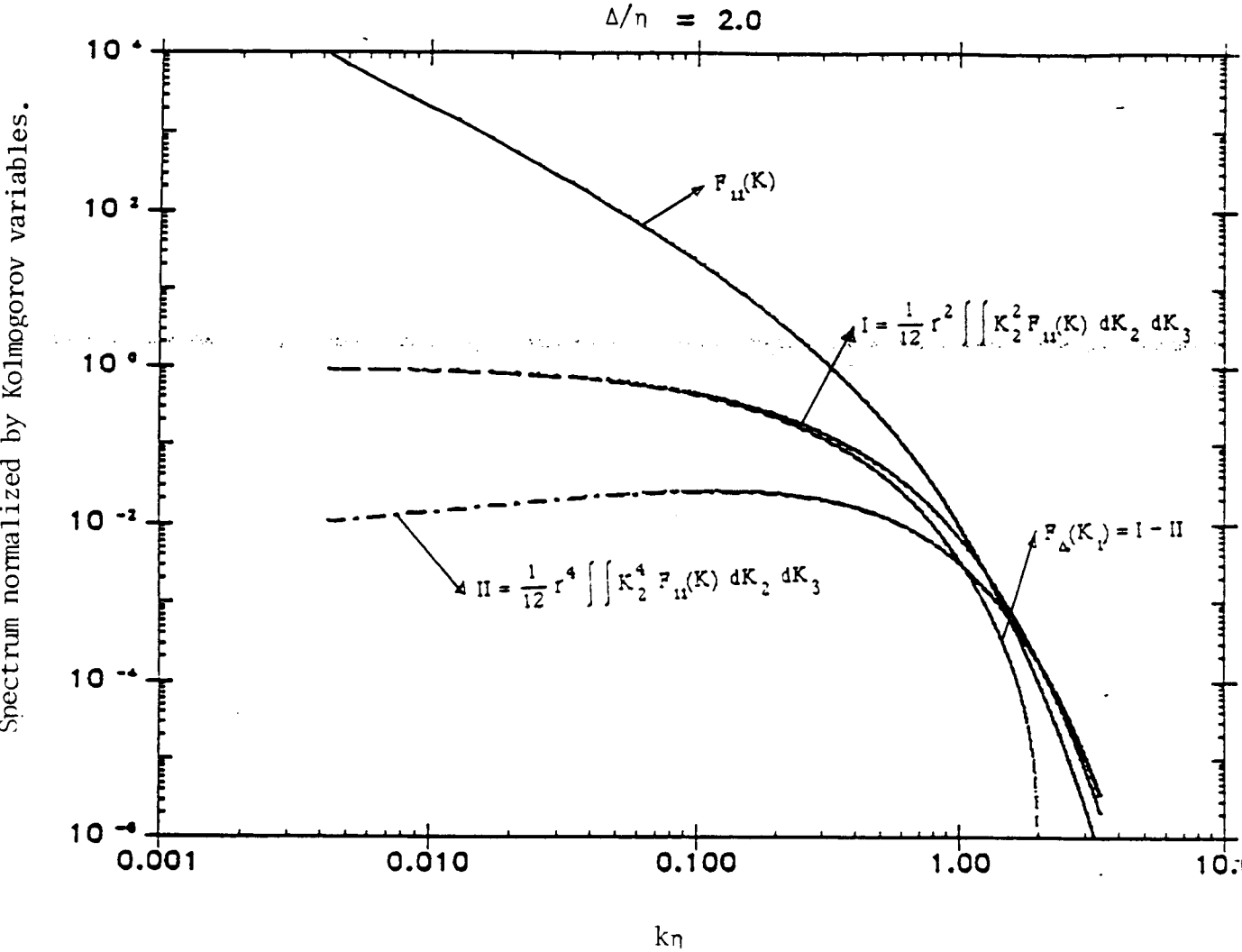

Figure 5.2 2c Comparison of Leading Terms for the Difference Spectra

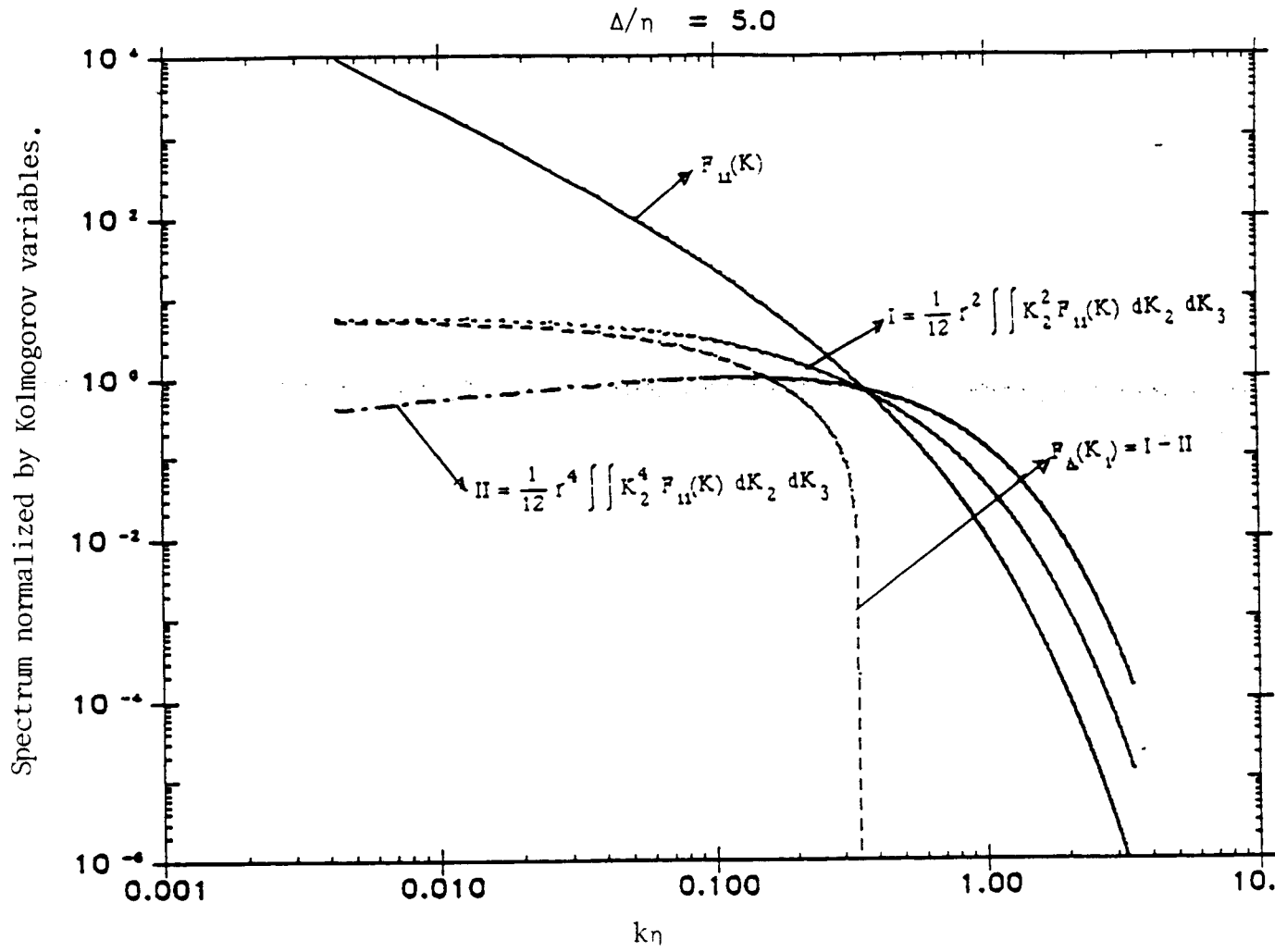

The cosine term in the above equation is a transfer function due to the separation between the two wires. Thus the separation acts as a low pass filter on a measured difference spectra. Writing the cosine term is a Taylor series expansion for small $k_2\Delta$ yields,

$$F_\Delta(k_1) = \Delta^2\left[\int\int_{-\infty}^{\infty} k^2{}_2 F_{11}(k)dk_2dk_3\right] - \Delta^4\left[\int\int_{-\infty}^{\infty} k^4{}_2 F_{11}(k)dk_2dk_3\right] \tag{5.2.16}$$

For an ideal probe the higher order terms would be negligible compared to the first term in equation (5.2.13) which can be seen to correspond to the mean square derivative in the 2-direction.

Calculations were carried out to evaluate the effect of the transfer function on the measured difference spectra. Figure 5.2.2 shows the measured difference spectrum compared with one-dimensional spectrum for three cases: Δ/η = 1,2 and 5. The one-dimensional spectrum was computed using Pao's model of the three dimensional velocity spectrum function (Pao 1965). The one-dimensional spectrum, the first and second terms in equation (5.2.6) and the difference of these two terms for several different spacings are shown in Figure 5.2.2. The difference spectrum progressively deviates from the derivative spectrum as the spacing between the wires is increased. For $\Delta = \eta$ the resulting measured difference spectra shows no effect of filtering. However a difference of 5η shows a large effect at wavenumbers above $k\eta$ of 0.2.

To show the effect of this spectral contamination on the measured derivative, the spectra were integrated to obtain the mean square derivative as a function of the spacing between the wires using,

$$\overline{\left[\frac{\partial u}{\partial y}\right]_m^2} = \int_{-\infty}^{\infty} F_\Delta(k_1)dk_1 \qquad (5.2.17)$$

The subscript m denotes the calculation for the measured quantity. Figure 5.2.3 shows results for the calculations comparing the measured streamwise derivative normalized by the derivative with the transfer function equal to unity. As shown in the plot, a wire spacing of $\Delta=\eta$ (which is what was used in this work) gives an accuracy of 95%.

5.3 Derivative Measurements

Two of the four experiments performed in this work were carried out with a parallel wire and the other two with the three wire AXI-probe described in Chapter 2. The AXI-probe provides all the information obtained with the parallel wire in addition to several transverse derivatives of the radial and azimuthal velocity components, as summarized in Table 5.1. Experiments 1 and 2 were performed with the parallel wires as shown on Figures 5.3.1a and 5.3.1b respectively, and give results that were used for verifications purposes. Experiment 1 was performed to obtain $\overline{(\partial u/\partial x)^2}$ and $\overline{(\partial u/\partial y)^2}$. Figure 5.3.2 shows the results from experiment 1. In experiment 2 the probe was rotated by 90^o as shown in Figure 5.3.1b. The term $\overline{(\partial u/\partial z)^2}$ shown on Figure 5.3.3 was obtained from experiment 2. Also in these experiments the term $\overline{(\partial u/\partial x)^2}$ was calculated from measured temporal derivatives by using Taylor's hypothesis as described in Appendix II.

Experiment 3 was performed with the triple wire probe oriented as shown on Figure 5.3.1c. The terms measured in this experiment were $\overline{(\partial u/\partial x)^2}$ and $\overline{(\partial v/\partial x)^2}$ which were computed from their corresponding temporal derivatives and the two terms $\overline{(\partial v/\partial z)^2}$ and $\overline{(\partial u/\partial z)^2}$ which were obtained by measuring u and v at two points which are in close

Figure 5.2.3 Effect of Wire Spacing on Measured Velocity Derivative

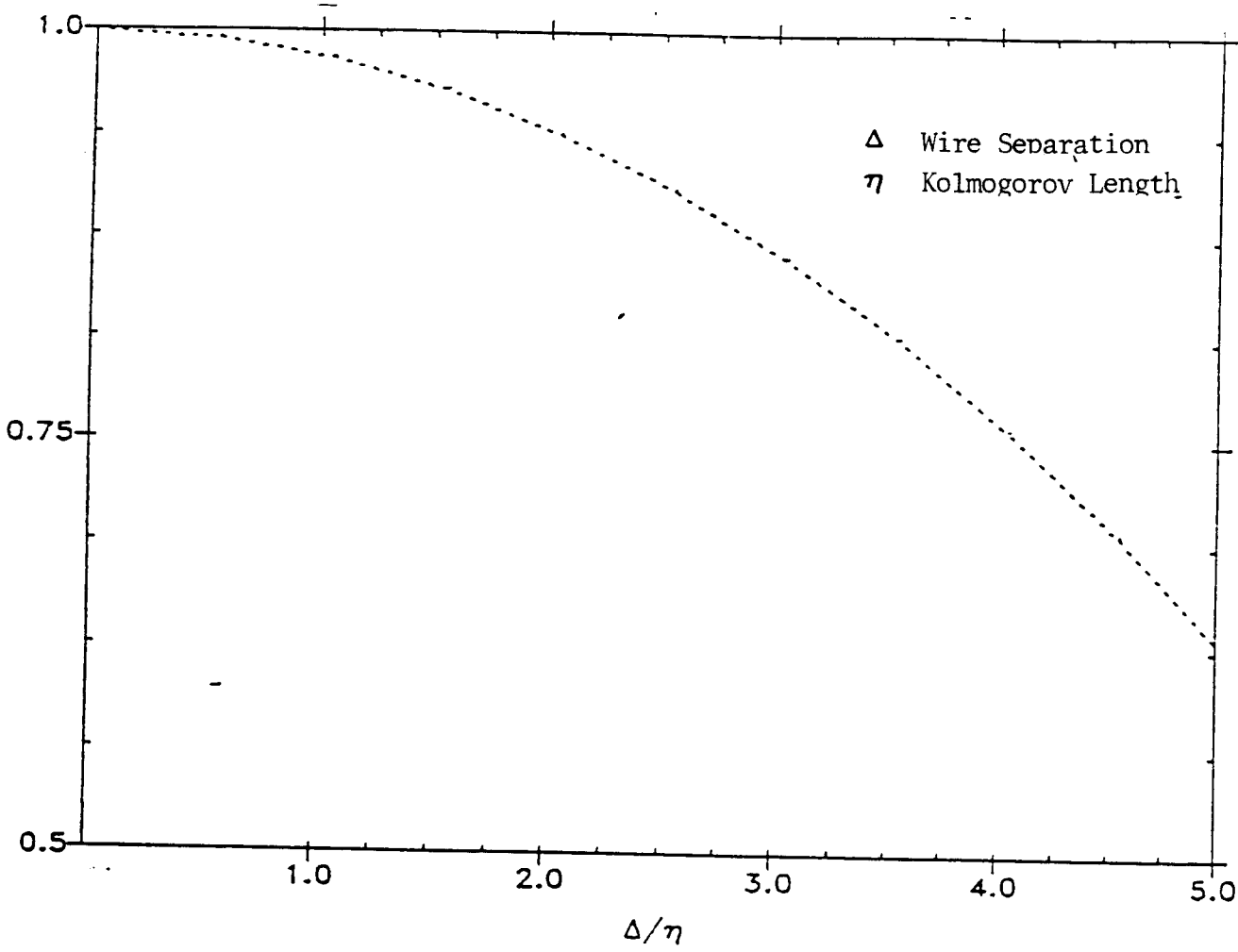

Figure 5.3.1 Orientation of Multiple Wire Probes for Different Experiments

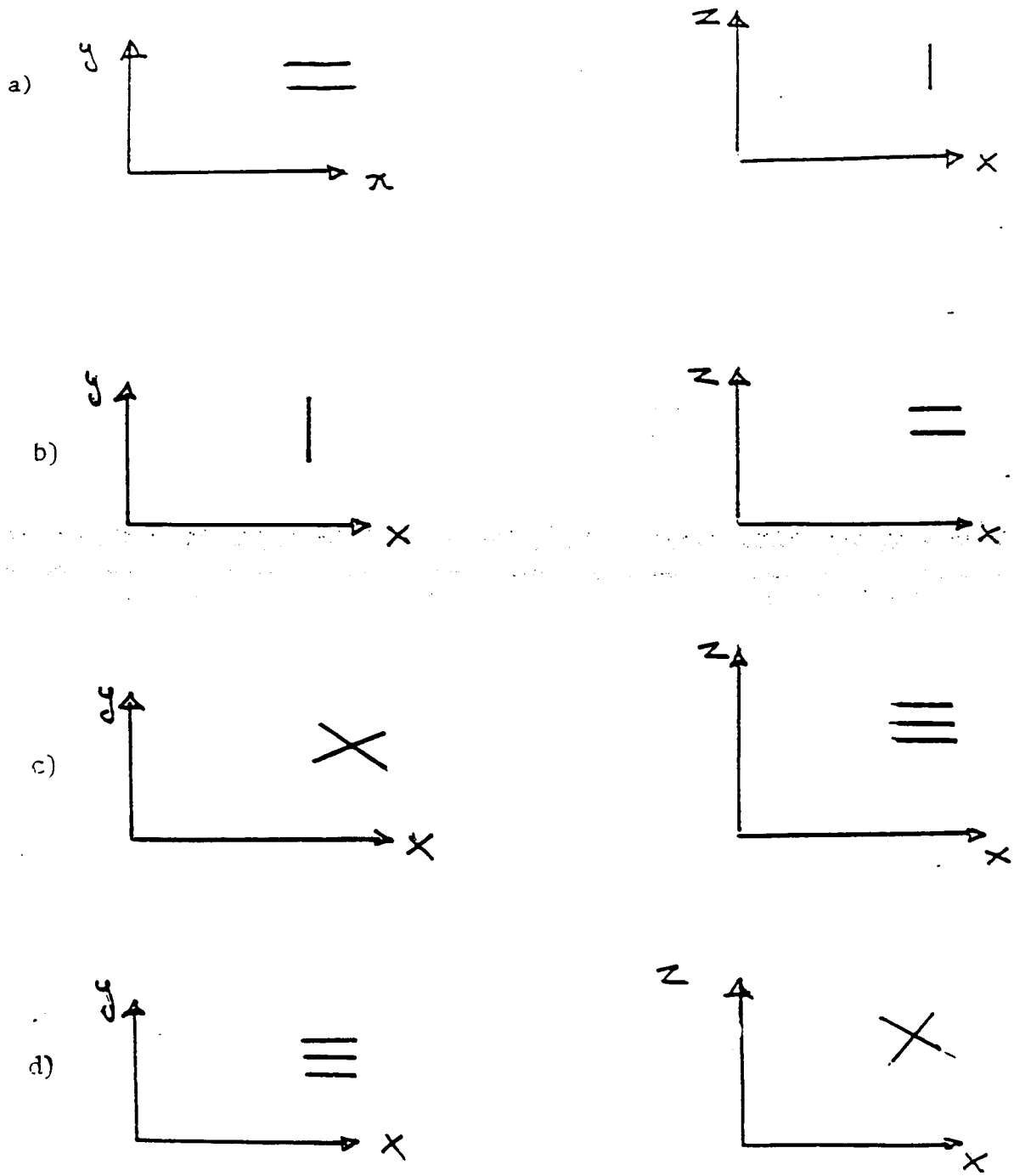

Figure 5.3.2 Radial Variation of $\overline{(\partial u/\partial x)^2}$ and $\overline{(\partial u/\partial y)^2}$ from Parallel Wire.

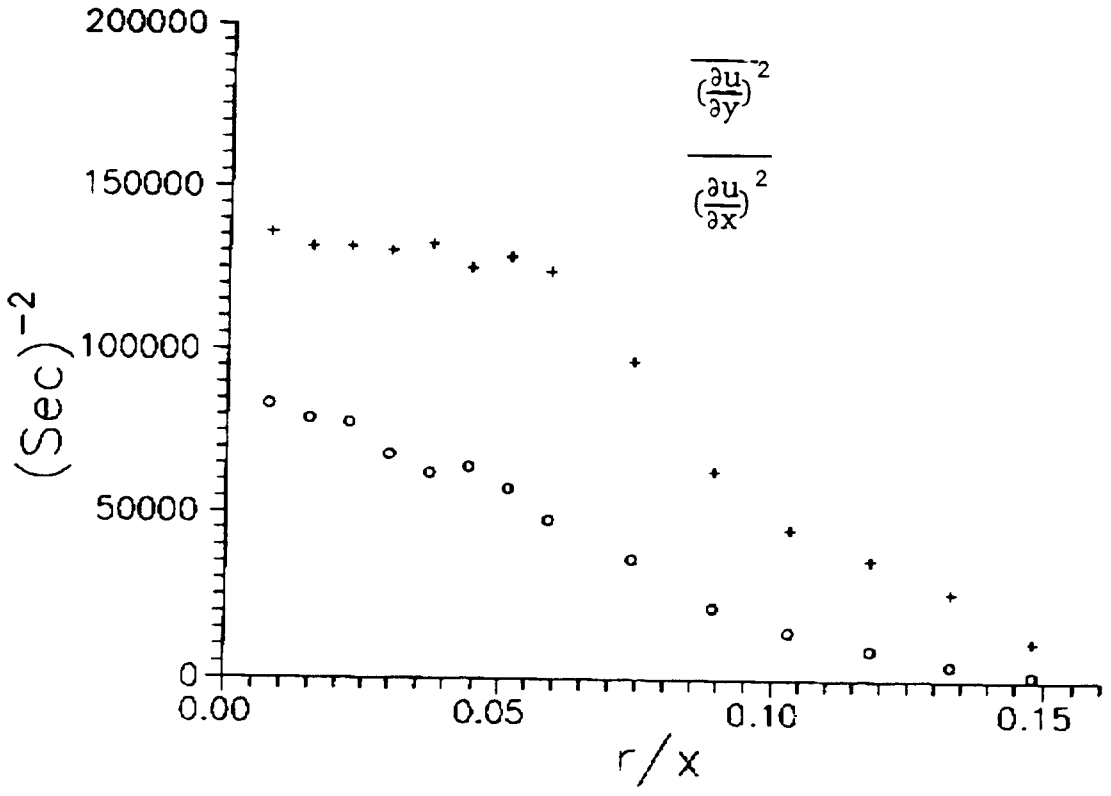

Figure 5.3.3 Radial Variation of $\overline{(\partial u/\partial x)^2}$ and $\overline{(\partial u/\partial z)^2}$ from Parallel Wire

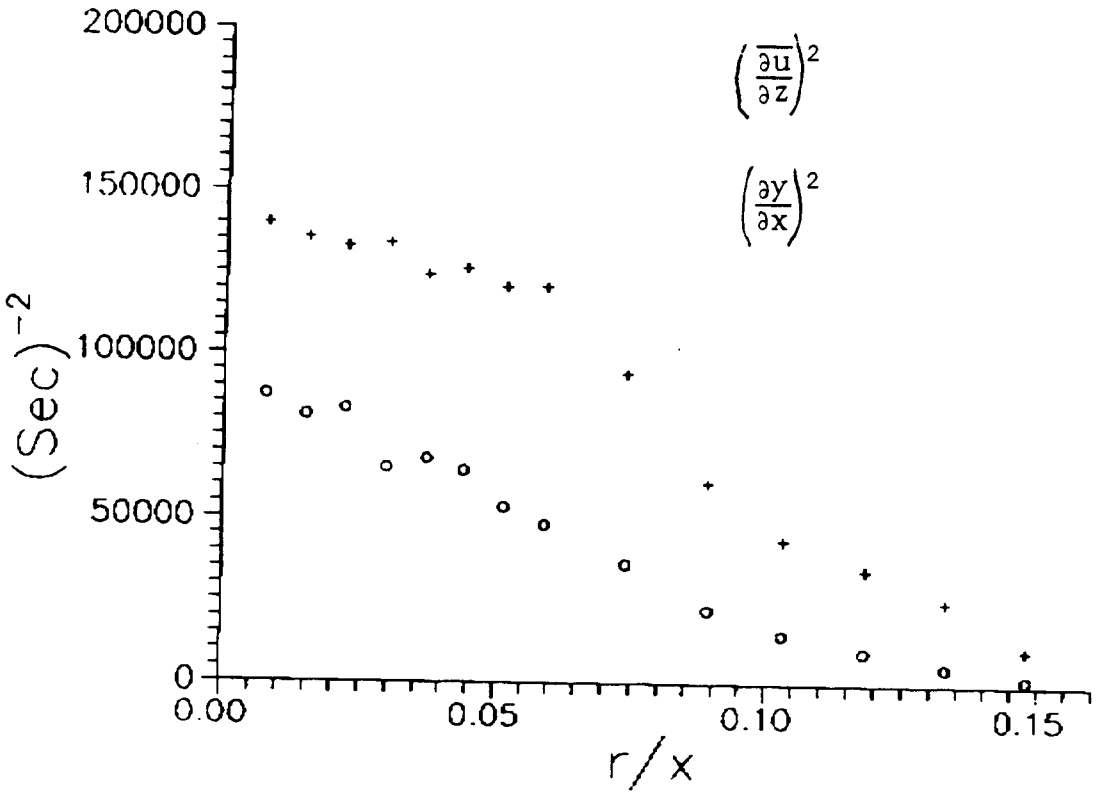

proximity. These terms are shown on Figures 5.3.4 and 5.3.5 respectively.

Experiment 4 was also performed with the triple wire probe but with it rotated 90^0 from the orientation of experiment 3 as shown on Figure 5.3.1d. The terms $\overline{(\partial u/\partial x)^2}$, $\overline{(\partial w/\partial x)^2}$, $\overline{(\partial w/\partial y)^2}$ and $\overline{(\partial u/\partial y)^2}$ were measured in this experiment and the results are shown on Figures 5.3.6 and 5.3.7.

The terms $\overline{(\partial u/\partial z)^2}$ and $\overline{(\partial u/\partial y)^2}$ should be equal for the locally axisymmetric flow be discussed in Appendix I. The results from the three wire AXI-probe for these two derivatives show a discrepency of about 10%. This discrepancy is attributed to an approximately 10% uncertainty in measuring the spacing between the wires. Unfortunately, this was realized after the completion of the experiments, so this explanation could not be verified.

TABLE 5.1

Experiment	Probe Used	Derivative Terms Measured
1	Parallel Wire	$\overline{\left[\frac{\partial u}{\partial x}\right]^2}$, $\overline{\left[\frac{\partial u}{\partial y}\right]^2}$
2	Parallel Wire	$\overline{\left[\frac{\partial u}{\partial x}\right]^2}$, $\overline{\left[\frac{\partial u}{\partial z}\right]^2}$
3	Triple Wire AXI-Probe	$\overline{\left[\frac{\partial u}{\partial x}\right]^2}$, $\overline{\left[\frac{\partial v}{\partial x}\right]^2}$, $\overline{\left[\frac{\partial u}{\partial z}\right]^2}$, $\overline{\left[\frac{\partial v}{\partial z}\right]^2}$
4	Triple Wire AXI-Probe	$\overline{\left[\frac{\partial u}{\partial x}\right]^2}$, $\overline{\left[\frac{\partial w}{\partial x}\right]^2}$, $\overline{\left[\frac{\partial u}{\partial y}\right]^2}$, $\overline{\left[\frac{\partial w}{\partial y}\right]^2}$

Figure 5.3.8 shows comparison of these terms between the results from the parallel probe and the AXI-probe. The parallel wire results have certain advantages because the spatial resolution is

Figure 5.3.4 Radial Variation of $\overline{(\partial u/\partial x)^2}$ and $\overline{(\partial v/\partial x)^2}$, AXI-probe.

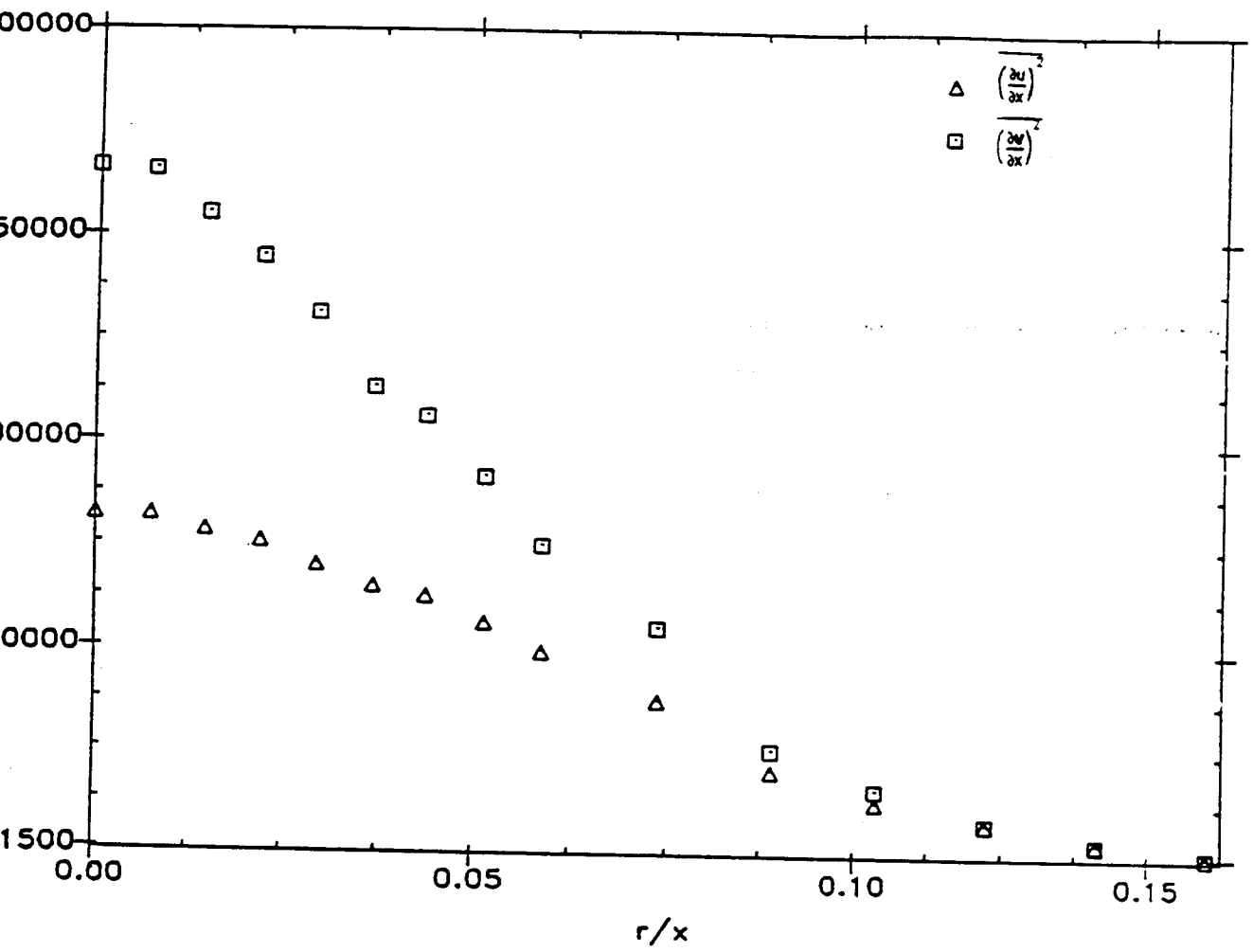

Figure 5.3.5 Radial Variation of $\overline{(\partial u/\partial z)^2}$ and $\overline{(\partial v/\partial z)^2}$, AXI-Probe

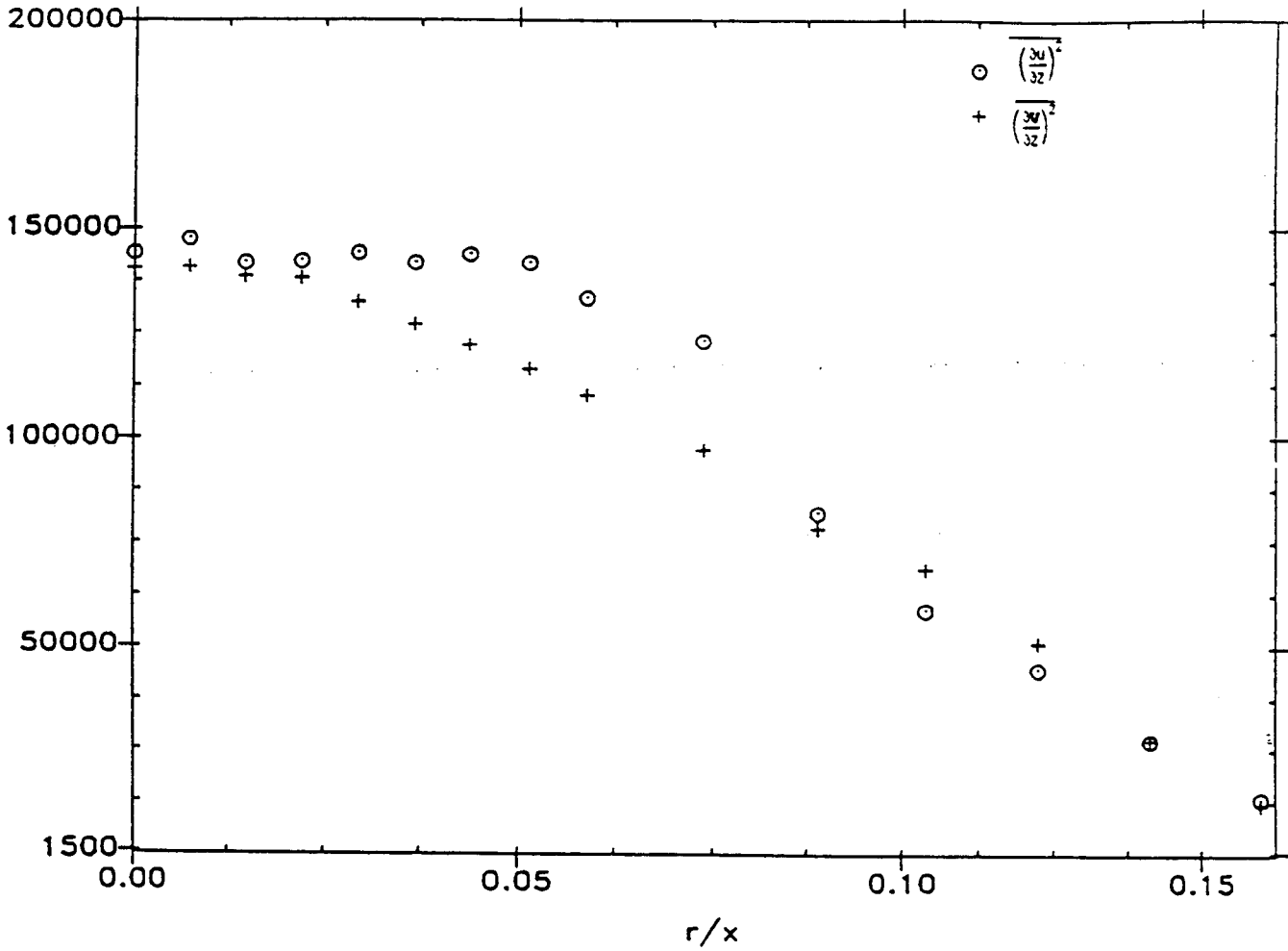

Figure 5.3.6 Radial Variation of $\overline{(\partial u/\partial x)^2}$ and $\overline{(\partial w/\partial x)^2}$, AXI-probe.

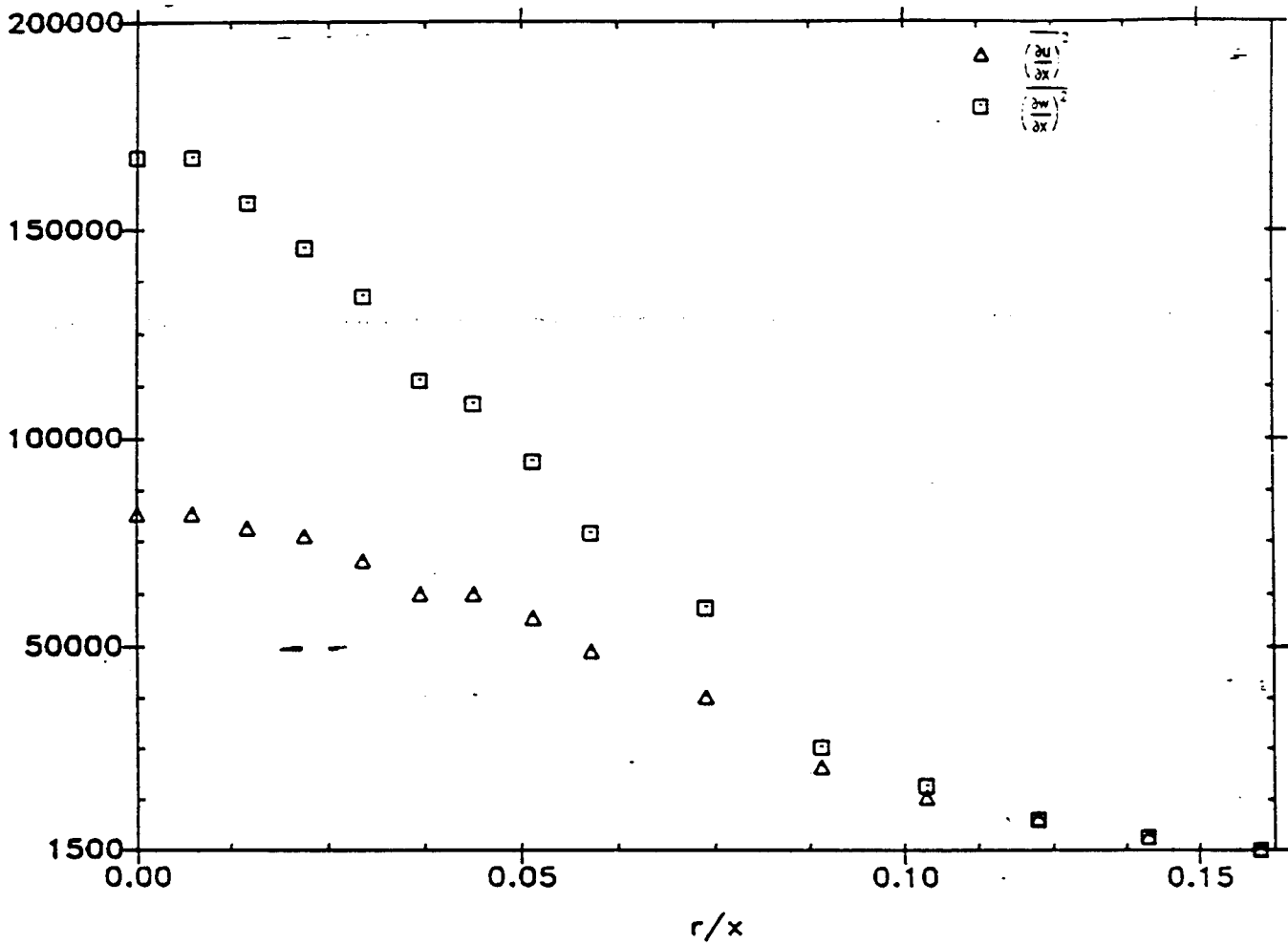

Figure 5.3.7 Radial Variation of $\overline{(\partial u/\partial y)^2}$ and $\overline{(\partial w/\partial y)^2}$, AXI-probe.

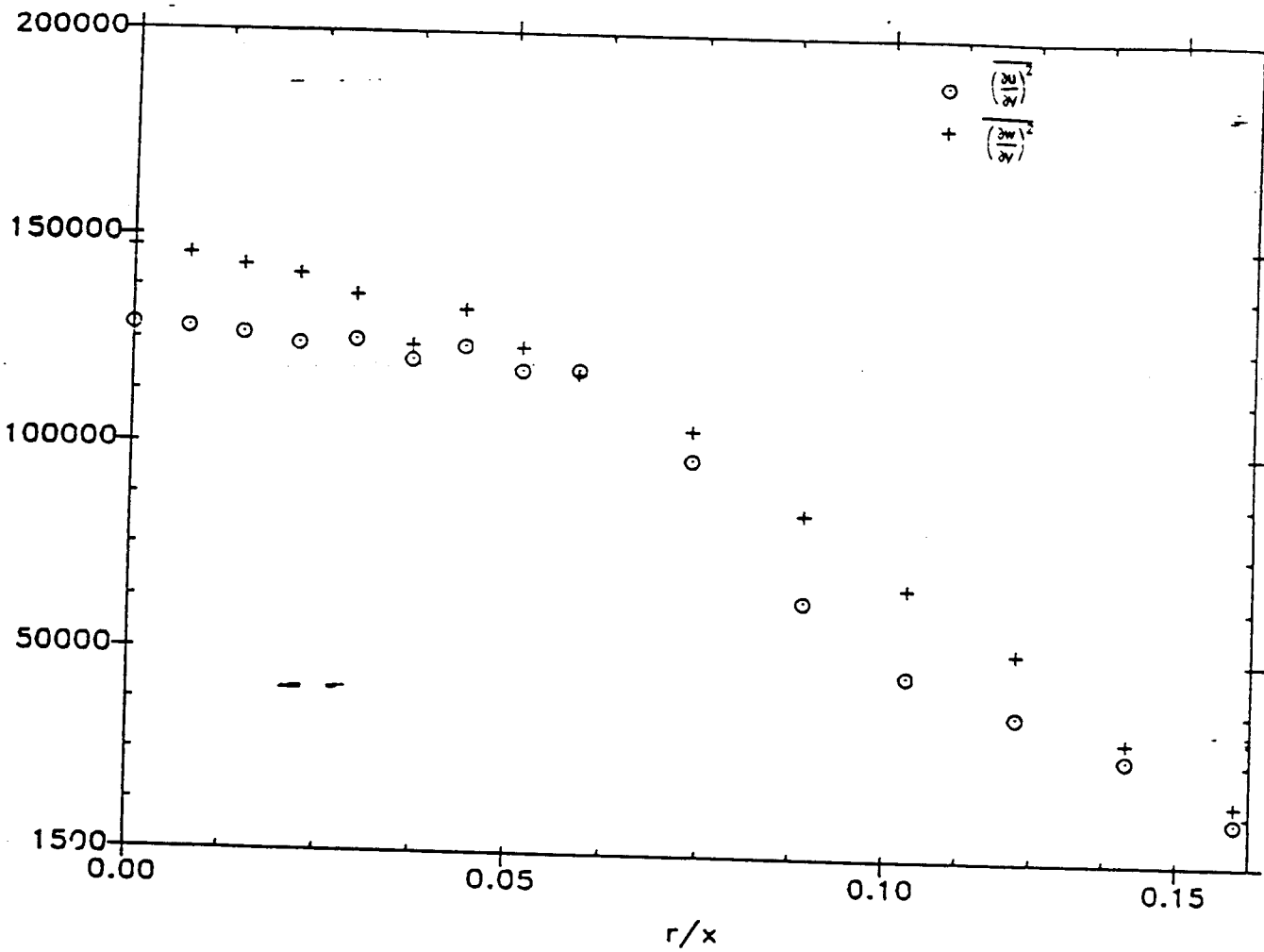

Figure 5.3.8 Comparison of $\overline{(\partial u/\partial z)^2}$ and $\overline{(\partial u/\partial y)^2}$

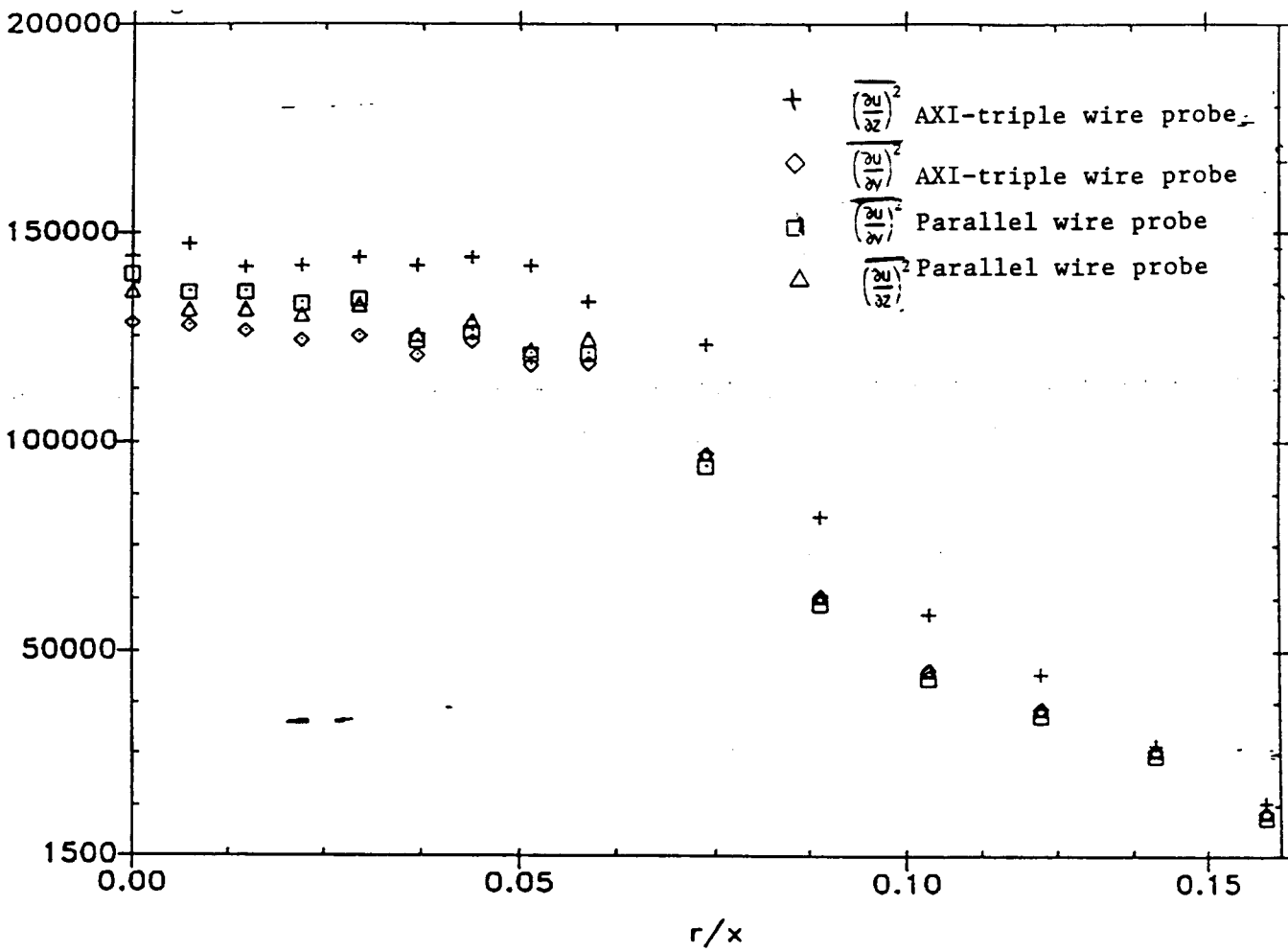

better, the measuring volume is smaller, and the calibration is easier since angle calibration is not necessary. This figure shows that the triple wire measurement of $\overline{(\partial u/\partial y)^2}$ has been slightly under-estimated and that of $\overline{(\partial u/\partial z)^2}$ over-estimated, at least when compared to the parallel wire results. Again, these are probably attributable to the 10% uncertainty in the wire spacing which results in a 20% uncertainty in the mean square derivative estimation. Thus, to within the accuracy of the measurements these terms satisfy the axisymmetric relationship.

In Appendix I it is argued that a large number of the velocity derivative correlations are zero in an axisymmetric flow. These correlations together with the other relations provide a basis for the verification of local axisymmetry. Four of these correlations that have been measured are:

$$\frac{\overline{\left[\frac{\partial v}{\partial x}\right]\left[\frac{\partial v}{\partial z}\right]}}{\sqrt{\left[\frac{\partial v}{\partial x}\right]^2}\sqrt{\left[\frac{\partial v}{\partial z}\right]^2}} \; ; \; \frac{\overline{\left[\frac{\partial v}{\partial x}\right]\left[\frac{\partial u}{\partial z}\right]}}{\sqrt{\left[\frac{\partial v}{\partial x}\right]^2}\sqrt{\left[\frac{\partial u}{\partial z}\right]^2}}$$

$$\frac{\overline{\left[\frac{\partial u}{\partial x}\right]\left[\frac{\partial u}{\partial z}\right]}}{\sqrt{\left[\frac{\partial u}{\partial x}\right]^2}\sqrt{\left[\frac{\partial u}{\partial z}\right]^2}} \; ; \; \frac{\overline{\left[\frac{\partial w}{\partial x}\right]\left[\frac{\partial w}{\partial y}\right]}}{\sqrt{\left[\frac{\partial w}{\partial x}\right]^2}\sqrt{\left[\frac{\partial w}{\partial y}\right]^2}}$$

These correlations are shown on Figures 5.3.9a and 5.3.9b and they are less than 5% over most of the jet, verifying that at least these aspects of local axisymmetry are satisfied to within the accuracy of the measurements.

Axisymmetry also requires that the terms $\overline{(\partial w/\partial y)^2}$ be equal to $\overline{(\partial v/\partial z)^2}$ and that $\overline{(\partial v/\partial x)^2}$ to be equal to $\overline{(\partial w/\partial x)^2}$, that is,

Figure 5.3.9a Radial Variation of Correlation Coefficient of $\partial w/\partial x$ and $\partial w/\partial y$.

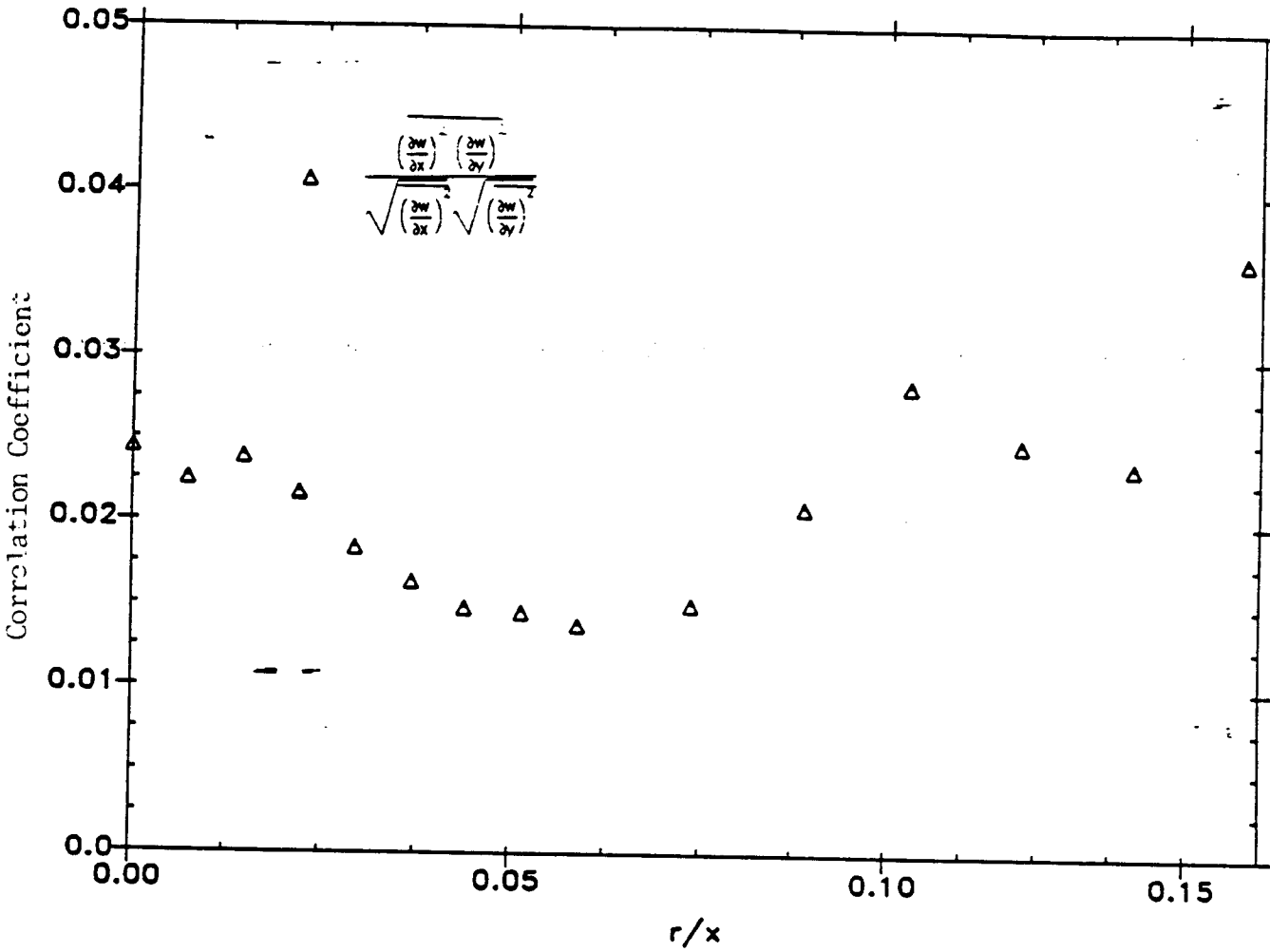

Figure 5.3.9b Radial Variation of Correlation Coefficients of $\partial u/\partial x$ and $\partial u/\partial z$, $\partial v/\partial x$ and $\partial u/\partial z$, and $\partial v/\partial x$ and $\partial v/\partial z$.

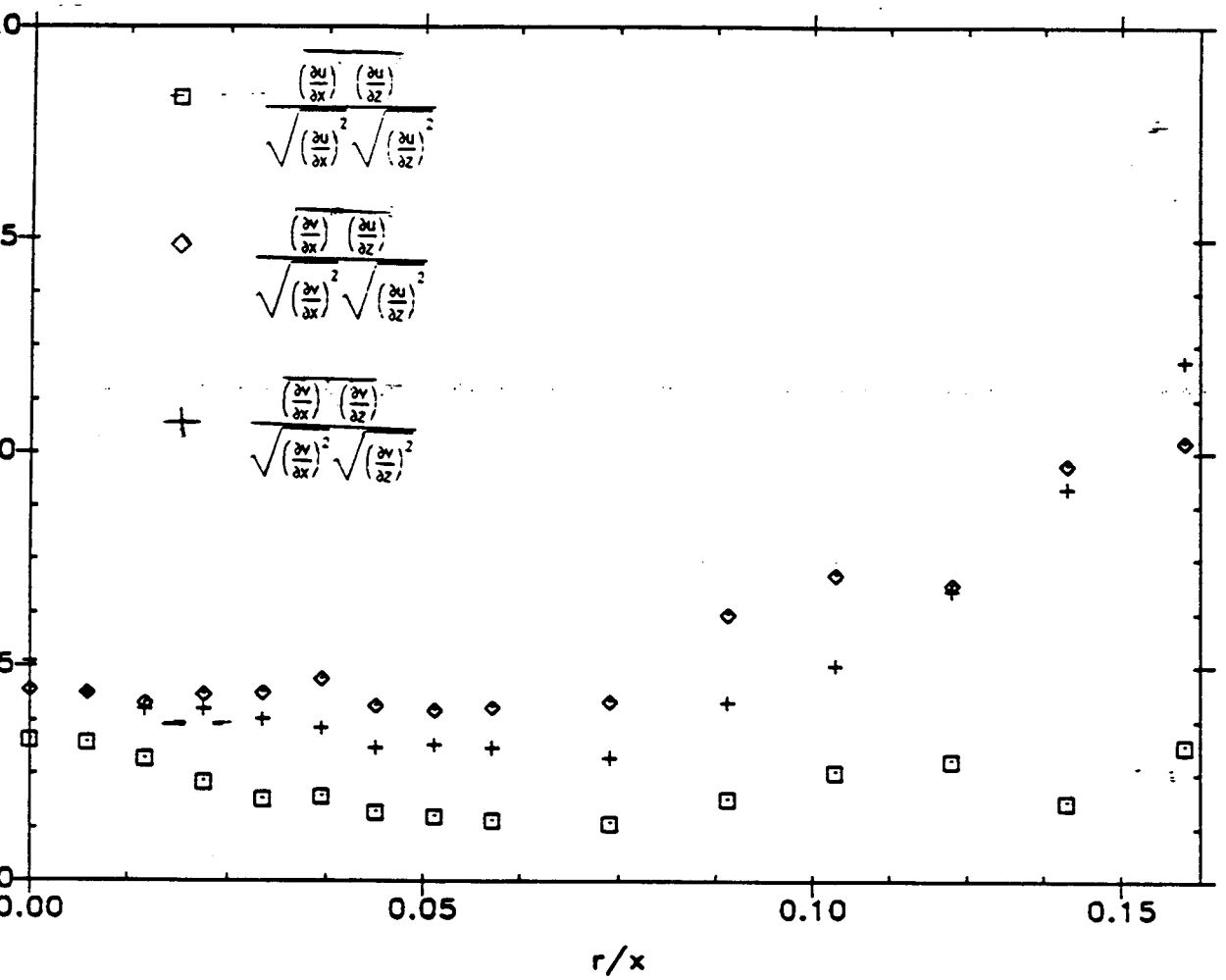

$$\overline{\left[\frac{\partial w}{\partial y}\right]^2} = \overline{\left[\frac{\partial v}{\partial z}\right]^2}$$

$$\overline{\left[\frac{\partial v}{\partial x}\right]^2} = \overline{\left[\frac{\partial w}{\partial x}\right]^2}$$

These terms are shown on Figures 5.3.10 and 5.3.11, and the results show that the flow appears to be truly axisymmetric in the small scales.

The full implications of this local axisymmetry is presented in Appendix I. The most significant consequence of these results for the present experiment is that the entire set of derivative correlations can be represented in terms of the four invariants which in turn, depend only on measureable quantities. Thus the determination of the dissipation and mean square fluctuating vorticity is limited only by the measurement accuracy of the invariants.

5.4 Calculation of Dissipation and Mean-Square Vorticity

Using the results obtained from Appendix I (A.I.27) the dissipation of turbulence can be directly calculated by using the four invariants α_{02}, α_{22}, β_{02} and β_{22}. Since these invariants can be calculated in a multitude of combinations of the velocity derivative correlations, a set providing the best results were chosen. The four independent terms chosen to calculate the dissipation are, $\overline{(\partial u/\partial x)^2}$ from experiment 1, $\overline{(\partial u/\partial y)^2}$ from experiment 2, $\overline{(\partial v/\partial x)^2}$ from experiment 3 and $\overline{(\partial w/\partial y)^2}$ from experiment 4. Thus,

Figure 5.3.10 Mean Square Derivatives of Velocity Fluctuations

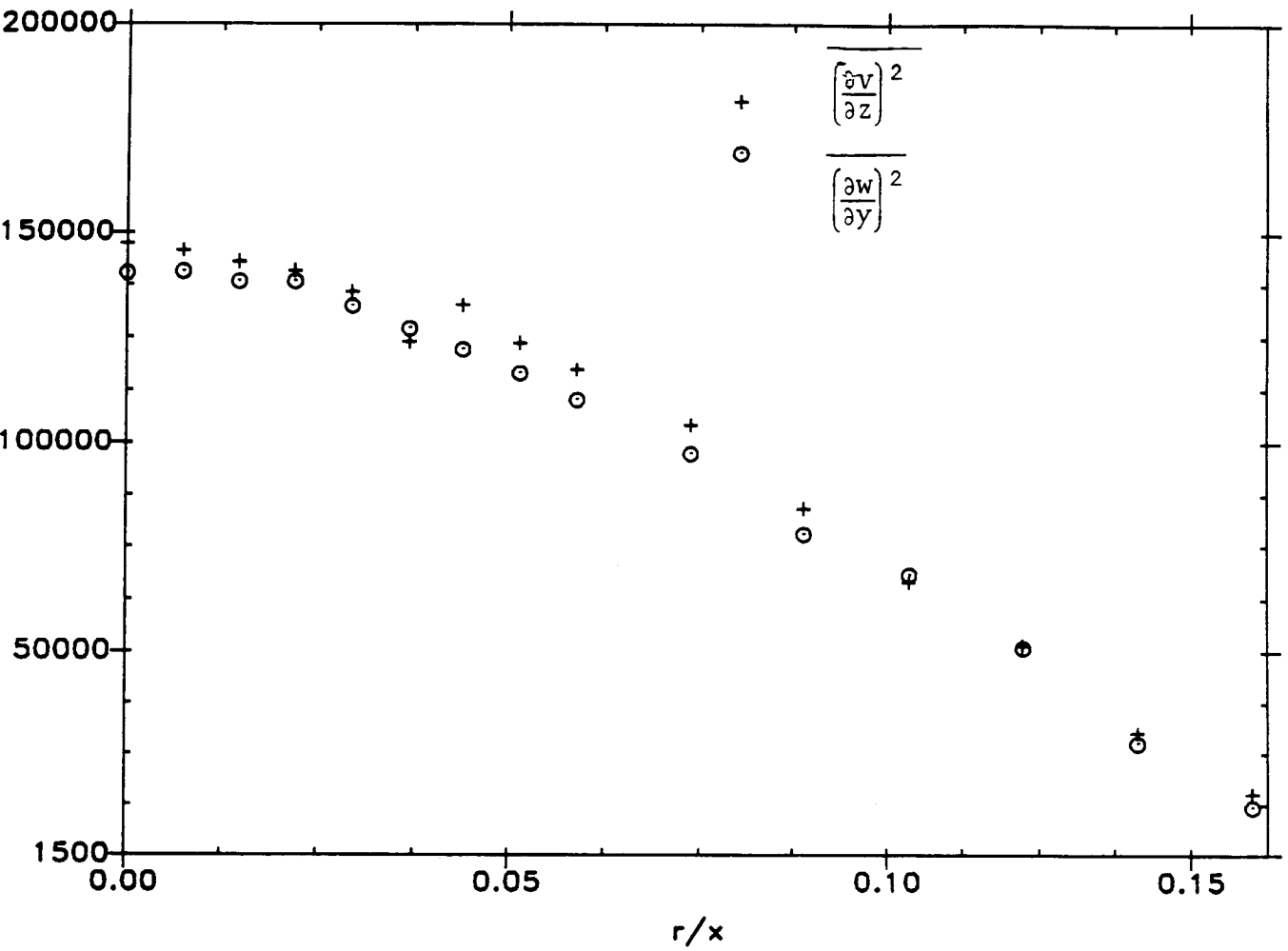

Figure 5.3.11 Mean Square Derivatives of Velocity Fluctuations

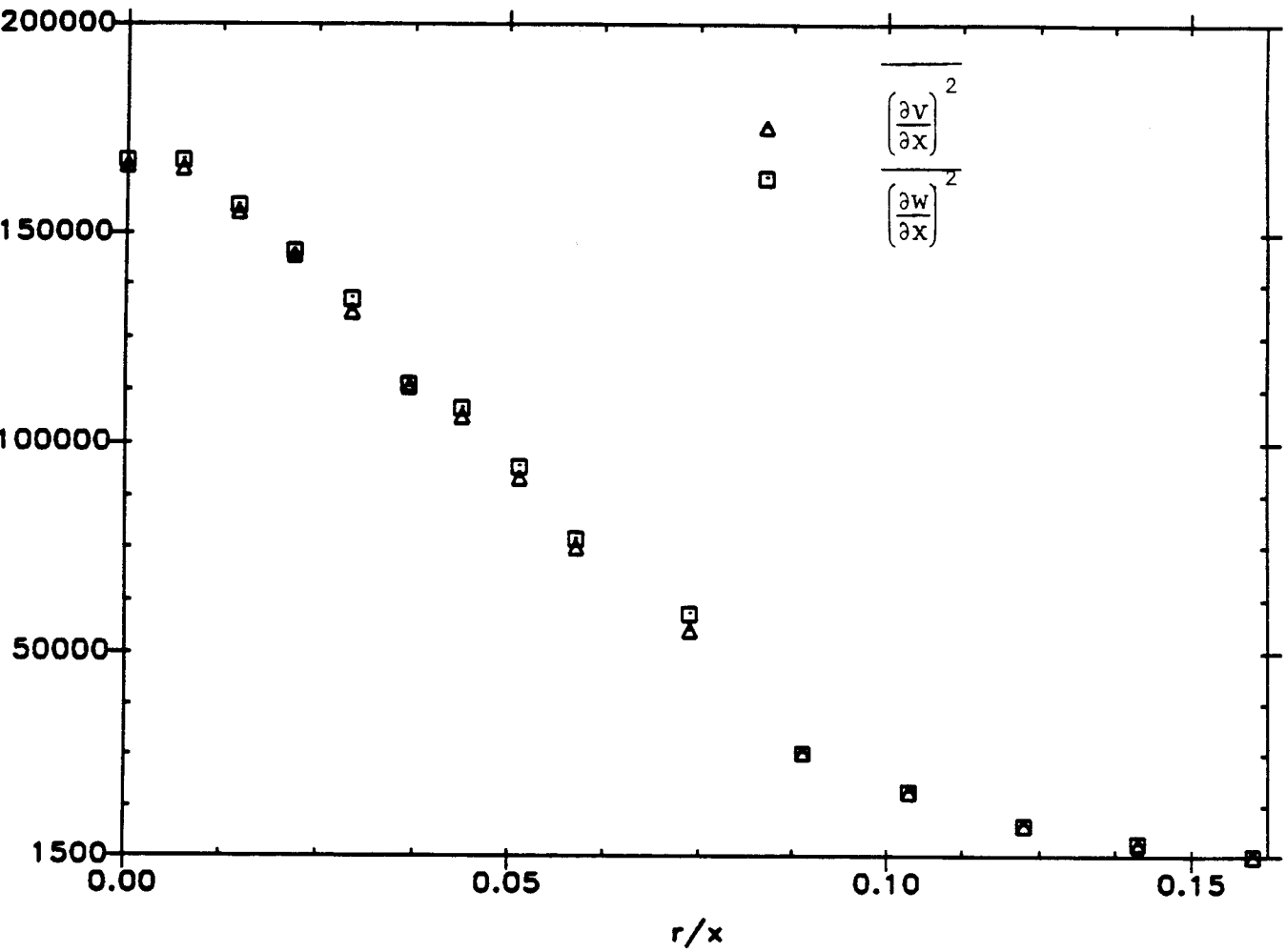

$$\alpha_{02} = \left[\frac{1}{8}\right] \overline{\left[\frac{\partial u}{\partial y}\right]^2} \tag{5.4.1}$$

$$\alpha_{22} = \left[\frac{1}{4}\right] \left[\overline{\left[\frac{\partial u}{\partial x}\right]^2} - \frac{1}{2} \overline{\left[\frac{\partial u}{\partial y}\right]^2} \right] \tag{5.4.2}$$

$$\beta_{02} = \left[\frac{1}{6}\right] \left[\overline{\left[\frac{\partial v}{\partial z}\right]^2} + \overline{\left[\frac{\partial u}{\partial x}\right]^2} - \left[\frac{3}{2}\right] \overline{\left[\frac{\partial u}{\partial y}\right]^2} \right] \tag{5.4.3}$$

$$\beta_{22} = \left[\frac{1}{2}\right] \left[\overline{\left[\frac{\partial v}{\partial x}\right]^2} + \overline{\left[\frac{\partial u}{\partial y}\right]^2} - \left[\frac{10}{3}\right] \overline{\left[\frac{\partial u}{\partial x}\right]^2} - \left[\frac{1}{3}\right] \overline{\left[\frac{\partial w}{\partial y}\right]^2} \right] \tag{5.4.4}$$

The results of the four invariants are shown on Figure 5.4.1. As shown on this figure α_{22}, β_{02} and β_{22} are much smaller than α_{02} near the centerline. This is expected since the jet is closer to isotropic near the centerline, and $\alpha_{22}=\beta_{02}=\beta_{22}=0$ for isotropy.

Figure 5.4.2 shows the comparison between ϵ_{axs} obtained with the assumption of local axisymmetry and ϵ_{iso}, calculated from $\overline{(\partial u/\partial x)^2}$ and $\overline{(\partial u/\partial y)^2}$ assuming local isotropy. For the jet, the isotropic results differ from the dissipation by about 25% at the centerline and by about 40% near the point of maximum mean shear ($r/x = 0.1$).

The mean square vorticity profile normalized by the centerline value is shown on Figure 5.4.3. The equation (5.1.2) was used to calculate for the vorticity and the only assumption made was that of local axisymmetry. Note that the mean square vorticity and mean square strain rates differ by only a factor of 2 for axisymmetric turbulence are equal, so Figure 5.4.3 is simply a scaled version of the dissipation profile of Figure 5.4.2.

Figure 5.4.1 Invariants of the Axisymmetric Jet

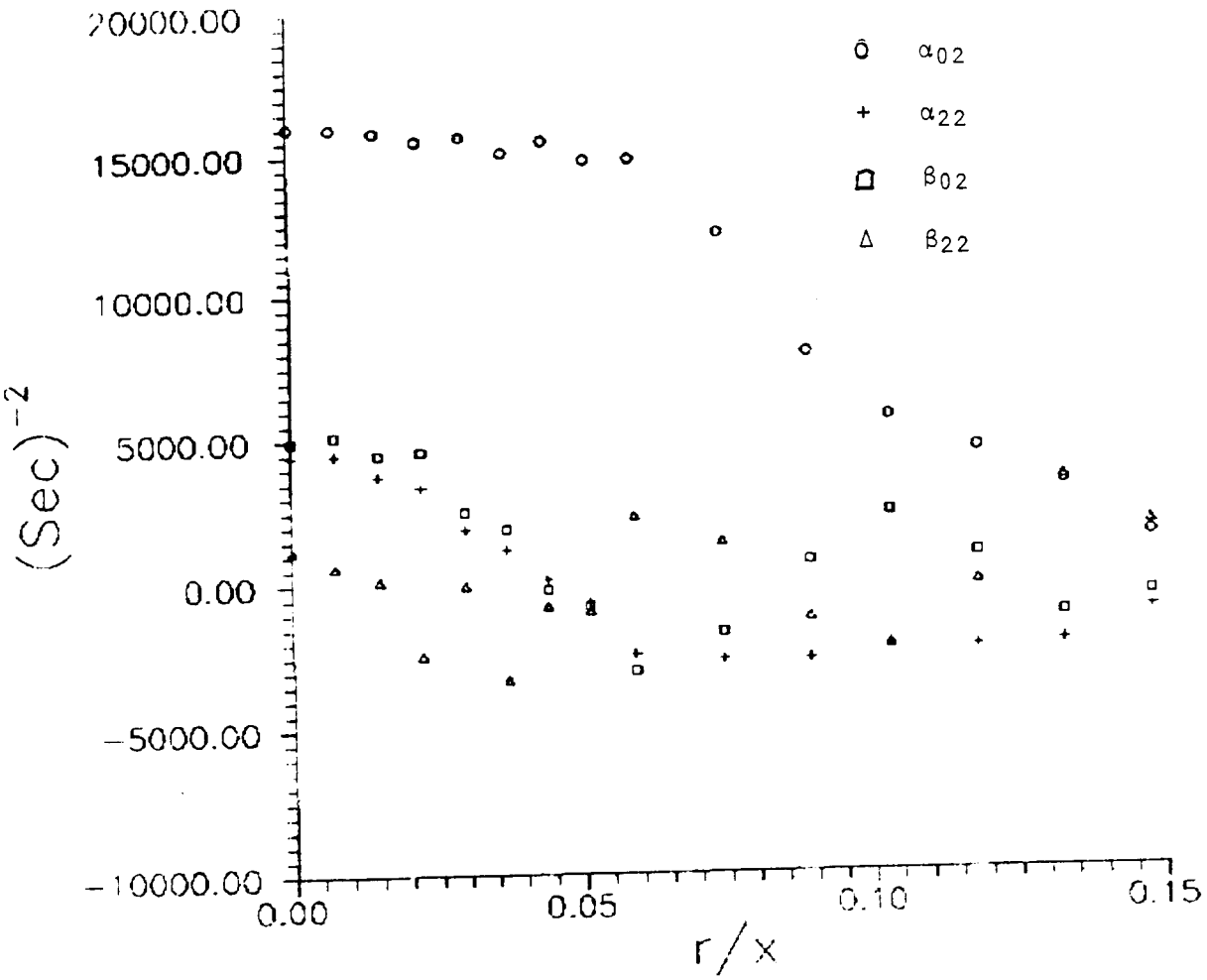

Figure 5.4.2 Dissipation Rate Profile

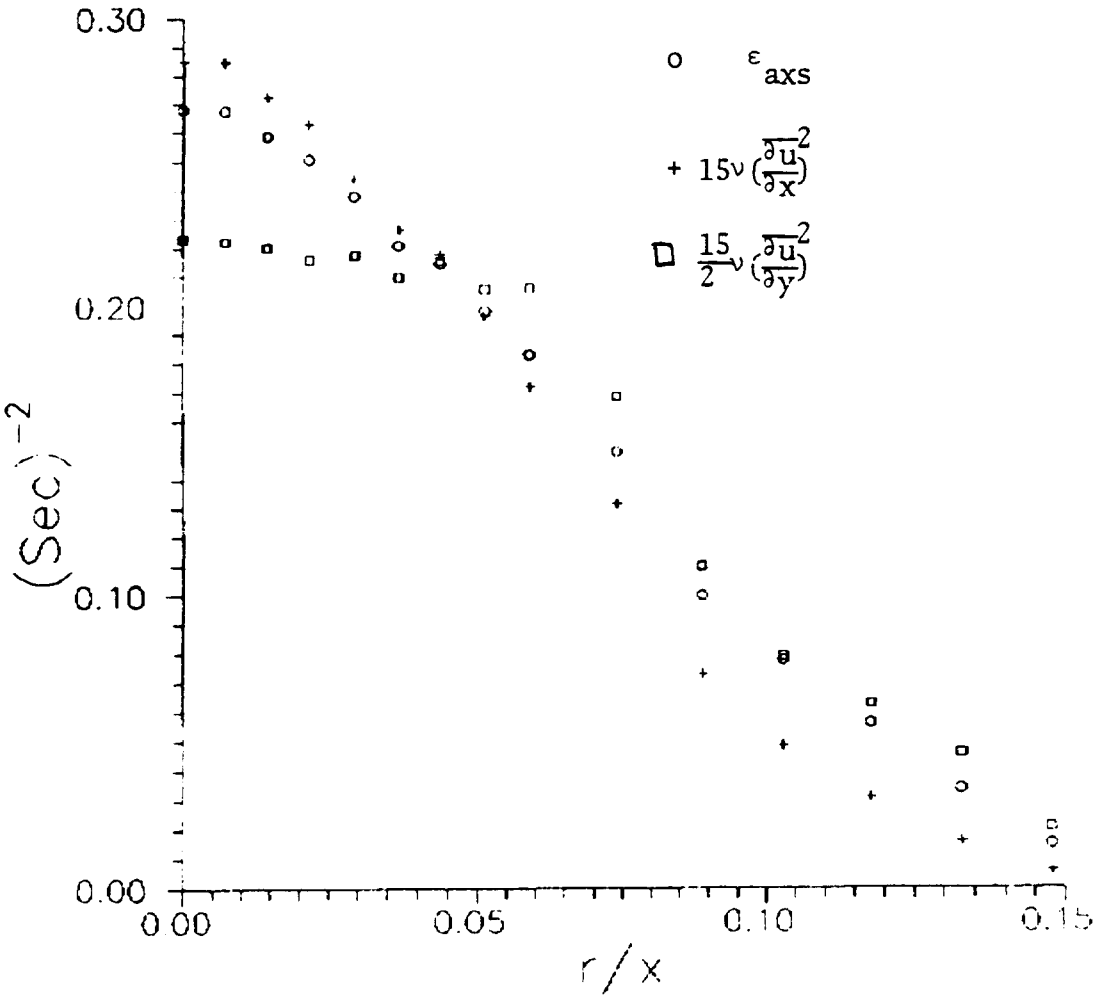

Figure 5.4.3 Mean Square Vorticity Profile

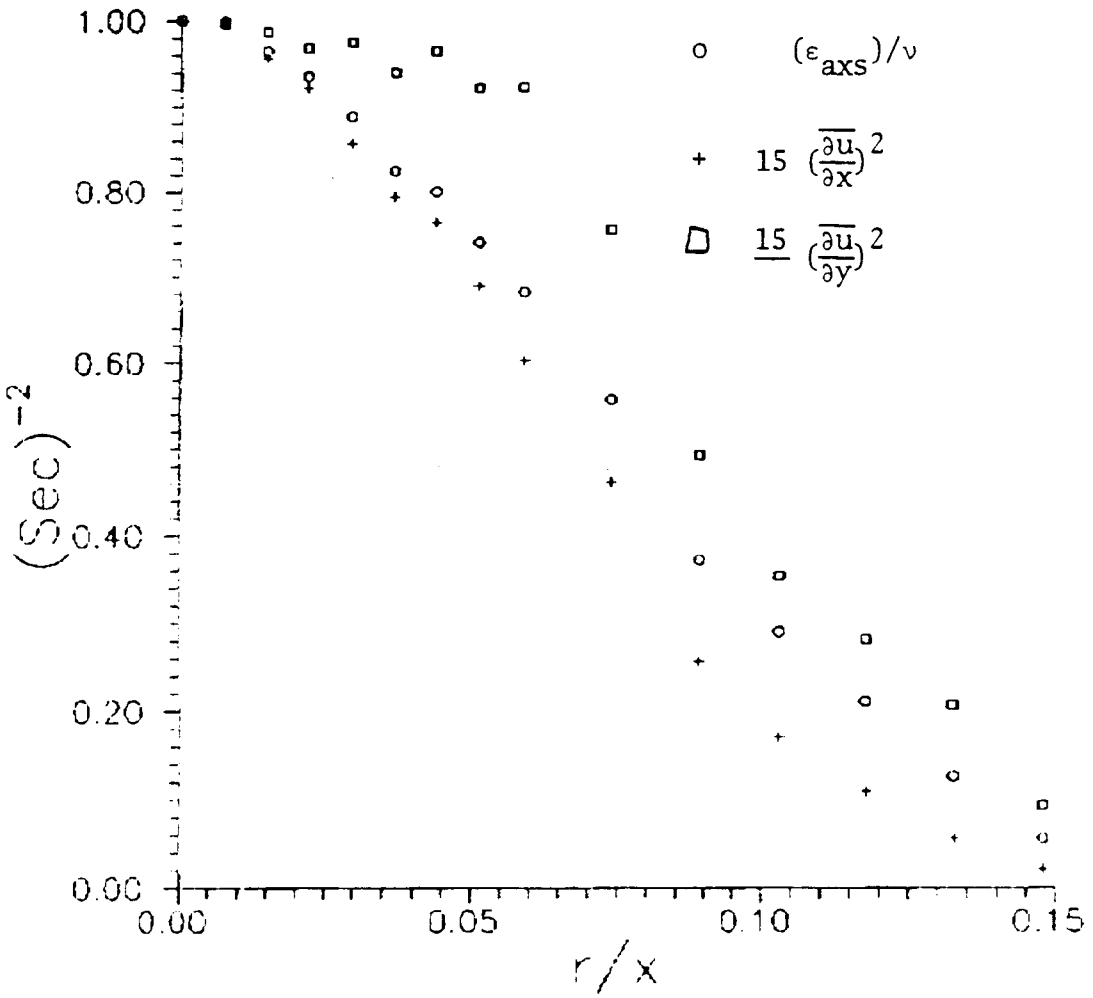

CHAPTER 6

Summary and Conclusions

The objective of this work was to provide a reliable set of data of the velocity moments and the dissipation for the axisymmetric turbulent jet. The mean velocity, second moment velocity, and velocity derivative profiles are presented in this work. Also the concept of local axisymmetry of the small scales is introduced. It was experimentally proven that the assumption of local axisymmetry is acceptable in this flow. The experiments required to accomplish this work provided ample opportunity to develop measurement techniques that are of use in all types of high turbulence intensity flows.

Three separate items that posed difficulties in this experimental investigation were addressed: The first was the requirement to design an appropriate probe for velocity derivative measurement, and the other two were related to the high intensity nature of the flow. The first item was brought about by the need to measure the numerous mean square derivative terms that make up the general mean square derivative tensor. The spatial resolution requirement for the correct measurement of the dissipative scales put a constraint on the size of the probe that could be used. Thus an analysis to determine exactly how many of the mean square derivative terms are pertinent for this flow was necessary before the probe needed could be designed. The introduction of the concept of local axisymmetry and the design and construction of the triple wire AXI-probe made it possible to measure the entire set of mean square derivative terms necessary for a direct determination of the dissipation.

Three of the mean-square derivatives in the dissipation were computed from their corresponding measured temporal derivatives. This conversion of temporal derivatives to spatial derivatives is normally done by using Taylor's frozen field hypothesis. The second difficulty in this investigation was due to the breakdown of this hypothesis for this high turbulence intensity flow. The use of the moving wire probe which reduces the effective turbulence intensity provides the only way to measure these terms accurately in this flow, since the Taylor's hypothesis does not apply for the stationary wire results. Having obtained a set of data with and without moving the wire, an assessment of the breakdown of this hypothesis was done. It was found that the correction model which was introduced by Lumley (1965) and George (1979) for the effect of fluctuating convection velocity on temporal derivative measured with stationary probe gives good results.

The third item in the instrument development aspect of this work was introduced by the difficulty in measuring with standard hot wires in this high turbulence intensity flow. More specifically the hot-wires which have a cross-flow and rectification errors give poor results at turbulence intensities that are higher than 30%. Comparisons between the results of the moving wire and stationary wire enabled an evaluation of these errors. The results for the error analysis for the moments of the velocity were presented in this work.

This work provides a considerable amount of data for the isothermal axisymmetric jet. It was proven that the jet is not locally isotropic but rather locally axisymmetric in the small scale. The direct measurement of the dissipation is presented for the first time for this type of flow. The techniques developed for

investigation of this flow can be used in other flows with similar high turbulence intensity characteristics, such as plane jets, axisymmetric thermal plumes, and flows in which there are regions of recirculation.

APPENDIX I

Theory of Axisymmetric Turbulence

A.I.1 Introduction

The theory of axisymmetric homogeneous turbulence described by Batchelor (1946) and Chandrasekhar (1950) provides a basis for the study of flows which are not locally isotropic. Unlike isotropic flows in which the small scales are independent of direction, axisymmetric homogeneous flows have a preferred direction. The functions of the velocities and their derivatives are invariant to rotations and reflections about the preferred direction. The study of these types of flows is of considerable importance since all laboratory flows have preferred directions in the direction of the mean shear. Thus it would not be too surprising if this were reflected in the turbulence statistics. In this Appendix a review of axisymmetric relations will be given and the equations for the mean dissipation rate and mean square vorticity fluctuations will be written for homogeneous flows with axial symmetry.

It will be seen that only four independent invariants are necessary to completely determine all of the single point second order derivative statistics, including the dissipation and mean square vorticity. The nine derivatives in a cartesian coordinate system are:

$$(\partial u_1/\partial x_1),\ (\partial u_1/\partial x_2),\ (\partial u_1/dx_3),$$

$$(\partial u_2/\partial x_1),\ (\partial u_2/\partial x_2),\ (\partial u_2/\partial x_3),$$

$$(\partial u_3/\partial x_1),\ (\partial u_3/\partial x_2),\ (\partial u_3/\partial x_3)$$

The most general form of the second order correlations of the derivatives is a tensor with 81 terms (see Table A.1). This tensor can be reduced to a manageable size by invoking the consequences of homogeneity and axisymmetry..

A.I.2 Implications of Homogeneity on the Second Order Derivative Correlation

The second order velocity correlations for a homogeneous flow can be written as:

$$\overline{u_i(\underline{x})\ u_j(\underline{x}+\underline{r})} = \overline{u_i(\underline{x}+\underline{r})\ u_j(\underline{x})} = \overline{u_i(\underline{x})\ u_j(\underline{x}-\underline{r})} \qquad \text{(A.I.1)}$$

where $r = \underline{x}'-\underline{x}$.

If

$$Q_{ij}(\underline{r}) = \overline{u_i(\underline{x})\ u_j(\underline{x}+\underline{r})}$$

it follows immediately that

$$Q_{i,j}(\underline{r}) = Q_{j,i}(-\underline{r}) \qquad \text{(A.I.2)}$$

Equation (A.I.2) implies that the diagonal elements are symmetrical in $\underline{r}$ so that

$$Q_{\alpha\alpha}(\underline{r}) = Q_{\alpha\alpha}(-\underline{r}) \quad \text{(no sum on } \alpha) \qquad \text{(A.I.3)}$$

The second order derivatives correlations form a fourth order tensor given by C_{ijkm} where

$$C_{ijkm} = \overline{\frac{\partial u_i}{\partial x_j}\frac{\partial u_k}{\partial x_m}} = \left.\overline{\frac{\partial u_i(x)}{\partial x_j}\frac{\partial u_k(x')}{\partial x_m'}}\right|_{\underline{x}=\underline{x}'}$$

$$= \left[\frac{\partial^2}{\partial x_m' \partial x_j}\ \overline{u_i(\underline{x})\ u_k'(\underline{x}')}\right]_{\underline{x}=\underline{x}'} \qquad \text{(A.I.4)}$$

TABLE A.1

$\left[\frac{\partial u}{\partial x}\right]^2$	$\left[\frac{\partial u}{\partial x}\right]\left[\frac{\partial v}{\partial x}\right]$	$\left[\frac{\partial u}{\partial x}\right]\left[\frac{\partial w}{\partial x}\right]$	$\left[\frac{\partial u}{\partial x}\right]\left[\frac{\partial u}{\partial y}\right]$	$\left[\frac{\partial u}{\partial x}\right]\left[\frac{\partial v}{\partial y}\right]$	$\left[\frac{\partial u}{\partial x}\right]\left[\frac{\partial w}{\partial y}\right]$	$\left[\frac{\partial u}{\partial x}\right]\left[\frac{\partial u}{\partial z}\right]$	$\left[\frac{\partial u}{\partial x}\right]\left[\frac{\partial v}{\partial z}\right]$	$\left[\frac{\partial u}{\partial x}\right]\left[\frac{\partial w}{\partial z}\right]$
$\left[\frac{\partial v}{\partial x}\right]\left[\frac{\partial u}{\partial x}\right]$	$\left[\frac{\partial v}{\partial x}\right]^2$	$\left[\frac{\partial v}{\partial x}\right]\left[\frac{\partial w}{\partial x}\right]$	$\left[\frac{\partial v}{\partial x}\right]\left[\frac{\partial u}{\partial y}\right]$	$\left[\frac{\partial v}{\partial x}\right]\left[\frac{\partial v}{\partial y}\right]$	$\left[\frac{\partial v}{\partial x}\right]\left[\frac{\partial w}{xy}\right]$	$\left[\frac{\partial v}{\partial x}\right]\left[\frac{\partial u}{\partial z}\right]$	$\left[\frac{\partial v}{\partial x}\right]\left[\frac{\partial v}{\partial z}\right]$	$\left[\frac{\partial v}{\partial x}\right]\left[\frac{\partial w}{\partial z}\right]$
$\left[\frac{\partial w}{\partial x}\right]\left[\frac{\partial u}{\partial x}\right]$	$\left[\frac{\partial w}{\partial x}\right]\left[\frac{\partial v}{\partial x}\right]$	$\left[\frac{\partial w}{\partial x}\right]^2$	$\left[\frac{\partial w}{\partial x}\right]\left[\frac{\partial y}{\partial y}\right]$	$\left[\frac{\partial w}{\partial x}\right]\left[\frac{\partial v}{\partial y}\right]$	$\left[\frac{\partial w}{\partial x}\right]\left[\frac{\partial w}{\partial y}\right]$	$\left[\frac{\partial w}{\partial x}\right]\left[\frac{\partial u}{\partial z}\right]$	$\left[\frac{\partial w}{\partial x}\right]\left[\frac{\partial v}{\partial z}\right]$	$\left[\frac{\partial w}{\partial x}\right]\left[\frac{\partial w}{\partial z}\right]$
$\left[\frac{\partial u}{\partial y}\right]\left[\frac{\partial u}{\partial x}\right]$	$\left[\frac{\partial u}{\partial y}\right]\left[\frac{\partial v}{\partial x}\right]$	$\left[\frac{\partial u}{\partial y}\right]\left[\frac{\partial w}{\partial y}\right]$	$\left[\frac{\partial u}{\partial y}\right]^2$	$\left[\frac{\partial u}{\partial y}\right]\left[\frac{\partial v}{\partial y}\right]$	$\left[\frac{\partial u}{\partial y}\right]\left[\frac{\partial w}{\partial z}\right]$	$\left[\frac{\partial u}{\partial y}\right]\left[\frac{\partial u}{\partial z}\right]$	$\left[\frac{\partial u}{\partial y}\right]\left[\frac{\partial v}{\partial z}\right]$	$\left[\frac{\partial u}{\partial y}\right]\left[\frac{\partial w}{\partial x}\right]$
$\left[\frac{\partial v}{\partial y}\right]\left[\frac{\partial u}{\partial x}\right]$	$\left[\frac{\partial v}{\partial y}\right]\left[\frac{\partial v}{\partial x}\right]$	$\left[\frac{\partial v}{\partial y}\right]\left[\frac{\partial w}{\partial x}\right]$	$\left[\frac{\partial v}{\partial y}\right]\left[\frac{\partial u}{\partial y}\right]$	$\left[\frac{\partial v}{\partial y}\right]^2$	$\left[\frac{\partial v}{\partial y}\right]\left[\frac{\partial w}{\partial y}\right]$	$\left[\frac{\partial v}{\partial y}\right]\left[\frac{\partial u}{\partial z}\right]$	$\left[\frac{\partial v}{\partial y}\right]\left[\frac{\partial v}{\partial z}\right]$	$\left[\frac{\partial v}{\partial y}\right]\left[\frac{\partial w}{\partial z}\right]$
$\left[\frac{\partial w}{\partial y}\right]\left[\frac{\partial u}{\partial x}\right]$	$\left[\frac{\partial w}{\partial y}\right]\left[\frac{\partial v}{\partial x}\right]$	$\left[\frac{\partial w}{\partial y}\right]\left[\frac{\partial w}{\partial x}\right]$	$\left[\frac{\partial w}{\partial y}\right]\left[\frac{\partial u}{\partial y}\right]$	$\left[\frac{\partial w}{\partial y}\right]\left[\frac{\partial v}{\partial y}\right]$	$\left[\frac{\partial w}{\partial y}\right]^2$	$\left[\frac{\partial w}{\partial y}\right]\left[\frac{\partial u}{\partial z}\right]$	$\left[\frac{\partial w}{\partial y}\right]\left[\frac{\partial v}{\partial z}\right]$	$\left[\frac{\partial w}{\partial y}\right]\left[\frac{\partial w}{\partial z}\right]$
$\left[\frac{\partial u}{\partial z}\right]\left[\frac{\partial u}{\partial x}\right]$	$\left[\frac{\partial u}{\partial z}\right]\left[\frac{\partial v}{\partial x}\right]$	$\left[\frac{\partial u}{\partial z}\right]\left[\frac{\partial w}{\partial x}\right]$	$\left[\frac{\partial u}{\partial z}\right]\left[\frac{\partial u}{\partial y}\right]$	$\left[\frac{\partial u}{\partial z}\right]\left[\frac{\partial v}{\partial y}\right]$	$\left[\frac{\partial u}{\partial z}\right]\left[\frac{\partial w}{\partial y}\right]$	$\left[\frac{\partial u}{\partial z}\right]^2$	$\left[\frac{\partial u}{\partial z}\right]\left[\frac{\partial v}{\partial z}\right]$	$\left[\frac{\partial u}{\partial z}\right]\left[\frac{\partial w}{\partial z}\right]$
$\left[\frac{\partial v}{\partial z}\right]\left[\frac{\partial u}{\partial x}\right]$	$\left[\frac{\partial v}{\partial z}\right]\left[\frac{\partial v}{\partial x}\right]$	$\left[\frac{\partial v}{\partial z}\right]\left[\frac{\partial w}{\partial x}\right]$	$\left[\frac{\partial v}{\partial z}\right]\left[\frac{\partial u}{\partial y}\right]$	$\left[\frac{\partial v}{\partial z}\right]\left[\frac{\partial v}{\partial y}\right]$	$\left[\frac{\partial v}{\partial z}\right]\left[\frac{\partial w}{\partial y}\right]$	$\left[\frac{\partial v}{\partial z}\right]\left[\frac{\partial u}{\partial z}\right]$	$\left[\frac{\partial v}{\partial z}\right]^2$	$\left[\frac{\partial v}{\partial z}\right]\left[\frac{\partial w}{\partial z}\right]$
$\left[\frac{\partial w}{\partial z}\right]\left[\frac{\partial u}{\partial x}\right]$	$\left[\frac{\partial w}{\partial z}\right]\left[\frac{\partial v}{\partial x}\right]$	$\left[\frac{\partial w}{\partial z}\right]\left[\frac{\partial w}{\partial x}\right]$	$\left[\frac{\partial w}{\partial z}\right]\left[\frac{\partial u}{\partial y}\right]$	$\left[\frac{\partial w}{\partial z}\right]\left[\frac{\partial v}{\partial y}\right]$	$\left[\frac{\partial w}{\partial z}\right]\left[\frac{\partial w}{\partial y}\right]$	$\left[\frac{\partial w}{\partial z}\right]\left[\frac{\partial u}{\partial z}\right]$	$\left[\frac{\partial w}{\partial z}\right]\left[\frac{\partial v}{\partial z}\right]$	$\left[\frac{\partial w}{\partial z}\right]^2$

since u_i is only a function of $\underline{x}$ and u_i' is only a function of $\underline{x}'$.

Defining

$$\underline{r} = \underline{x}' - \underline{x}$$

and

$$\underline{y} = \underline{x} + \underline{x},$$

we can map $\underline{x}', \underline{x} \rightarrow \underline{r}, \underline{y}$. The derivatives are related by the chain rule by

$$\frac{\partial}{\partial x_j} = \frac{\partial r_i}{\partial x_j}\frac{\partial}{\partial r_i} + \frac{\partial y_i}{\partial x_j}\frac{\partial}{\partial y_i}$$

$$= -\frac{\partial}{\partial r_j} + \frac{\partial}{\partial y_j}$$

Similarly,

$$\frac{\partial}{\partial x_m'} = \frac{\partial}{\partial r_m} + \frac{\partial}{\partial y_m}$$

Therefore the second derivative can be written in terms of $\underline{r}$ and $\underline{y}$ by

$$\frac{\partial^2}{\partial x_j \partial x_m'} = \left[-\frac{\partial}{\partial r_j} + \frac{\partial}{\partial y_j}\right]\left[\frac{\partial}{\partial r_m} + \frac{\partial}{\partial y_m}\right]$$

Since $\overline{u_i(\underline{x})u_j(\underline{x}')} = Q_{ij}(\underline{r})$ for homogeneous flow and is thus a function of r only,

$$\frac{\partial^2}{\partial x_m' \partial x_j}\overline{u_i u_k'} = -\frac{\partial^2}{\partial r_m \partial r_j} Q_{i,k}$$

It follows that

$$C_{ijkm} = \overline{\frac{\partial u_i}{\partial x_j}\frac{\partial u_k}{\partial x_m}} = -\left[\frac{\partial^2}{\partial r_m \partial r_j} Q_{i,k}\right]_{\underline{r}=0} \qquad \text{(A.I.5)}$$

Thus for homogeneous flows:

$$\overline{\frac{\partial u_i}{\partial x_j}\frac{\partial u_k}{\partial x_m}} = \overline{\frac{\partial u_i}{\partial x_m}\frac{\partial u_k}{\partial x_j}} \qquad \text{(A.I.6)}$$

This means that C_{ijkm} is symmetric in j and m, i.e.,

$$C_{ijkm} = C_{imkj} \tag{A.I.7}$$

Using $Q_{ij}(\underset{\sim}{r})=Q_{ji}(-\underset{\sim}{r})$ we find that

$$C_{ijkm} = -\frac{\partial^2}{\partial r_m \partial r_j} Q_{i,k}(\underset{\sim}{r})\Big|_{\underset{\sim}{r}=0} = -\frac{\partial^2}{\partial r_m \partial r_j} Q_{k,i}(-\underset{\sim}{r})\Big|_{\underset{\sim}{r}=0} = C_{kjim} \tag{A.I.8}$$

Thus C_{ijkm} is also symmetric in k and i.

The net result is that for homogeneous flows the number of independent 2nd order derivative correlations is:

$$\frac{81-9}{2} + 9 = 45$$

Table A.2 illustrates this reduction of Table A.1.

A.I.3 Representation of Second Order Velocity Tensor for Axisymmetric Homogeneous Turbulence

Chandrasekhar (1950) showed that the second order velocity correlation tensor for axisymmetric homogeneous turbulence could be expanded for small values of x; the result to second order is:

$$\begin{aligned} Q_{i,j} = {} & 2\left[\alpha_{02} - \alpha_{22} + \beta_{02}\right] r_i r_j \\ & + \left[-\left[2\alpha_{00} + \beta_{00}\right] + r^2\left\{\left[-4\alpha_{02} + 2\alpha_{22} - 3\beta_{02}\right]\right.\right. \\ & \qquad \left.\left. + \mu^2\left[2\beta_{02} - \beta_{22} - 8\alpha_{22}\right]\right\}\right]\delta_{ij} \\ & + \left[\beta_{00} + r^2\left[3\beta_{02} - 2\alpha_{22} + \beta_{22}\,\mu^2\right]\right]\lambda_i\lambda_j \\ & + 2r\mu\left[\lambda_i r_j + r_i\lambda_j\right]\left[2\alpha_{22} - \beta_{02}\right] \end{aligned} \tag{A.I.9}$$

TABLE A.2

$\left[\frac{\partial u}{\partial x}\right]^2$	$\left[\frac{\partial u}{\partial x}\right]\left[\frac{\partial v}{\partial x}\right]$	$\left[\frac{\partial u}{\partial x}\right]\left[\frac{\partial w}{\partial x}\right]$	$\left[\frac{\partial u}{\partial x}\right]\left[\frac{\partial u}{\partial y}\right]$	$\left[\frac{\partial u}{\partial x}\right]\left[\frac{\partial v}{\partial y}\right]$	$\left[\frac{\partial u}{\partial x}\right]\left[\frac{\partial w}{\partial y}\right]$	$\left[\frac{\partial u}{\partial x}\right]\left[\frac{\partial u}{\partial z}\right]$	$\left[\frac{\partial u}{\partial x}\right]\left[\frac{\partial v}{\partial z}\right]$	$\left[\frac{\partial u}{\partial x}\right]\left[\frac{\partial w}{\partial z}\right]$
	$\left[\frac{\partial v}{\partial x}\right]^2$	$\left[\frac{\partial v}{\partial x}\right]\left[\frac{\partial w}{\partial x}\right]$	$\left[\frac{\partial v}{\partial x}\right]\left[\frac{\partial u}{\partial y}\right]$	$\left[\frac{\partial v}{\partial x}\right]\left[\frac{\partial v}{\partial y}\right]$	$\left[\frac{\partial v}{\partial x}\right]\left[\frac{\partial w}{xy}\right]$	$\left[\frac{\partial v}{\partial x}\right]\left[\frac{\partial u}{\partial z}\right]$	$\left[\frac{\partial v}{\partial x}\right]\left[\frac{\partial v}{\partial z}\right]$	$\left[\frac{\partial v}{\partial x}\right]\left[\frac{\partial w}{\partial z}\right]$
		$\left[\frac{\partial w}{\partial x}\right]^2$	$\left[\frac{\partial w}{\partial x}\right]\left[\frac{\partial y}{\partial y}\right]$	$\left[\frac{\partial w}{\partial x}\right]\left[\frac{\partial v}{\partial y}\right]$	$\left[\frac{\partial w}{\partial x}\right]\left[\frac{\partial w}{\partial y}\right]$	$\left[\frac{\partial w}{\partial x}\right]\left[\frac{\partial u}{\partial z}\right]$	$\left[\frac{\partial w}{\partial x}\right]\left[\frac{\partial v}{\partial z}\right]$	$\left[\frac{\partial w}{\partial x}\right]\left[\frac{\partial w}{\partial z}\right]$
			$\left[\frac{\partial u}{\partial y}\right]^2$	$\left[\frac{\partial u}{\partial y}\right]\left[\frac{\partial v}{\partial y}\right]$	$\left[\frac{\partial u}{\partial y}\right]\left[\frac{\partial w}{\partial z}\right]$	$\left[\frac{\partial u}{\partial y}\right]\left[\frac{\partial u}{\partial z}\right]$	$\left[\frac{\partial u}{\partial y}\right]\left[\frac{\partial v}{\partial z}\right]$	$\left[\frac{\partial u}{\partial y}\right]\left[\frac{\partial w}{\partial x}\right]$
				$\left[\frac{\partial v}{\partial y}\right]^2$	$\left[\frac{\partial v}{\partial y}\right]\left[\frac{\partial w}{\partial y}\right]$	$\left[\frac{\partial v}{\partial y}\right]\left[\frac{\partial u}{\partial z}\right]$	$\left[\frac{\partial v}{\partial y}\right]\left[\frac{\partial v}{\partial z}\right]$	$\left[\frac{\partial v}{\partial y}\right]\left[\frac{\partial w}{\partial z}\right]$
					$\left[\frac{\partial w}{\partial y}\right]^2$	$\left[\frac{\partial w}{\partial y}\right]\left[\frac{\partial u}{\partial z}\right]$	$\left[\frac{\partial w}{\partial y}\right]\left[\frac{\partial v}{\partial z}\right]$	$\left[\frac{\partial w}{\partial y}\right]\left[\frac{\partial w}{\partial z}\right]$
						$\left[\frac{\partial u}{\partial z}\right]^2$	$\left[\frac{\partial u}{\partial z}\right]\left[\frac{\partial v}{\partial z}\right]$	$\left[\frac{\partial u}{\partial z}\right]\left[\frac{\partial w}{\partial z}\right]$
							$\left[\frac{\partial v}{\partial z}\right]^2$	$\left[\frac{\partial v}{\partial z}\right]\left[\frac{\partial w}{\partial z}\right]$
								$\left[\frac{\partial w}{\partial z}\right]^2$

where $r_i = x_i' - x_i$, $\underline{\lambda}$ is a unit vector for the preferred direction and $\mu = \underline{r}.\underline{\lambda}/r$. In the above equation the six coefficients, α_{oo}, α_{o2}, α_{22}, β_{oo}, β_{o2}, and β_{22} are the independent invariants.

If the preferred direction is chosen to be the 1-direction, then $\underline{\lambda} = (1,0,0)$ and $\mu = r_1/r$. Also,

$$\alpha_{00} = -\frac{\overline{u_1^2}}{2} \tag{A.I.10}$$

$$\beta_{00} = \overline{u_1^2} - \overline{u_2^2} = \overline{u_1^2} - \overline{u_3^2} \tag{A.I.11}$$

These will not enter the derivative relations.

It is easy to see that the diagonal elements depend only on r_1^2, r_2^2, and r_3^2; i.e.,

$$Q_{1,1}(\underline{r}) = -2\alpha_{00} + r_1^2\left[-2\alpha_{02} - 2\alpha_{22}\right] + (r_2^2+r_3^2)\left[-4\alpha_{02}\right] \tag{A.I.12}$$

$$Q_{2,2} = -\left[2\alpha_{00}+\beta_{00}\right] + r_1^2\left[-4\alpha_{02}-6\alpha_{22}-\beta_{02}-\beta_{22}\right] + r_2^2\left[-2\alpha_{02}-\beta_{02}\right]$$

$$+ r_3^2\left[-4\alpha_{02} + 2\alpha_{22} - 3\beta_{02}\right] \tag{A.I.13}$$

$$Q_{3,3} = -\left[2\alpha_{00}+\beta_{00}\right] + r_1^2\left[-4\alpha_{22}-6\alpha_{22}-\beta_{02}-\beta_{22}\right]$$

$$+ r_2^2\left[-4\alpha_{02} + 2\alpha_{22} - 3\beta_{02}\right] + r_3^2\left[-2\alpha_{02} - \beta_{02}\right] \tag{A.I.14}$$

The above results show that $Q_{2,2}$ and $Q_{3,3}$ have similar forms which is the expected consequence of axisymmetry.

For the off-diagonal elements we know from homogeneity that $Q_{i,j}(\underline{r}) = Q_{j,i}(-\underline{r})$. From equation (A.I.9) the three independent terms are given by

$$Q_{12} = 2(\alpha_{02}+\alpha_{22})r_1r_2 \tag{A.I.15}$$

$$Q_{13} = 2(\alpha_{02}+\alpha_{22})r_1r_3 \tag{A.I.16}$$

$$Q_{23} = 2(\alpha_{02}-\alpha_{22}+\beta_{02})r_2r_3 \tag{A.I.17}$$

A.I.4 Consequences of Axisymmetry on Second Order Derivatives

From equation (A.I.5) and equations (A.I.12)-(A.I.17), it can be shown that only 15 of the remaining derivative correlations are non-zero. These can in turn be related to the four invariants α_{02}, α_{22}, β_{02}, and β_{22}. The non-zero terms are given by

$$\overline{\left[\frac{\partial u_1}{\partial x_1}\right]^2} = 4\alpha_{02}+4\alpha_{22} \tag{A.I.18}$$

$$\overline{\left[\frac{\partial u_1}{\partial x_2}\right]^2} = \overline{\left[\frac{\partial u_1}{\partial x_3}\right]^2} = 8\alpha_{02} \tag{A.I.19}$$

$$\overline{\left[\frac{\partial u_2}{\partial x_1}\right]^2} = \overline{\left[\frac{\partial u_3}{\partial x_1}\right]^2} = 8\alpha_{02}+12\alpha_{22}+2\beta_{02}+2\beta_{22} \tag{A.I.20}$$

$$\overline{\left[\frac{\partial u_2}{\partial x_2}\right]^2} = \overline{\left[\frac{\partial u_3}{\partial x_3}\right]^2} = 4\alpha_{02}+2\beta_{02} \tag{A.I.21}$$

$$\overline{\left[\frac{\partial u_2}{\partial x_3}\right]^2} = \overline{\left[\frac{\partial u_3}{\partial x_2}\right]^2} = 8\alpha_{02}-4\alpha_{22}+6\beta_{02} \tag{A.I.22}$$

$$\overline{\frac{\partial u_1}{\partial x_2}\frac{\partial u_2}{\partial x_1}} = \overline{\frac{\partial u_1}{\partial x_3}\frac{\partial u_3}{\partial x_1}} = \overline{\frac{\partial u_1}{\partial x_2}\frac{\partial u_2}{\partial x_1}} = \overline{\frac{\partial u_1}{\partial x_3}\frac{\partial u_3}{\partial x_1}} = -2\alpha_{02}-2\alpha_{22} \tag{A.I.23}$$

$$\overline{\frac{\partial u_2}{\partial x_3}\frac{\partial u_3}{\partial x_2}} = \overline{\frac{\partial u_2}{\partial x_3}\frac{\partial u_3}{\partial x_2}} = -2\alpha_{02}+2\alpha_{22}-2\beta_{02} \tag{A.I.24}$$

A.1.5 Representation of ϵ and $\overline{\omega^2}$

In the last section it was determined that all of the independent terms of the velocity derivative correlations can be represented by the four invariants α_{02}, α_{22}, β_{02}, β_{22}. In this section this result is implemented to represent the dissipation ϵ and mean square vorticity $\overline{\omega^2}$ in terms of the four invariants. The significance of this is that the dissipation can be calculated from these directly measured invariants.

The dissipation of turbulence is given by,

$$\epsilon = 2\nu\,\overline{e_{ij}e_{ij}} = \nu\left\{2\left[\overline{\left(\frac{\partial u_1}{\partial x_1}\right)^2} + \overline{\left(\frac{\partial u_2}{\partial x_2}\right)^2} + \overline{\left(\frac{\partial u_3}{\partial x_3}\right)^2}\right]\right.$$

$$+ \left[\overline{\left(\frac{\partial u_1}{\partial x_2}\right)^2} + \overline{\left(\frac{\partial u_1}{\partial x_3}\right)^2} + \overline{\left(\frac{\partial u_2}{\partial x_1}\right)^2} + \overline{\left(\frac{\partial u_2}{\partial x_3}\right)^2} + \overline{\left(\frac{\partial u_3}{\partial x_1}\right)^2} + \overline{\left(\frac{\partial u_3}{\partial x_2}\right)^2}\right]$$

$$\left. + 2\left[\overline{\left(\frac{\partial u_2}{\partial x_1}\right)\left(\frac{\partial u_1}{\partial x_2}\right)} + \overline{\left(\frac{\partial u_3}{\partial x_1}\right)\left(\frac{\partial u_1}{\partial x_3}\right)} + \overline{\left(\frac{\partial u_3}{\partial x_2}\right)\left(\frac{\partial u_2}{\partial x_3}\right)}\right]\right\} \qquad \text{(A.I.25)}$$

Substituting equations (A.I.18) to (A.I.24) into equation (A.I.25) yields the dissipation as,

$$\epsilon = \nu\left[60\alpha_{02} + 20\alpha_{22} + 20\beta_{02} + 4\beta_{22}\right] \qquad \text{(A.I.26)}$$

For isotropic flows, $\alpha_{22} = \beta_{02} = \beta_{22} = 0$ so that the isotropic dissipation can be recovered from equation (A.I.18) and (A.I.19) as

$$\epsilon = \nu\ 60\alpha_{02} = \frac{15}{2}\ \nu\ \overline{\left(\frac{\partial u}{\partial y}\right)^2} = 15\ \nu\ \overline{\left(\frac{\partial u}{\partial x}\right)^2} \qquad \text{(A.I.27)}$$

In a similar manner, the mean square vorticity can also be shown to be given by

$$\overline{\omega_i \omega_i} = 60\ \alpha_{02} + 20\ \alpha_{22} + 20\ \beta_{02} + 4\beta_{22} \qquad \text{(A.I.28)}$$

which is equal to $2\overline{e_{ij} e_{ij}}$ as required for homogeneous turbulence. (Note that equations 129 and 130 of Chandrasekar (95) are incorrect for $\overline{\omega_i \omega_i}$).

APPENDIX II

The Application of Taylor's Hypothesis to Velocity Derivative Measurements

Lumley (1965) and Wyngaard and Clifford (1977) have presented analyses of the effect of the fluctuating convection velocity on spectral and derivative analyses. In both cases, the analysis of the fluctuating derivatives began with the truncation of an assumed Gaussian characteristic function for the turbulence, and it was therefore believed to be limited in some manner. The purpose of the brief analysis presented below which is due to George and Beuther (1979) is to illustrate that their result can be obtained without the Gaussian assumption, and should therefore be applicable over a wider range of turbulence intensities than might have been believed from the earlier analysis.

We begin by analyzing the response of a randomly moving probe in a homogeneous velocity field, $\underline{u}(\underline{x})$. Let us assume the probe to respond only to the 1-component of the turbulent velocity. Let us further assume that the turbulent field is frozen and that the probe moves through it. The time varying signal seen by the probe can then be written as

$$u_m(t) = \int e^{i\underline{k}\cdot\underline{X}_p} \hat{u}(\underline{k})d\underline{k} \qquad (A.II.1)$$

where $\underline{X}_p(t)$ represents the motion of the probe and $\hat{u}$ is the Fourier transform of the velocity field.

We seek a relation between the time derivative of $u_m(t)$ and the spatial derivative of $u(\underline{x})$. Differentiating equation (A.II.1) we have,

have,

$$\dot{u}_m = \int e^{i\underline{k}\cdot\underline{X}_p} (i\underline{k}\cdot\dot{\underline{X}}_p)\, \hat{u}(\underline{k})\, d\underline{k} \qquad \text{(A.II.2)}$$

from which it follows that

$$\overline{(\dot{u}_m)^2} = -\iint e^{i(\underline{k}-\underline{k}')\cdot\underline{X}_p} (\underline{k}\cdot\dot{\underline{X}}_p)(\underline{k}'\cdot\dot{\underline{X}}_p)\, \overline{\hat{u}(\underline{k})\, \hat{u}^*(\underline{k}')}\, d\underline{k}\, d\underline{k}'$$

If we assume the motion of the probe to be statistically independent from the turbulence we can write

$$\overline{(\dot{u}_m)^2} = -\int e^{i(\underline{k}-\underline{k}')\cdot\underline{X}_p} \overline{(\underline{k}\cdot\dot{\underline{X}}_p)(\underline{k}'\cdot\dot{\underline{X}}'_p)}\; \overline{u(\hat{\underline{k}})u(\hat{\underline{k}}')}\, d\underline{k}\, d\underline{k}' \qquad \text{(A.II.3)}$$

Since the field is assumed homogeneous

$$\overline{\hat{u}(\underline{k})\hat{u}^*(\underline{k}')}\, d\underline{k}\, d\underline{k}' = F_{11}(\underline{k})\, \delta(\underline{k}'-\underline{k}) d\underline{k}\, d\underline{k}' \qquad \text{(A.II.4)}$$

where F_{11} is the three-dimensional spectrum of the turbulent velocity.

The position of the probe is simply the time integral of its velocity added to its initial position, i.e.

$$\underline{X}_p(t) = \underline{X}_p(0) + \int_0^t \tilde{\underline{u}}_p(t_1) dt_1 \qquad \text{(A.II.5)}$$

where $\tilde{\underline{u}}_p$ is the instantaneous probe velocity. Thus

$$\begin{aligned} \dot{\underline{X}}_p(t) &= \tilde{\underline{u}}_p(t) \\ &= \underline{U}_p + \underline{u}_p \end{aligned} \qquad \text{(A.II.6)}$$

where $\underline{U}_p$ is the mean probe velocity and $\underline{u}_p$ is its fluctuating component. It follows immediately that

$$\overline{\left[\dot{u}_m(t)\right]^2} = \int \overline{\left[\underline{k}\cdot\underline{U} + \underline{k}\cdot\underline{u}_p\right]^2} F_{11}(\underline{k})\, d\underline{k} \qquad \text{(A.II.7)}$$

We consider the mean motion of the probe to be only in the 1-direction while we allow its fluctuating motion to be in all directions, i.e.,

$$\underline{U}_p = (U_p, 0, 0)$$

and

$$\underline{u}_p = (u_{p1}, u_{p2}, u_{p3})$$

Inserting these into equation (A.II.7) yields the measured mean square time derivative as

$$\begin{aligned}
\overline{[\dot{u}_m(t)]^2} = {} & U_p^2 \int k_1^2 F_{11}(\underline{k})d\underline{k} \\
& + \overline{u_{p_1}^2} \int k_1^2 F_{11}(\underline{k})d\underline{k} \\
& + 2\overline{u_{p1}u_{p2}} \int k_1 k_2 F_{11}(\underline{k})d\underline{k} \\
& + 2\overline{u_{p1}u_{p3}} \int k_1 k_3 F_{11}(\underline{k})d\underline{k} \\
& + \overline{u_{p2}^2} \int k_2^2 F_{11}(\underline{k})d\underline{k} \\
& + 2\overline{u_{p2}u_{p3}} \int k_2 k_3 F_{11}(\underline{k}\, d\underline{k} \\
& + \overline{u_{p3}^2} \int k_3^2 F_{11}(\underline{k}d\underline{k}
\end{aligned} \qquad \text{(A.II.8)}$$

The integrals of equation (A.II.8) can be readily recognized as the mean square velocity derivatives. Thus

$$\begin{aligned}
\overline{(\dot{u}_m)^2} = {} & \overline{(U_{p1}+u_{p_1})^2}\ \overline{(\partial u_1/\partial x_1)^2} + \overline{(u_{p2}^2)}\ \overline{(\partial u_1/\partial x_2)^2} \\
& + \overline{(u_{p3})^2}\ \overline{(\partial u_1/\partial x_3)^2} \qquad \text{(A.II.9)} \\
& + 2\overline{u_{p1}u_{p2}} \left[\overline{\frac{\partial u_1}{\partial x_1}\frac{\partial u_1}{\partial x_2}}\right] + 2\overline{u_{p1}u_{p3}} \left[\overline{\frac{\partial u_1}{\partial x_1}\frac{\partial u_1}{\partial x_3}}\right] + 2\overline{u_{p2}u_{p3}} \left[\overline{\frac{\partial u_1}{\partial x_2}\frac{\partial u_1}{\partial x_3}}\right] \\
& + \overline{2u_{p2}u_{p3}} \left[\overline{\frac{\partial u_1}{\partial x_2}\frac{\partial u_1}{\partial x_3}}\right] .
\end{aligned}$$

For a homogeneous flow:

$$\overline{\frac{\partial u_1}{\partial x_1}\frac{\partial u_1}{\partial x_2}} = \overline{\frac{\partial u_1}{\partial x_1}\frac{\partial u_1}{\partial x_3}} = \overline{\frac{\partial u_1}{\partial x_2}\frac{\partial u_1}{\partial x_3}} = 0 \qquad \text{(A.II.10)}$$

Therefore,

$$\overline{\left[u_m^2\right]^2} = U_{p1}^2\overline{\left[\frac{\partial u_1}{\partial x_1}\right]^2} + \overline{u_{p1}}^2\overline{\left[\frac{\partial u_1}{\partial x_1}\right]^2} + \overline{u_{p2}}^2\overline{\left[\frac{\partial u_1}{\partial x_2}\right]^2} + \overline{u_{p3}}^2\overline{\left[\frac{\partial u}{\partial x_3}\right]^2} \qquad \text{(A.II.11)}$$

At this point we identify our probe velocity to be equal and opposite to the local fluid velocity (which corresponds to a probe at rest in a moving field). In doing this we of necessity violate the condition of independence of probe and fluid motions introduced earlier. However, we may assume the condition to be approximately valid if we confine our attention to the small scale turbulence which is nearly independent of that containing the turbulent energy (Lumley (1965) has discussed the validity of this). The assumption is particularly good if we confine our attention to high turbulence Reynolds number flows because we are interested only in mean square velocity gradients which receive their primary contribution from the dissipative scales, while the convection of disturbances past the probe is primarily due to the more energetic turbulence.

If we are further willing to assume the small scale turbulence to be locally isotropic, then derivatives are related by

$$\overline{(\partial u_1/\partial x_2)^2} = \overline{(\partial u_1/\partial x_3)^2} = \overline{2(\partial u_1/\partial x_1)^2}$$

Using these, the mean square derivative signal seen by a stationary probe in a moving turbulent field is

$$U^{-2}\,\overline{(\dot{u}_m)^2} = \overline{(\partial u/\partial x_1)^2}\left[1 + \frac{\overline{u_1^2}}{U^2} + 2\,\frac{\overline{u_2^2}+\overline{u_3^2}}{U^2}\right] \qquad \text{(A.II.12)}$$

Thus a primitive application of Taylor's hypothesis to the time derivative of the streamwise velocity yields a value of $\overline{(\partial u_1/\partial x_1)^2}$ which is too high by a factor of

$$\frac{\overline{\left(\frac{\partial u_1}{\partial x_1}\right)^2}_{meas}}{\overline{\left(\frac{\partial u_1}{\partial x_1}\right)^2}} = \left[1 + \frac{\overline{u_1^2}}{U^2} + 2\left(\frac{\overline{u_2^2}+\overline{u_3^2}}{U^2}\right)\right]$$

This is exactly the result obtained by Lumley (1965), but with fewer assumptions.

REFERENCES

Baker, C.B. (1980) "An Analysis of the Turbulent Buoyant Jet", Ph.D. Dissertation, Pennsylvania State University.

Baker, C.B., W.K. George and D.B. Taulbee (1980) "An Analysis of the Axisymmetric Turbulent Buoyant Jet", Proc. 7th Inter. Heat Trans. Conf. Sept. 6-10, 1982, Munich, West Germany.

Batchelor, G.K. (1946) "Theory of Axisymmetric Turbulence", Proc. Roy.Soc. A, 186, 480.

Beuther, P.D. (1980) "Experimental Investigation of the Axisymmetric Turbulent Buoyant Plumes", PhD Dissertation, University at Buffalo, SUNY.

Beuther, P.D., A. Shabbir and W.K. George (1987) "X-Wire Response in Turbulent Flows with High Intensity Turbulence and Low Mean Velocity", ASME Proc. Symp. on Thermal Anemometry, Cincinnati, OH

Cantwell, B. and C. Coles (1983) "An Experimental Study of Entrainment and Transport in the Turbulent Near Wake of a Circular Cylinder, J. Fluid Mech. 136, 321-374.

Capp et al. (1988) In preparation.

Capp, S.P. (1983) "Experimental Investigation of the Turbulent Axisymmetric Jet", PhD Dissertation, University at Buffalo, SUNY.

Champagne, F.H. (1978) "The Fine Scale Structure of the Turbulent Velocity Field", J. Fluid Mech., 86, Pt. 1, 67.

Chandraseklar, S. (1950) "Theory of Axisymmetric Turbulence", Proc. Roy Soc. A., 242, 855.

Corrsin, S. (1943) National Advisory Committee, Aeronaut. Wartime Reports., No. 94.

Corrsin, S. and M.S. Uberoi (1949) National Advisory Committee, Aeronaut. Tech. Notes No. 1865.

Corrsin, S. and M.S. Uberoi (1951) "Spectra and Diffusion in a Round Turbulent Jet", NACA Rep. 1940 (originally published as NACA Tech. Note 2124, Aug. 1950).

Corrsin, S. (1951) "The Decay of Isotropic Temperature Fluctuations in an Isotropic Turbulence", J. Aeronaut. Sci., 18, No. 6, 417-423.

Corrsin, S. and A.L. Kistler (1954) National Advisory Committee Aeronaut. Tech. Notes No. 3133.

Doughman, E.L. (1972) "Development of a Hot-Wire Anemometer for Hypersonic Turbulent Flows". The Review of Scientific Instruments, 43, 8, 1200.

Durst,F., A. Melling, J.H. Whitelaw (1976) "Principles and Practice of Laser-Doppler Anemometry", New York: Academic Press.

George, W.K. and P.D. Beuther (1979) "Interpretation of Turbulent Measurements in High Intensity Shear Flow", Bull. Am.Phys.Soc., Ser.II, 24, No. 8.

George, W.K., A.A. Seif and C.B. Baker (1982) "Momentum Balance Considerations in Axisymmetric Turbulent Jets", unpublished.

George, W.K., A. Shabbir and D.B. Taulbee (1985) "The Effects of Screens on Attempts to Generate Free Turbulent Shear Flows", 38th APS, Bull. V. 30, 10.

George, W.K., P.D. Beuther and A. Shabbir (1987) "Polynomial Calbirations for Hot Wires in Thermally Varying Flows", ASME Appl. Mech., Bioengr and Fluids Engr. Conf., Cincinnati, OH

George, W.K. (1980a) "Governing Equations, Experiments and the Experimentalist", 1st World Cobnference on Heat Transfer, Fluid Mechanics and Thermodynamics, Dubrovnik, Yugoslavia, Sept. 5-9.

George, W.K. (1988) "The Self-Preservation of Turbulent Flows and its Relation to Initial Conditions and Coherent Structures", Advances in Turbulence (George and Arndt, ed.), Hemisphere Pub.

Hinze, J.O. and B.G. van der Hegge Zijnen (1949) "Transfer of Heat and Matter in the Turbulent Mixing Zone of an Axially Symmetrical Jet", Appl.Sci. Res., V.1A, 435-461.

Launder, B.E., G.J. Reece and W. Rodi (1975) "Progress in the Development of a Reynolds Stress Turbulence Closure", J. Fluid Mech. 68, 537-566.

Lee, M. and W.C. Reynolds (1985) "Bifurcating and Blooming Jets", Rept. TF-22, Thermosciences Div., Dept. of Mech. Engr., Stanford Univ.

Lehrmann, B. (1986) "Laser Doppler Measurements in a Turbulent Free Jet", DFVLR–Forschungsbericht, 55-86.

Lumley, J.L. (1965) "Interpretation of Time Spectra Measured in High-Intensity Shear Flows" Physics of Fluids, 8, 1056-1062.

Lumley, J.L. (1970) "Stochastic Tools in Turbulence", Academic Press.

Lumley, J.L. (1978) "Computational Modeling of Turbulent Flows, Advances in Applied Mechanics", 18, 123-176.

Monin, A.S. and A.M. Yaglom (1971) "Statistical Fluid Mechanics, Mechanics of Turbulence, 1, MIT Press.

Morel, T. (1975) "Comprehensive Design of Axisymmetric Wind Tunnel Contractions" J. Fluids Engr., ASME Trans. Sec. I, V.97, 225-233.
Panchapaken (1987)

Panchapakesan, N.R. and J.L. Lumley (1986) "Round Jet Measurements with a Hot-Wire Probe Mounted on a Shuttle", Bull. Am.Phys. Soc., Ser. II, 31, No. 10.

Panchapakesan, N.R. and J.L. Lumley (1987) "Shuttle Mounted X-Wire Measurements in a Round Jet", 40th APS, Eugene, OR.

Pao, Y.H. (1965) "Structure of Turbulent Velocity and Scalar Fields at Large Wavenumbers" Physics of Fluids, 8, 1063-75.

Peng, D. (1985) "Hot Wire Measurements in a Momentum Conserving Axisymmetric Jet", MS Thesis, University at Buffalo, SUNY.

Reichardt, H. (1951) 2nd Ed. Forsch. Gebiete Ingenieurw., No. 414.

Rodi, W. and D.B. Spaulding (1970) "A Two-Parameter Model of Turbulence and Its Application to Free Jets", Warme und Stoffubertragung, 3, 85.

Rodi, W. (1975) "New Method of Analyzing Hot-Wire Signals in Highly Turbulent Flow and its Evaluation in Round Jets", Disa Info. No. 17.

Schneider, W. (1985) "Decay of Momentum Flux in Submerged Jets" J. Fluid Mechanics, 154, 91-110.

Seif, A.A. (1981) "Higher Order Closure Model for Turbulent Jets", PhD Dissertation, University at Buffalo, SUNY.

Shabbir, A. and W.K. George (1987) "Energy Balance Measurements in an Axisymmetric Turbulent Buoyant Plume in a Neutral Environment", 6th Symp. on Turbulent Shear Flows, Toulouse, France.

Tan-atichat, J. (1980) "Effects of Axisymmetric Contractions on Turbulence of Various Scales" Ph.D. Thesis, Illinois Inst. Tech.

Taulbee, D.B., H.J. Hussein and S.P. Capp (1987) "The Round Jet Experiment and Inferences on Turbulence Modeling", 6th Symp. on Turbulent Shear Flows, Toulouse, France.

Taulbee, D.B. (1988) "Engineering Turbulence Models. A State-Of-The-Art Review" to appear in New Horizons in Turbulence, Hemisphere Pub.

Tollmien, W., (1926) "Berechnung Turbulenter Auxbreitunsvorgange", ZAMM, 6, 468-478.

Townsend, A.A. (1976) "The Structure of Turbulent Shear Flows", 2nd Ed., Cambridge University Press.

Tutu, N. and R. Chevray (1975) "Cross-wire Anemometry in High Intensity Turbulence" J. Fluid Mechanics, 71, 785-800.

Uberoi, M.S. and L.S.G. Kovasznay (1953) "On Mapping and Measurement of Random Fields", Quarterly of Applied Mathematics, 10, 375.

Uberoi, M.S. (1975) Presentation at APS/DFD 36th Annual Meeting, College Park, MD.

Watmuff, J.H., A.E. Perry and M.S. Chang (1983) "A Flying Hot-Wire System", Experiments in Fluids, 1, 63-71.

Wyngaard, J.C. (1968) "Measurement of Small Scale Turbulence Structure with Hot-Wires" J. Sq. Instrum. 1, 1105-1108.

Wyngaard, J.C. and S.F. Clifford (1977) "Taylor's Hypothesis and High Frequency Turbulence Spectra" J. Atm. Sci., 34, 922.

Wygnanski, I. and H.E. Fiedler (1969) "Some Measurements in the Self-Preserving Jet" J. Fluid Mech., 38, 577-612.